Trends and internal variability in Brazilian hydropower catchments

Emilie Byermoen
Master's thesis in Energy
Geophysical Institute
University of Bergen

June 1, 2023

Acknowledgements

Abstract

Hydropower is a major energy source in Brazil, and long-term hydropower production planning is crucial both for maintaining energy and water security in the country. The amount of water that is available to electricity production in the reservoirs have changed in the recent years, and there is an urgent need to understand the cause(s) of these changes, and whether observed streamflow trends will persist, reverse or amplify in the future.

In this thesis, I therefore separate externally forced precipitation and evaporation trends and variability from internal variations originating in the ocean for three hydrographic catchments in Brazil: Óbidos catchment in Amazon, Propria catchment in São Francisco and Porto Murtinho catchment in Paraguay. I compare an ocean anomaly assimilation experiment of Norwegian Climate Prediction Model (NorCPM) to an externally forced historical experiment and observed streamflow, precipitation and evaporation in the catchments.

The results indicate that the multi-decadal increasing streamflow trend in Amazon is (partly) externally forced, and might therefore persist, but that the SON streamflow is tightly connected to JJA precipitation variation which is shown to be driven by ocean variation, and may therefore reverse in the future. The long-term decrease of precipitation in São francisco is likely to be caused by internal variability, and is therefore likely to (partly) restore in the future, but results indicate that decadal streamflow variations in the basin is substantially impacted by other factors than precipitation as well. São Francisco catchment is found to be strongly connected to DJF precipitation variations that the model is unable to replicate. In Paraguay, I find that the austral summer streamflow is tightly connected to interannual precipitation variability that originates in the ocean in austral winter and spring. The steep significant decrease in streamflow over the last decades in Paraguay catchment is likely to have additional causes than precipitation, according to the results.

All the results have implications for hydropower and water management planning in the three catchments in Brazil.

Contents

Chapter 1

Introduction

Hydropower is the largest contributor to renewable energy in the world (International Energy Agency, 2022b), and Brazil is the country that produces the second most hydropower (International Energy Agency, 2012). More than 65 % of the electricity in the country is hydropower, making Brazil one of the least carbon-intensive energy sectors in the world, and one of the countries that relies the most on electricity from hydropower (International Energy Agency, 2022a). Hydropower production planning in the country is crucial, both for maintaining energy security and for reducing carbon emissions in the future.

At the same time, water scarcity is projected to increase in South America (Caretta et al., 2022 and references therein), and most of Brazil is projected to become drier (Zaninelli et al., 2019; Reboita et al., 2022) and to experience more rainfall variability in the future (Alves et al., 2020).

Droughts have already started to affect hydropower production and energy security in recent years. All of the most severe and intense droughts over the last 60 years have occurred after 2011, and 2012-2014 were the first years where all regions of Brazil experienced drought at the same time (Cunha et al., 2019). Sobradinho reservoir in the northeastern part of the country reached filling degrees of 1 percent in 2015 and 2 precent in 2017, and Cantareira reservoir in the state of Sao Paulo was down to 5 percent capacity in 2015 (Abatan et al., 2022).

There is an urgent need to understand the reason(s) for these recent changes, as this can help to understand if the changes will persist, amplify or reverse in the future. The knowledge on the reasons for changed precipitation and inflow into Brazilian hydropower plants is essential to ensure successful planning, both for energy companies and government. Identifying climatic factors that influence hydropower production is also valuable in the development of seasonal prediction models.

As pointed out in the IPCC 6th Assessment report (2022): "In the energy sector, a large number of studies document the impact of extreme climate events (e.g., droughts or extreme temperature days) on production of hydropower and thermoelectric power, yet there are limited studies that measure trends in energy production due to long-term climate change. This remains a knowledge gap." (Caretta et al., 2022, pp. 586).

Part of this missing knowledge is what I will try to uncover, when I use the Norwegian Climate prediction model to separate influence from long term climate change and slow natural variability in the climate system for three large hydrographic catchments in Brazil. The aim of the thesis is to be able to identify whether the recent observed changes in streamflow - especially over the last decades - can be traced back to internal variability or not, and using this result to make a certified guess to whether the observed trends of decreasing or increasing water flow over the last decades are likely to reverse, amplify or persist.

Chapter 2

Background

In this chapter, I will explain why research on hydropower is important in Brazil, and why information about precipitation and evaporation variability and trends in the basins is key to good planning. I will then introduce the three catchment areas that are analysed in the thesis, and describe their climates as well as relevant large scale patterns that influence the rainfall in the chosen regions. Lastly, I will explain modes of variability that are influencing precipitation in the three catchment areas.

2.1 Hydropower

2.1.1 Basic principles of hydropower

Hydropower is a method of generating electricity by leading water flow to drive a turbine, utilizing the potential energy in the height difference between the water surface and the turbine. The potential energy is transformed to mechanical energy in the turbine, which is transformed to electrical energy in the generator (Jaffe, 2018, pp. 593). Hydropower is a renewable energy source: it is the hydrological cycle that is "recharging" the water, bringing water back to higher elevations (Locher and Scanlon, 2012).

There exists many different types of hydropower installations, made for different purposes. Run-of-river systems are the most simple ones. They produce energy mainly from the natural river flow, and make little changes to the surroundings. The production varies greatly on daily, weekly and seasonally time scales (International Energy Agency, 2012).

Reservoirs - made artificially or by damming up existing lakes - is another typical installation. Reservoirs are less variable on shorter time scales, because producers can control the water outflow based on demand. Large

reservoirs can save water for months, seasons, and some even years. Most reservoirs are multi-purpose: providing services like irrigation or flood protection in addition to electricity production (International Energy Agency, 2012). Hydropower plants come in a wide size range. By the Brazilian government, plants with a capacity of < 30 MW are considered small-scale hydropower plants (International Energy Agency, 2012)

Hydropower reservoirs are often installed along a river in a cascade, where the inflow into a reservoir depends on the outlet from the upstream reservoir (among other variables, see equation 2.2). Pumped storage is a type of reservoir that - in addition to a turbine - has an electric pump that can pump water back to the upper reservoir at low demand, which can be used to produce electricity at high demand, thereby "storing" surplus energy (International Energy Agency, 2012).

Even though hydropower installations may harm the local environment by disturbing ecosystems and local wildlife (Jaffe, 2018) and causing population displacement and disturbance of local communities and ingenious people (Locher and Scanlon, 2012), the technology holds several advantages over other sources of energy. Compared to other sources of renewable energy, hydropower is a mature, flexible and reliable technology (Locher and Scanlon, 2012).

Furthermore, hydropower offers production control and grid stabilizing effects (Locher and Scanlon, 2012). As opposed to other renewable energy sources such as solar power and wind power, where energy production varies greatly throughout the day, week and month - and electricity is produced accordingly - hydropower generation is controllable (Wörman, 2012). Operators control the energy production from a hydropower plant by regulating the flow from the reservoir. In that way, hydropower can be used to balance the grid (Wörman, 2012). Hence, hydropower is especially convenient to ensure a steady electricity flow in the grid with irregular renewable energy sources taking a growing share of the energy mix. For these reasons, knowledge about the future water available for hydropower production is key to safe grid planning, and to utilize this powerful renewable energy source in the most optimal way possible.

Electricity produced by hydropower is proportional to the river flow through the turbine. It also depends on other factors, which are more or less constant. The power generated by a hydropower plant is expressed as in equation 2.1 (Wörman, 2012, pp. 43, Jaffe, 2018, pp. 593).

$$P = \eta \cdot Q_p \cdot \rho \cdot g \cdot h \qquad (2.1)$$

Where Q_p is the river flow used for production (m^3/s), h is the hydraulic

head (the height difference between the reservoir and the outlet, m), ρ is the density of water (kg/m^3), g is the gravitational constant (m/s^2), and η is the efficiency of the plant (depending on type of turbine etc.). Large turbines in modern hydroelectric plants can operate at an efficiency of 96 % or more (Jaffe, 2018, pp. 594).

The streamflow - which limits the electricity production - is controlled by precipitation and runoff patterns (International Energy Agency, 2012). Precipitation is the main restrictor of water availability, although evaporation and deep infiltration into the soil also affect the amount of water flowing into the reservoirs (Wörman, 2012, pp. 42). This is why hydropower production typically varies on an annual time scale, and annual total river discharge sets a limit to the amount of energy that can be produced (Wörman, 2012, pp. 41).

The streamflow in a specific river leading to a reservoir depends on the total drainage area for that river (the catchment area), the total rainfall, the evaporation and other factors that are expressed in the following equation (Wörman, 2012, pp. 42).

$$Q_R = A_W(P - ET - D) + dS/dt \qquad (2.2)$$

Where Q_R is the total natural river flow (m^3/s), A_W is the size of the catchment (m^2, the area leading downhill to the river), P is the precipitation rate (m/s), ET is the evapotranspiration rate (m/s), D is the net groundwater discharge (m/s) and dS/dt is the change in stored water in the upstream reservoir (m^3/s). Note that Q_R is only explaining the natural flow. Competing water use purposes such as irrigation and water consumption along the river will also change the amount of water available for hydropower production (Wörman, 2012).

Climate change studies for hydroelectric management often include the above mentioned variables in different combinations, where precipitation is considered the most important variable to study (Dias et al., 2018). Other meteorological variables such as temperature and evapotranspiration and non-meteorological variables such as land use changes and water consumption changes, are also often studied in combination with precipitation (Dias et al., 2018 and references therein).

Due to the limited scope of a master thesis, I will focus on the meteorological variables in this thesis. I will mainly look at precipitation - and its relationship with streamflow. Additionally, I will include evaporation in some of the analyses.

2.1.2 Energy market and hydropower in Brazil

Brazil is one of the countries in the world with the larges share of hydropower in the energy mix, and the country is the second largest hydroelectricity producer in the world (International Energy Agency, 2012). More than 65 % of the electricity in Brazil comes from hydropower (International Energy Agency, 2022a). Fossil fuels and biofuels are the second and third largest sources for electricity in the country, and over the last ten years, wind power electricity production has increased rapidly (International Energy Agency, 2022a). Still, Brazil remains heavily reliant on hydropower.

There are 1313 operating hydropower plants in the country, out of which 218 are considered medium- or large-sized with a capacity of > 30 MW (Dias et al., 2018). These 218 hydroelectric power plants stands for more than 94 % of the total installed hydropower capacity. The hydropower plants are located in all main regions of the country, with the main concentration in the southeast part (Dias et al., 2018).

Itaipu is Brazil's largest - and the world's second largest - hydroelectric power plant with an installed installed capacity of 14 000 MW. Itaipu is located along the Parana River in the southern part of the country. Brazil's second largest hydroelectric power plant is Belo Monte in the Amazon region. This plant has a total installed capacity of 11 233 MW, and is the third largest in the world. Other important hydroelectric power plants are Sobradinho (1050 MW) in the Sao Francisco river in the northeast part of the country, Itumbiara (2280 MW) in the Paranaiba river in the midwest/southeast part, and Tucurui (8370 MW) in the Tocantins river in the north (Dias et al., 2018).

The hydroelectric power plants with the highest useful volume are Serra da Mesa (in the Southeast/Midwest) and Tucurui (in the North), both located along the Tocantins river, with 43.25 km^3 and 38.98 km^3 storage capacity respectively (Dias et al., 2018).

In Brazil, the prices of hydropower have a strong effect on the prices in the entire electricity market, and these vary throughout the year depending on water availability (Julia Ribeiro de Oliveira in Statkraft, personal communication). Therefore, any major changes in the total available water for electricity production, as well as the timing of the water availability, will affect the energy market and prices substantially.

Furthermore, the heavy reliance on hydropower in Brazil makes the population vulnerable to abrupt changes in inflow. This vulnerability is a motivation for investigating the reasons for altered inflow rates, and for wanting to understand the future of Brazilian precipitation that controls it.

2.2 Catchment regions

Figure 2.1 shows a map of the catchment areas I have chosen to analyse, and the location of the corresponding streamflow observations. Also, the main rivers are marked on the map. The catchments that are marked in the map are areas, in which all flowing water will eventually reach the bottom of the basin, where there is a streamflow observation.
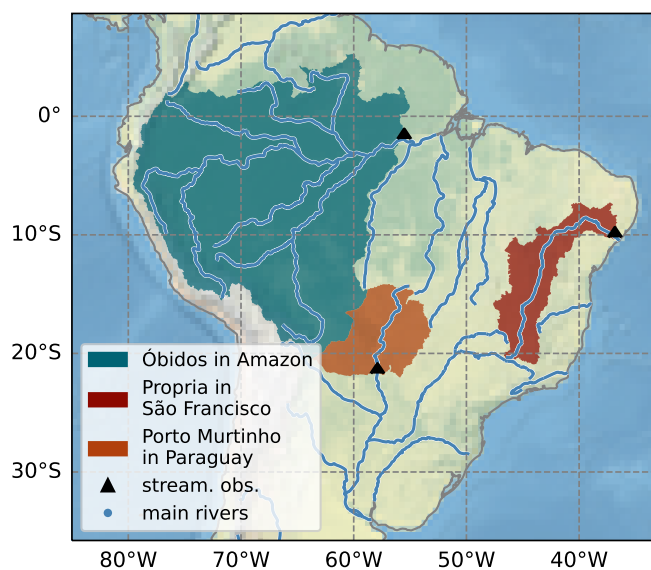
Figure 2.1: Catchments analyzed in this thesis. The black triangles are locations of streamflow observations corresponding to the catchment areas. The blue lines are main river systems.

Note that the streamflow measurements might not necessarily be located *at* hydropower plants, but rather be a streamflow observation that corresponds to a drainage area. The analysis will nevertheless be very relevant for existing hydropower production in the same or nearby areas, as well as for new possible projects. Enhanced knowledge on the relation between the streamflow out of the catchment and the precipitation into the catchment - as well as the driving mechanisms for the precipitation trends compared to the flow trends in the area - is applicable to hydropower hydrological flow in the same areas too.

2.2.1 Amazon

The first region I have chosen, is the Óbidos catchment in the Amazon region (the blue region in figure 2.1), because the potential for new hydropower projects in Brazil is considered to be mainly in the Amazon region, due to the near exhaustion of the hydroelectric potential in the rest of the country (Dias et al., 2018). This basin is characterized by a peak in streamflow around May/June, a rainfall peak in February/March, and relatively even evapotranspiration all year around (figure 2.2).
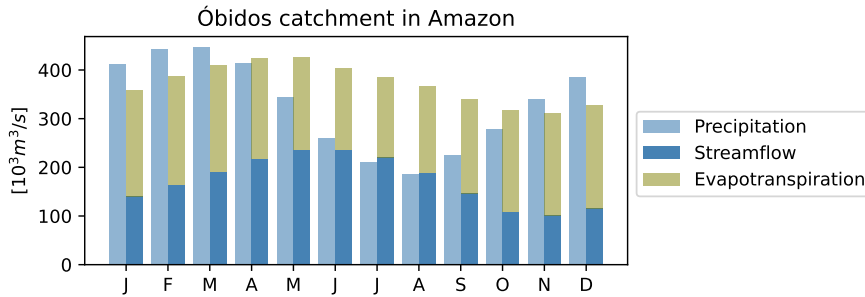
Figure 2.2: Monthly climatological streamflow, evapotranspiration and precipitation in Óbidos catchment in Amazon. The climatological period is 1981-2011. Evapotranspiration data is GLEAM and precipitation data is CHIRPS. The precipitation and evapotranspiraiton is calculated from mm/month to monthly mean $10^3 m^3/s$ using the catchment size provided in the CAMELS-BR data. Streamflow data is from the National Water Agency of Brazil (ANA), obtained through CAMELS-BR.

Amazon basin largely consist of tropical rain forest with dense vegetation. According to the aridity/Budyko/dryness index, Amazon is characterized as humid (Zaninelli et al., 2019). The region has a rainy season from October to May, and a dry period from June to September. The annual rainfall are the highest in the country - between 2000 and 3500 mm annual rainfall (based on data from 1975 to 2005) - with higher amounts in the western part and the northern part (see figure 2.5). The Amazon typically has between 150 and 250 rainy days a year (Luiz-Silva et al., 2021).

The two main sources of moisture in the Amazon are (i) evaporation from the Tropical Atlantic Ocean that is brought inland with the trade winds (see figure 2.6) and (ii) moisture originating from the forest itself (Luiz-Silva et al., 2021). The precipitation in this area is linked to the Intertropical Convergence Zone, which I will explain in more detail in section 2.3.1. The year-to-year rainfall variability in the area is linked to different oscillations

in the climate system and remote teleconnections, which I will both explain in section 2.4.

2.2.2 São Francisco

The second catchment is the Propria catchment in the São Fransisco basin (the red region in figure 2.1). São Fransisco is a highly interesting area to analyze in regard to hydropower production because it is the only area in Brazil with significantly decreasing streamflow over the second half of the twentieth century, combined with a decrease in precipitation (Luiz-Silva et al., 2021). Furthermore, São Fansisco basin inhabits the Sobradinho hydropower plant with a power capacity of 1050 MW (large HHP$> 30MW$), which is considered one of Brazil's main hydropower plants (Dias et al., 2018).

Propria catchment has high evaporation values compared to streamflow (figure 2.3). The northeastern inland in Brazil is the only semi-arid area in the country (Zaninelli et al., 2019) and is commonly referred to as the "drought polygon" (Luiz-Silva et al., 2021). This dry area makes up parts of the São Francisco basin. This area has lowest annual accumulated rainfall, with numbers in the rage of 500-1000 mm, as well as the lowest number of rainy days in a year, lowest total precipitation on the wettest day, and lowest wetness during rainy days (Luiz-Silva et al., 2021). This dryness - relative to other regions in Brazil - is due to subsidence by the meridionally oriented Walker circulation (illustrated with yellow arrows in figure 2.6), as well as topographic inversion/blocking of the trade winds. This region has several plateaus of high elevation.
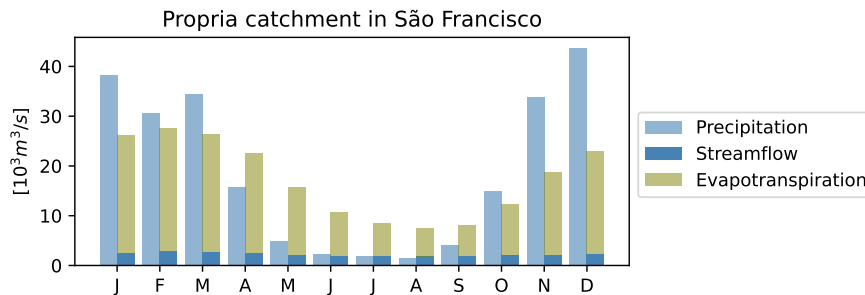
Figure 2.3: Like figure 2.2, but for Propria catchment in São Francisco.

2.2.3 Paraguay

The third basin, Porto Murtinho in Paraguay (the orange region in figure 2.1), I have chosen because of its energy storing capacity. Paraguay is located

in the southwest, the region that holds 70 % of the energy storage capacity in the country (Dias et al., 2018). Thus, knowledge on expected streamflow for the Paraguay basin is very valuable, as available surplus water is what needed to enable planned water storage in the reservoirs. For long-term energy planning, it is very useful to understand more about the trends, as the reservoirs need to be larger to utilize the energy storage if the amount of water increases. Also, for lower streamflow values, it is useful to planners to know whether there will be enough water to sustain the energy storage.

The catchment consists of Cerrado - a highland savanna - and wetland in the northern part, called the Pantanal (Marques et al., 2021), and the general climate in the region is characterized as humid and semi-humid according to the aridity/Budyko/dryness index (Zaninelli et al., 2019).

Paraguay basin is located in the subtropical climate zone, and is characterized by a well-defined rainy seasons and a monsoon pattern. The wettest period is during austral summer, and the driest is during austral winter. Typical annual rainfall values are between 1000 and 2000 mm, reaching a maximum in the coastal areas. Number of rainy days throughout the year is around 50-180 in the area (Luiz-Silva et al., 2021). The evapotranspiration also varies throughout the year, with a maximum around December/January (figure 2.4).
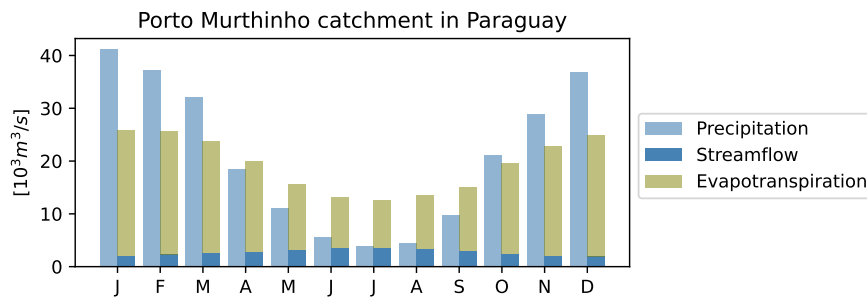
Figure 2.4: Like figure 2.2, but for Porto Murtinho catchment in Paraguay.

Substantial amounts of the rainfall in the region originates from moisture from the Amazon. The moisture is carried southwards by the wind, from the Amazon along the east side of the Andes mountain range, feeding the convection in the southeast and interior part of Brazil (Villela, 2017, see figure 2.6). Therefore, particularly the central region is strongly influenced by the heat and moisture content in the Amazon forest (Luiz-Silva et al., 2021). This circulation pattern is a part of the South Atlantic Convergence Zone, which I will treat in detail in section 2.3.2.

2.3 Precipitation patterns in Brazil

There are two large-scale rainfall patterns that affect the catchment regions that I assess in the thesis: The Intertropical Convergence Zone (section 2.3.1) and the South Atlantic Convergence Zone (section 2.3.2). The patterns are also illustrated in figure 2.6. Figure 2.5 shows the climatological seasonal precipitation in the country.
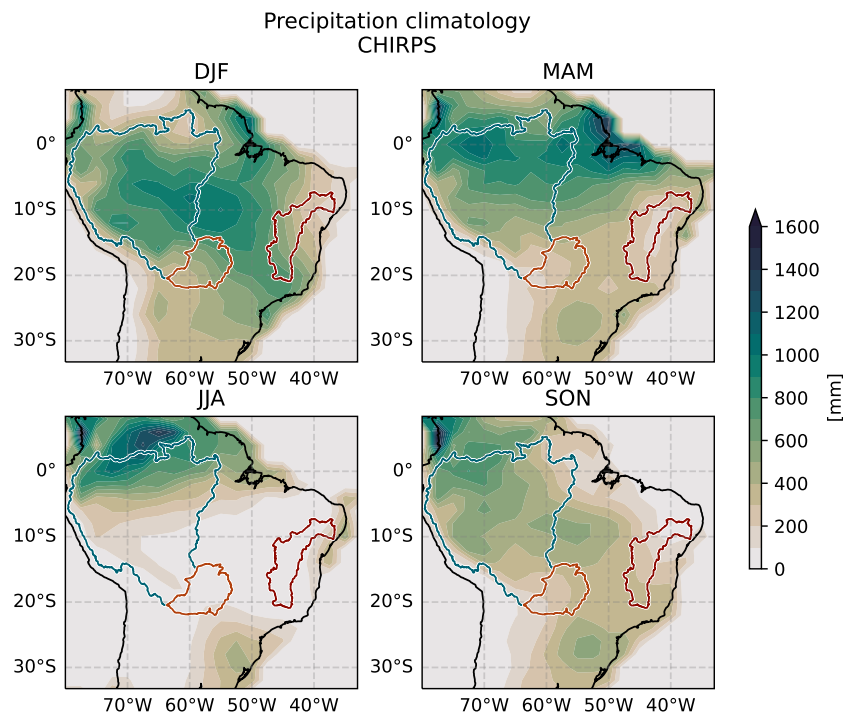
Figure 2.5: Seasonal total precipitation with CHIRPS data, mean over the years 1981-2011. The regions indicated on the map are the catchemnts that are analysed in this thesis (described in section 2.2).

2.3.1 Intertropical Convergence Zone (ITCZ)

The Intertropical Convergence Zone (ITCZ) is a belt near the equator associated with heavy precipitation, that dominates the precipitation regime in the north and northeast of Brazil (Garreaud et al., 2009). The Amazon basin and the northern part of São Francisco basin is affected by the ITCZ. In the ITCZ, along the surface, the moisture-heavy trade winds from both
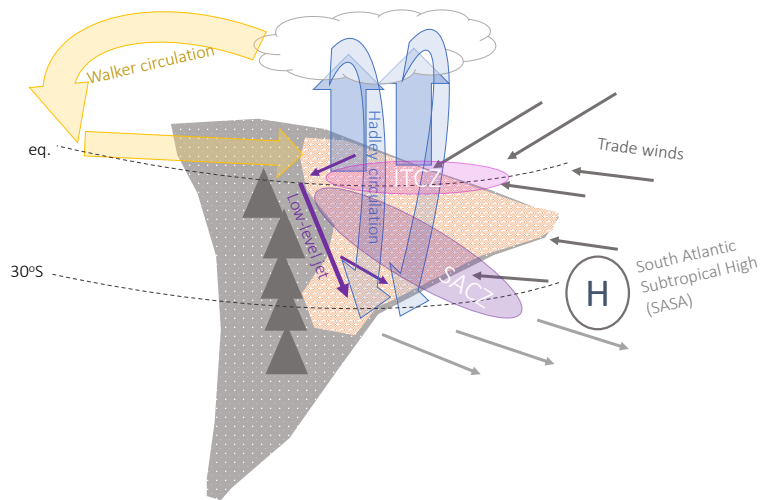
Figure 2.6: Illustration of important large-scale atmospheric patterns over Brazil. Blue arrows illustrate the Hadley cell circulation of rising air at the equator, with associated moisture condensation and cloud formation. The yellow arrows illustrate meridional oriented Walker circulation under neutral ENSO conditions. The dark gray arrows are the trade winds, converging approximately at the equator, creating the Intertropical convergence zone (ITCZ), and the purple arrows are the low-level southwards flowing winds that bring moist air from the Amazon to the south and southeastern part of the country. These wind are steered by the topography of the Andes mountain chain, and converge with the southeasterly winds at the coast and make the South Atlantic Convergence Zone (SACZ). The high pressure system is the South Atlantic Subtropical Anticyclone (SASA).

hemispheres converge, which causes the air to rise and form high tropical clouds and produce thunderstorms, tropical cyclones and other precipitation-producing weather systems (Hartmann, 2016, pp. 134, as illustrated in figure 2.6). The position of the ITCZ oscillates north- and southwards throughout a year, depending on the position of maximum incoming solar radiation. Near the tropopause over the ITCZ, the air diverge polewards, and this dry air descend gently over the subtropics, forming the Hadley circulation (Garreaud et al., 2009, see figure 2.6), also often referred to as the Hadley cell (Hartmann, 2016). This descending dry air explains why the climate in the sub-tropics is drier than in the tropics (Garreaud et al., 2009).

2.3.2 South Atlantic Convergence Zone (SACZ)

Roughly, it can be said that rainfall over Brazil originates from synoptic systems in the south, ITCZ in the north, and SACZ in the middle of the country (see figure 2.6). I will give SACZ a more in-depth introduction, as this particular large-scale system is of greatest relevance for the hydropower production in Brazil. The reason for the importance of SACZ to hydropower in the country is that several of the large river systems carrying water northward and southward to hydro-electrical plants are formed in the highlands in the middle of the country (Dias et al., 2018) where the SACZ regime dominates (Rosa et al., 2020). The southern part of Amazon, and the southern and most important part of the São Francisco basin is affected by SACZ, and the entire Paraguay rainfall originates from SACZ.

The SACZ is a band of deep convection and associated precipitation. It is oriented in the northeast/southwest direction, stretching from the Amazon, over large parts of tropical and subtropical Brazil, to the South Atlantic Ocean (Villela, 2017, as illustrated in figure 2.6). Precipitation in the system result from convergence of moist low-level winds and subsequent convection. The dynamics of the SACZ are similar to convergence zones in the South Pacific Ocean, the Asiatic East Ocean and the South Indian Ocean. In the SACZ, the South American low-level jet brings moisture from the Amazon southwards along the Andes mountain range that converge with winds containing moisture from the tropical Atlantic (Villela, 2017).

The SACZ plays a significant role in the rainfall regime in central Brazil (Villela, 2017; Luiz Silva et al., 2019). It is responsible for a large part of the total summer precipitation in the country (Rosa et al., 2020).

The active phase of SACZ is during austral summer, and the most active period is between December and February. November and March are also important to include in SACZ event detection because 30 percent of the active SACZ days occur in these two months (Rosa et al., 2020).

SACZ variation is linked to severe droughts and floods in southeast Brazil (Rosa et al., 2020). The intense drought in the state of São Paulo during the austral summers of 2014 and 2015 was partly caused by SACZ not moving as far south as usual. This drought had several severe socioeconomic impacts, including the effect on hydropower production capacity (Abatan et al., 2022).

SACZ is expected to move southwards due to climate change (Luiz Silva et al., 2019), and there are indications that a poleward shift of the SACZ already has occurred in recent decades (Zilli et al., 2019). Understanding and predicting variations in SACZ is crucial to understand rainfall variability over southeastern Brazil, but the variability of the system is not well understood (Abatan et al., 2022).

SACZ intensity and position has been related to SSTs in the South Atlantic. The relationship between the South Atlantic SSTs and the SACZ is complex. SST variation influences the SACZ position, and the SACZ position influences SSTs (Jorgetti et al., 2014). The relationship between SACZ and SSTs in the Atlantic will be interesting to keep in mind in the analysis of this thesis.

2.4   Natural variability and teleconnections influencing climate and precipitation Brazil

The global climate system has natural modes of variability that arises from the internal dynamics of the system itself without any specific cause or forcing (Hartmann, 2016). Internal variability occurs on time scales from weeks to seasons, years, decades, centuries and even thousands of years. The shorter scales of variability are often connected to variations within the atmosphere, and the inter-seasonal, interannual and decadal variations are often coupled dynamics between the atmosphere and the ocean (Hartmann, 2016, pp. 233-234). These variations can be seen as low frequency oscillations controlling the timing and magnitude of anomalies. Regional SST anomalies can affect the regional atmospheric patterns.

The anomalies in one region might also affect atmospheric patterns in other parts of the world, through *teleconnections*. A teleconnection is a link between climate anomalies and atmospheric patterns separated by great distances (Reboita et al., 2021). Some teleconnections can be explained as energy redistribution through atmospheric waves propagating from an anomalous heat source - for instance an anomalously warm ocean basin heating the local atmosphere - to another part of the globe (Reboita et al., 2021, pp. 1). The planetary atmospheric waves dissipate energy and restore the

atmosphere back to a stable state, and thereby disrupting the atmospheric pattern along the anomalous wave train (Reboita et al., 2021).

I will focus this section on the natural variability and the teleconnections originating in the *ocean*. There are two reasons for this restriction. Firstly, I am interested in looking at the slow oscillations in the climate system, as these are more easily confused with climate change signals. The slow climate variability - on interannual and decadal scales - mostly originates in the ocean (Hartmann, 2016, pp. 254; Reboita et al., 2021).

Secondly, teleconnections that originate in the ocean are also especially pronounced from tropical to subtropical regions (Liu and Alexander, 2007), which is where Brazil is located. This is because SST anomalies in the tropics modifies the subtropical and extra-tropical atmosphere by perturbing the Hadley cell, establishing stationary waves and interacting with mid-latitude storm tracks (Liu and Alexander, 2007).

I have chosen to explain five natural variability/slow oscillations that (1) originate in the ocean basins and (2) are important for precipitation variations in Brazil (Reboita et al., 2021). I divide the following part into modes of variability in the Pacific ocean (section 2.4.1) and modes of variability in the Atlantic ocean (section 2.4.2). The focus will be on what parts of the country the modes of variability affect, the climate mechanisms that cause it, and the time scale in which they vary.

2.4.1   Pacific Ocean modes of variability

El Niño Southern Oscillation (ENSO) is a coupled ocean-atmosphere mode of variability, connected to SST variability in the tropical Pacific and associated surface pressure patterns and atmospheric circulation (Hartmann, 2016, pp. 246), and is considered one of the most important teleconnections for the Brazilian climate and precipitation patterns (Reboita et al., 2021). The relationships between ENSO and droughts in Northern Brazil and floods in Southern Brazil his well known (Cai et al., 2020).

ENSO is an oscillation between the El Niño conditions and La Niña conditions, driven by the ocean-atmosphere coupled dynamics (Hartmann, 2016, pp. 249). The system is self restoring, and typically oscillates with a period of 2-7 years, with strongest variability in the periods from 3 to 5 years, and significant variance in the range between 2 and 20 years (Hartmann, 2016, pp. 249). During El Niño, the SST in the east and central Pacific is anomalously warm - peaking around Christmas time - and during La Niña, the SSTs are colder than usual in the east and central Pacific (Hartmann, 2016, pp. 249).

The anomalous heat sources in the Pacific during an El Niño event influence early summer precipitation over Brazil through two mechanisms: (1) perturbation of the Hadley and Walker circulation and (2) generation of a Rossby wave train reaching the subtropical part of Brazil (Grimm, 2003). The perturbation of the Walker circulation during the El Niño event cause (anomalous) subsidence over the northern part of the country, leading to drier conditions and weakened moisture transport to central Brazil (Cai et al., 2020; Grimm, 2003).

Hence, during El Niño events, there is reduction in precipitation over northeast Brazil and the east of the Amazon (Reboita et al., 2021; Grimm, 2003) in the magnitude of 3 mm/day during DJF (Tedeschi and Collins, 2017). The suppression of precipitation is strongest during DJF, and extends to Northest Brazil in SON and MAM (Cai et al., 2020). El Niño also leads to reduced annual rainfall over the Brazilian central Plateau - the Cerrado (Correia Filho et al., 2022).

The subsidence over Amazon - together with atmospheric Rossby waves - also cause anticyclonic low-level anomalies over central-east Brazil which favors moisture inflow from the Atlantic Ocean towards southern Brazil, giving positive precipitation anomalies there. Therefore, precipitation increase during El Niño in the very south of the country (Grimm, 2003).

During La Niña conditions, it is opposite: the northern part of the country - stretching from the Amazon via Northeast and the SACZ region - is wetter and the southern is drier (Grimm, 2003). The annual rainfall in the Brazilian Cerrado is also higher during La Nina years (Correia Filho et al., 2022).

The Pacific Decadal Oscillation (PDO) - like the ENSO - originates in the Pacific ocean. The PDO pattern consists of opposite SST anomalies between the tropical/northeastern and central/northwestern North Pacific Ocean (Reboita et al., 2021, pp. 10). In the warm PDO phase, warmer and drier periods are observed in northern and northeastern Brazil (Reboita et al., 2021). PDO events typically lasts for 20-30 years (Reboita et al., 2021). Time series of ENSO and PDO are correlated. Hence, it can be argued that PDO is the low-frequency component of the ENSO (Hartmann, 2016, pp. 255; Reboita et al., 2021).

The Pacific ocean also has variability on an inter-decadal time scale, with periods of 60-70 years, in addition to the period of 20-30 years. Inter-decadal SST anomalies in the Pacific ocean are characterized by warm anomalies in the tropical central and eastern part of the basin, with an extended "comma"-pattern in the northern part of the basin, along the western North American coast, surrounded by two anomalous cold tongues stretching from eastern Asian and Oceania (Villamayor et al., 2018). The Pacific inter-decadal variability affect rainfall in Brazil in the following way: positive anomalies in

the tropical Pacific ocean lead to less rainfall in the Amazon, less rainfall in the very northern part of Northeast, more rainfall in the southern part of the São Francisco basin, and positive rainfall anomalies in Paraguay basin (Villamayor et al., 2018).

The impact of Pacific ocean variability on Brazilian precipitation is complex. The effects of El Niño and La Niña also depend on factors such as local land-surface interactions, timing with various conditions of other modes of interannual climate variability originating in the Atlantic (see section **??**) and Indian Ocean, as well as inter-basin interaction between the Pacific and Atlantic ocean basins (Cai et al., 2020).

2.4.2 Atlantic Ocean modes of variability

The modes of variability in the Atlantic ocean are important to the precipitation and weather patterns in Brazil. For instance, weather and climate of Brazil is profoundly impacted by the meridional gradient of SSTs in the Atlantic basin (Garreaud et al., 2009). Additionally, droughts in Amazon and Northeast Brazil have been linked to anomalous high SSTs in the tropical North Atlantic (Garreaud et al., 2009).

Atlantic Multidecadal Oscillation (AMO) is the leading mode of decadal SST variability in the North Atlantic (north of 20 °S), with a typical period of several decades (Hartmann, 2016, pp. 257). The warm phase of AMO reduces the MAM, JJA and SON precipitation in central and northeastern parts of Brazil, and may enhance the rainfall in northeast Brazil during DJF (Reboita et al., 2021).

Tropical Atlantic Ocean Dipole (TAD) - also known as the decadal tropical Atlantic SST variability - is characterized by a dipole pattern between SST anomalies in the tropical North and South Atlantic. The positive phase is defined as when the tropical North Atlantic has warm anomalies and the tropical South Atlantic has cold anomalies, and the negative phase when the pattern is opposite (Reboita et al., 2021). During a positive phase of the TAD, the northeasterly trade winds are weakened and the sea level pressure reach low anomalies. The TAD is strongly influencing the north/south position of the ITCZ (Reboita et al., 2021 and references therein).

South Atlantic Dipole (SAD) is the dominant mode of ocean-atmosphere coupled anomalies in the South Atlantic, which is a dipole that is typically oriented in the northeast-southwest direction with SST anomalies in the tropical and extra-tropical part of the Atlantic basin in each of the phases of this mode of variability (Reboita et al., 2021). The SAD varies on both interannual and inter-decadal scales, and has been found to affect sea surface pressure and wind anomalies, which cause precipitation anomalies over

Brazil (Reboita et al., 2021 and references therein). A positive SAD mode - with warmer than usual northeast (tropical) region and colder than usual southwest (extra-tropical) region of the south Atlantic basin - may cause late onset and dry austral summers in the southeast of Brazil and early onset and wet summers in the northeast part of Brazil (Reboita et al., 2021).

Chapter 3

Data and methods

In this chapter, I will describe the observational data (see table 3.1 for an overview and table 3.2 for the providers) and the model including experiments I compare. I will also argue why these data sets are well suited for my analysis of hydropower and climate in Brazil. Then I will describe how I process the various gridded data to obtain time series that match the catchments that I analyse (section 3.5). Lastly, I will describe the steps in both of the two methods I use for time series analysis: (I) statistical significance trend test (section 3.6) and (II) filtering and correlation analysis (section 3.7).

Table 3.1: Data used in the thesis.

Data	Variables	Type	Spatial resolution	Temporal res.	Years
ERA5	precip. evap. SST	renalysis	0.25° x 0.25°	monthly	1950-2022
CHIRPS	precip.	satellite and gauge obs. combined and gridded	0.05° x 0.05°	monthly	1981-2022
CAMELS-BR	inflow, catchments, evap.	observations	897 catchments	daily	1940-2018[1]
NorCPM	precip. evap. SST	model, historical and assimilation	2.5° x 2°	monthly	1850-2014 1950-2018

Table 3.2: Data providers.

Data	Provider
ERA5	European Centre for Medium-Range Weather Forecasts (ECMWF)
CHIRPS	Climate Hazards Group InfraRed Precipitation with Stations (Funk et al., 2015)
CAMELS-BR	Chagas et al. (2020)

3.1 CHIRPS gridded precipitation data

3.1.1 Description of CHIRPS

In situ observations of precipitation in Brazil is scarce. Rain gauge data in Brazil is often characterized by low spatial coverage, a high-proportion of missing data, as well as short time series, typically less than 15 years (Jones et al., 2013). The lack of adequate rainfall data in parts of the country, makes products like CHIRPS valuable for precipitation analysis in Brazil (de Oliveira-Júnior et al., 2021; Paredes-Trejo et al., 2017).

The Amazon in particular is an area where rainfall measurement quality is low, because of low density of stations due to remote and inaccessible areas, as well as insufficient maintenance and broken records many places. Furthermore, few stations in the Amazon are automatic, and local technicians are responsible for noting down the measured values, which might introduce errors and inconsistent methods (Paca et al., 2020).

Climate Hazards Group InfraRed Precipitation with Stations (CHIRPS) is a product made specifically with the aim of obtaining reliable and useful gridded data in regions of scarce observations, such as Africa and South America. The CHIRPS data set is created with satellite observations, in combination with available station data. Precipitation estimated from infrared Cold Cloud Duration observations are interpolated with some available gauge observations to create a 0.05 ° gridded monthly precipitation dataset beginning in 1981 (Funk et al., 2015).

3.1.2 Evaluation of CHIRPS in Brazil

CHIRPS precipitation data is found to compare well with observations across all regions in Brazil (Costa et al., 2019). Statistical analysis of rain gauge

---

[1]Inflow data start and end date varies from station to station. See an overview of the data time range in table 3.3 about the chosen catchments.

time series and CHIRPS data for the period 1998-2011 indicate that the determination between the two are high in all regions of the county in that period. Northwest of Amazon and the southwest of Para state are the regions where CHIRPS showed a somewhat lower similarity with the rain gauge data (Costa et al., 2019).

Paredes-Trejo et al. (2017) concluded that the dataset is well suited for studying spatial and temporal variability of rainfall in Northeast Brazil, which is where the São Francisco catchment is located. CHIRPS monthly precipitation correlates adequately with observations from 21 ground stations in the period 1981-2013, with a correlation coefficient of 0.94 (Paredes-Trejo et al., 2017).

Even though the data is evaluated as well suitable for analysis in the Northeast region, it is worth mentioning that there are spatial and temporal variations of the quality of the CHIRPS dataset in the area: The worst estimations are found in high elevation regions with complex terrain and warm precipitation processes. Furthermore, CHIRPS is less accurate in drier parts of Northeast Brazil. When it comes to temporal variations, rainfall events are best detected during the last part of the rainy season in eastern part of Northeast Brazil, from June to August (Paredes-Trejo et al., 2017).

The CHIRPS dataset is also found to be suitable to assess rainfall trends in Amazon - across all of Óbidos basin (Paca et al., 2020). Several national institutes of Brazil and the alike institutions in Peru, Bolivia, Colombia and Ecuador - countries which also make up parts of the Óbidos basin - have been recording precipitation on ground in the Amazon region over the last decades. The CHIRPS gridded data match very well with these gauge measurement, with a coefficient of determination, $R^2 = 0.96$. CHIRPS were also able to reproduce the local trends within the basin in accordance with the gauge measurements (Paca et al., 2020).

In the region of the Paraguay catchment, de Oliveira-Júnior et al. (2021) concluded that the CHIRPS dataset is satisfactory for spatiotemporal analysis of regional precipitation. Time series from ten gauge rain gauge stations in the topical/subtropical regions Mato Grosso and Mato Grosso du Sul and the CHRIPS data in the region for the period 1985-2014/2018, had a correlation coefficient of 0.86. CHIRPS is able to identify drought and wet periods under any ENSO condition in the Brazilian Midwest (de Oliveira-Júnior et al., 2021).

CHIRPS also reproduces ENSO variability in the region well. Although the tendency towards over- and underestimation varies across the region, CHIRPS leans towards overestimating the rainfall in this tropical part of South America (López-Bermeo et al., 2022).

An important notion about the CHIRPS dataset in Brazil, is that it tends

to overestimate low rainfall events (< 100 mm/month) and overestimate high rainfall events in some areas (> 100 mm/month). This is true for both the Brazilian Northeast (Paredes-Trejo et al., 2017) and Midwest (de Oliveira-Júnior et al., 2021) where the São Francisco and Paraguay basins are located, respectively. This error of often estimating rainfall when there is none, or more when there is little, makes CHIRPS inadequate for identifying drought events, as its precision in detecting no-rain events is poor (Paredes-Trejo et al., 2017).

The above described shortcoming is not problematic when analysing rainfall trends for hydropower production. The total accumulated rainfall over periods longer than one month - typically a year - is what controls the production from an electrical hydropower plant with a reservoir (Wörman, 2012, pp. 41). In this thesis, I analyse accumulated precipitation over several seasons or years. Underestimation of low rainfall months would not alter the accumulated precipitation much, since the low-rainfall months contribute proportionally less to the accumulated rainfall anyways. The overestimation of high-rainfall months, on the other hand, could influence the analysis more, because the accumulated precipitation over several months would add up, and the error would grow when accumulating.

Nevertheless, the CHIRPS rainfall data is a dataset that is recommended for analyzing precipitation changes in Brazil in all the catchment regions (Paredes-Trejo et al., 2017; de Oliveira-Júnior et al., 2021; Paca et al., 2020), and it holds advantages such as high spatial resolution and a consistent methodology across the country and neighbouring countries. And since the data is gridded, it is well comparable with other gridded model data.

3.2   ERA5 reanalysis data

Since the CHIRPS data records does not begin until 1981, another precipitation dataset is used as an additional comparison dataset: namely the ECMWF Reanalysis v5 (ERA5). This reanalysis begins in 1950, and therefore allows me to look at oscillations in the climate system that exceed those limited by the 34 years between 1981 and 2018 in the CHIRPS data. The ERA5 *evaporation* data is used in the analysis as well, for the same reason, as an extension to the evapotranspiration data provided for each catchment in the CAMELS-BR (that will be presented in section 3.4).

3.2.1 Description of ERA5

ERA5 is a state-of-the-art reanalysis product made by the European Centre for Medium-Range Weather Forecasts (ECMWF, Hersbach et al., 2020). A reanalysis is made by optimally combining observations and models. ERA5 builds on an atmospheric weather forecast model, and the reanalysis includes several components, including a land component, an ocean surface wave component, as well as an atmospheric ozone component. The ocean component and the land component are both coupled with the atmospheric model, and two-way interactions are included (wind generates waves, and the waves affect the surface winds etc.). The horizontal grid resolution is 31 km, and the model has 137 vertical levels, reaching up to 1 hPa. ERA5 runs from 1950 to present. A 12-hourly assimilation is done, and the model runs as a short forecast 9 hours into the next 12-hour assimilation window (starting at 1800UTC and 0600UTC) where it suggests the next starting point of the next assimilation (Hersbach et al., 2020).

ERA5 is assimilated with a two-dimensional optimal interpolation scheme of 2 m temperature and relative humidity, as well as three soil moisture layers in the top 1 m of soil. ERA5 uses satellite data for assimilation. Note that precipitation is not assimilated directly. The global correlation between ERA5 monthly mean precipitation and observations is 77 % globally (Hersbach et al., 2020).

3.2.2 Evaluation of ERA5 in Brazil

ERA5 precipitation data has been evaluated against river flow observations and daily precipitation measurements on ground in Brazil. ERA5 has a bias of between -5 and -10 mm/day in the Amazon - with a an absolute maximum in the western part of the basin. The absolute value bias in the semi-arid region of the northeast is smaller. Generally, the ERA5 bias is negative in all regions of Brazil. The RMSE is largest in the southern part of the country and in the Amazon. Furthermore, the correlation with gauge observations are largest on the SACZ region - in the middle-southeast Atlantic region (Almagro et al., 2021). Almagro et al., 2021 found that satellite-based products was better at simulating precipitation over Brazil than ERA5 in five out of six biomes.

Furthermore, when assessing the suitability of ERA5 precipitation as input in a hydrological model that simulates daily river discharge and horological signatures in Brazilian catchments, ERA5 was outperformed by the satellite-based data. Satellite-based products performed better in simulating the mean discharge in Caatinga (the semi-arid interior region in the

NE, which make up parts of the São Francisco catchment) and Cerrado (the grassland in the inland middle country, which make up parts of the Paraguay catchment and parts of the São Francisco catchment). ERA5 performed similarly as the satellite-based data in Atlantic forest (along the eastern coast) and the Amazon. They also found that satellite-based products were better predictors than ground-based observations in Cerrado and Caatinga biomes, and that it was as good as ground-based rainfall observations in the Amazon (Almagro et al., 2021).

The ERA5 precipitation monthly anomalies show varying closeness to the satellite observed data across the country: The correlation between ERA5 monthly anomaly precipitation reanalysis and version 7 of NASA's TRMM Multi-satellite Precipitation Analysis (TMPA) 3B43 dataset in the time span 1998-2008 are very low ($< 30\%$) in the Amazon region, but the correlations are higher on the eastern coast of Brazil, with values around 80-90 % (Hersbach et al., 2020).

The bias of the monthly ERA5 precipitation (when compared to the NASA satellite data in the same period) is positive along the coast with a mean difference of about -(1-2) mm/day on the eastern coast and -(2-3) mm/day on the northeastern coast. In the Amazon drainage area, the precipitation biases are around -(2-3) mm/day in the western part, and positive values of around 2-3 mm/day in the eastern part of the Amazon basin, and 4-6 mm/day in the Andes mountain range (Hersbach et al., 2020).

3.3 Norwegian Climate Prediction Model (Nor-CPM)

3.3.1 Model components

NorCPM1 is based on an Earth system model that assimilates sea surface temperature (SST) and temperature/salinity-profile (T/S-profile) anomalies. The aim of the NorCPM is to enable climate reanalyses and research on seasonal-to-decadal climate predictions (Bethke et al., 2021).

NorCPM1 uses the medium-resolution coupled earth system model NorESM1-ME (Bentsen et al., 2013). An earth system model includes components that simulate chemical and biological factors and their interactions with the other components, in addition to the simulation of general circulation of the atmosphere and ocean (Hartmann, 2016, pp. 325). NorESM1-ME is based on the Community Earth System Model (CESM1.0.4, Hurrell et al., 2013) combined with CAM4-OSLO and Bergen Layered Ocean Model (BLOM; that originates from the Miami Isopycnic Coordinate Ocean Model). The Com-

munity Land Model (CLM4; Lawrence et al., 2011) is the same in NorESM as in the CESM1.0.4. (Bethke et al., 2021). The resolution of the atmospheric component of NorCPM1 is 2.5 degrees longitude and about 1.8 degrees latitude.

NorESM is found to overestimate the flux of water vapor from ocean to land with about 8 % (Bentsen et al., 2013). Also, the intensity of the water cycle is slightly too high (Bentsen et al., 2013). The cloud cover in the model is too low globally. This is also true for Brazil, where the cloud fraction in the historical run has a negative bias of 25-35% in the southwestern part of Amazon and 5-25% in the rest of the country (Bentsen et al., 2013). Generally, in the model, although the cloud fraction is too low, the liquid water content is exaggerated, resulting in precipitation rates with less bias than the low cloud cover would imply (Bentsen et al., 2013).

3.3.2 Historical experiment

The historical experiment for the NorCPM1 is following the Coupled Model Intercomparison Project phase 6 (CMIP6) protocol, and runs from 1850 until 2014 (Bethke et al., 2021). Using a spin-up time of 700 years, the historical NorESM model runs are initialized with the conditions of the model in year 699. The external forcings in the historical simulation are: observation-based variations in (1) solar irradiance, (2) volcanic activity, (3) concentrations of greenhouse gases (GHG), (4) aerosols and (5) other particles in the atmosphere (Bentsen et al., 2013, pp. 693). Apart from the restrictions caused by these external forcing sources, each model run runs freely. The historical ensemble used in NorCPM1 contains 30 members.

3.3.3 Reanalysis experiment

In a 30-member reanalysis experiment, assim-i1, the model assimilates observed ocean variables: sea surface temperature (SST) and temperature/salinity-profiles (T/S-profiles). This means that each of the assim-i1 runs will have a timing of the ocean variation that is close to observed values.

The assimilation data for assim-i1 are: EN4.2.1 hydrographic profile data (Good et al., 2013), Hadley Centre Sea Ice and Sea Surface Temperature dataset (HadISST2, reference is cited as personal communication in Bethke et al., 2021) and National Oceanic and Atmospheric Administration (NOAA) Optimum Interpolation SST version 2 (OISSTV2, available only from 1982, Reynolds et al., 2002). The model climatology is taken from the ensemble mean of the 30-member historical experiment, with the climatological reference period defined as 1980-2010 (Bethke et al., 2021).

The ocean variables in the reanalysis experiment are updated using *anomaly assimilation* where observed monthly mean anomalies (from the climatology period 1980-2010) are added to the model climatology (computed from the historical experiment) and used to update the instantaneous model state.

Updating only the ocean variables during data assimilation in the assim-i1 reanalysis experiment, makes it a *weakly coupled data assimilation system*. This means that the atmospheric part of the model is only affected indirectly by the data assimilation. Since no atmospheric variables are used in the data assimilation, atmospheric variables - such as temperature and precipitation - are only affected by the assimilation through the influence from the ocean variables that are updated throughout the model integration (Bethke et al., 2021).

For assim-i1, the anomaly correlation coefficients (ACCs) for surface atmosphere temperature (SAT) in both the tropical Atlantic and the tropical Pacific are high (> 0.9). For the land temperatures in Brazil, the ACCs vary more, with higher correlations along the coastlines (both northern and eastern coast) with values around $0.4 - 0.7$. The inland temperatures show lower correlations (figure 10a in Bethke et al., 2021).

For precipitation, the assim-i1 ACC values in north and northeastern Brazil are in the range of $0.2 - 0.7$ (with highest correlation in the NE tip of the country). The ACC in the southernmost part are positive, and below approximately 0.5. In the middle of the country, and in the SACZ region, there is no significant ACC for precipitation (not locally significant, Bethke et al., 2021, figure 10b).

Precipitation ACCs are higher in the assim-i1 experiment than the historical experiment for all the areas of Brazil along the coast, as well as in the Amazon region. This means that the reanalysis run does capture the precipitation variability better than the historical run in large parts of Brazil. In other interior parts of the country, the reanalysis run and the historical run seem to perform similarly when it comes to ACC (Bethke et al., 2021, figure 10f).

3.3.4 Historical vs. reanalysis comparison

The historical NorCPM1 experiment is expected to contain anomalies of the same magnitude as the observed oscillations in the climate system - for instance variations connected to ENSO - but the timing in each individual historical run is arbitrary. That means that, when calculating the ensemble mean of the 30 runs, the internal variability in the model that is connected to ocean variability will presumably cancel out (since the probability that the individual runs have the same timing for the maximum and minimums is very

low). The trends and variations that are contained in the historical runs - and therefore in the historical ensemble mean - are those connected to external forcing (by GHGs, aerosols, solar irradiation and volcanic eruptions).

The assim-i1 reanalysis ensemble mean, on the other hand, will contain both long term climate change from forcing *and* in-sync internal variability. This is because variability originating in the ocean will have the right timing in all individual runs, following the ocean variable anomaly data assimilation. The assimilation restricts the model, and keeps it close to the anomaly ocean observations. The ensemble mean of all assim-i1 runs will then represent the climate that is both consistent with the model set-up, and in-sync with the SST and T/S-profiles. This means that each assim-i1 run includes observed internal variability - such as ENSO, AMO and PDO - if the related mechanisms are properly included in the model.

Assuming that the physical processes causing teleconnections are included in the coupled model, the assim-i1 runs will also include atmospheric response to ocean anomalies in other parts of the globe. The assim-i1 ensemble spread will contain the uncertainty of the model and variations due to internal atmospheric variability.

Subtracting the historical ensemble mean from the assim-i1 ensemble mean will therefore isolate oscillations and trends related to ocean variability (equation 3.1).

$$\overline{A} - \overline{H} = (F_{ext} + F_{int}) - F_{ext} = F_{int} \tag{3.1}$$

Where $\overline{A}$ is the mean of the 30 assim-i1 ensemble members, and $\overline{H}$ is the mean of the 30 historical ensemble members, F_{ext} is the response to external forcing, F_{int} is the response to internal variability forcing (originating in the ocean).

This also means, that if the assim-i1 ensemble mean is very similar to the historical ensemble mean in a region, the internal variability originating in the ocean might not be very important in that region, and the long term external forcing (by GHGs for instance) is what is mainly driving the changes in that area. In contrast, if assim-i1 run is much more similar to the observations, the ocean variability might play an important role to the changes in that area.

3.4   CAMELS-BR data

Catchment Attributes and MEteorology for Large-sample Studies Brazil (CAMELS-BR) is a set of hydro-meteorological time series and landscape attributes for 897 catchments in Brazil. Similar datasets are previously made for the United

States, Chile and Great Britain. The aim of the data is to enable large-scale hydrological research by providing a consistent dataset across the country. The dataset is made by combining relevant (gridded) meteorological variables like precipitation, evapotranspiration and temperature from different sources, and processing them to match the observed inflow series in specific catchments across the country. Additionally, the dataset includes 65 attributes covering a range of topographic, climatic, hydrologic, land cover, geologic, soil, and human intervention variables, as well as data quality indicators (Chagas et al., 2020).

3.4.1 Streamflow and catchment data

The streamflow data in CAMELS-BR is a subset of raw streamflow data provided by Brazilian National Water Agency (ANA). ANA originally provided 3679 time series - unevenly distributed across the country, with the highest density of gauge measurements in the southeastern part of the country and the lowest in the Amazon. The raw data can be accessed at ANA's web portal HidroWeb (ANA - Brazilian National Water Agency, 2023).

ANA has been responsible for planning, inspections, standardization of procedures and tools, quality check and publication of the hydrometeorological data in Brazil since year 2000 (ANA - Brazilian National Water Agency, 2023). Hydro-meteorological variables has been monitored by the state of Brazil since the beginning of the 1900 - and some places since mid-1800 - but the time series vary in length from place to place (ANA - Brazilian National Water Agency, 2023). ANA estimates daily streamflow by taking two daily stream stage measurements - at 07:00 and 17:00 local time - which are averaged and calculated into discharge, using a stage-discharge relationship. In situations where no stream stage measurement is available, regionalization methods are used (Chagas et al., 2020).

Chagas et al. (2020) selected 897 streamflow time series, based on the following criteria: (i) less than 5% of the data between 1990 and 2009 is missing, and (ii) the catchment boundaries have been estimated by a second provider, and these catchment boundaries compare well with the area estimated by ANA (Chagas et al., 2020). The catchment connected to each of these 897 streamflow time series are the basis of the CAMELS-BR dataset: The meteorological variables are post-processed to become catchment averages for the areas.

Out of these datas, I chose a subset of three catchment areas and their corresponding streamflow time series (as listed in table 3.3 with name, registered gauge ID, location of streamflow measurement, catchment size and time span of collected streamflow time series). These chosen catchment areas

can also be seen on the map in figure 2.1 in the introduction. Due to the scarce resolution of the NorCPM data, I chose the largest catchments possible in each of the three regions. This was to be able to generate meaningful mean time series from the model data.

Table 3.3: Catchment regions used in the thesis.

Region	Catchment name	Gauge ID	Gauge location	Catchment size $[km^2]$	Timeseries
Amazon	Obidos	17050001	1.919°S 36.824°W	4720020.0	1968-2018
São Francisco	Propria	49705000	10.214°S 55.513°W	638461.7	1977-2019
Paraguay	Porto Murtinho	67100000	21.700°S 57.891°W	565154.2	1939-2018

3.4.2 Meteorological data

Chagas et al. (2020) used three products to create daily precipitation time series for each selected catchment: (i) CHIRPS version 2.0 (Funk et al., 2015) with spatial resolution of 0.05°and temporal coverage 1981-2018, (ii) CPC Global Unified (NOAA, 2023) with spatial resolution of 0.5°and temporal coverage 1980-2018 and (iii) Multi-Source Weighted-Ensemble Precipitation version 2.2 (MSWEP v2.2; Beck et al., 2019) with spatial resolution of 0.1°and temporal coverage 1980-2016.

For actual evapotranspiration, they used Global Land Evaporation Amsterdam Model version 3.3a (GLEAM v3.3a; Martens et al., 2017) with spatial resolution of 0.25°and temporal coverage 1980-2018 and Modelo hidrológico de Grandes Bacias (MGB; Siqueira et al., 2018) of 0.5°spatial resolution and 1980-2014 temporal coverage. CPC Global Unified (NOAA, 2023) is used for calculating average temperatures for the catchments.

Of the 13 different climate indices - most of them related to precipitation - that are calculated for the catchments, I use the catchment averages of mean daily precipitation, based on CHIRPS v2.0 and the mean daily actual evpotranspiration based on GLEAM v3.3a, summed into monthly, seasonal and yearly values.

3.5 Masking areas and making time series for each region

To be able to compare the different types of gridded data at hand for each of the three regions, I generate masks to locate the grid cells that are within the catchment areas, using the catchemnt boundaries from CAMELS-BR. For each of the data sets with different resolutions (ERA5, CHIRPS and NorCPM), I generated one mask for each of the chosen catchments fitting the grid resolution (see figure 3.1). On the figure, the massive resolution difference between observational and modelled data is visible.

I use the python package `regionmask` to create the masks (read more on https://regionmask.readthedocs.io/en/stable/index.html). These masks were then used to create time series for each of the above mentioned areas.

The purpose of masking the data sets, is to create time series from the mean over each of the catchments. These time series, generated from the different data sets, I will then compare using various time series analyses, including trend significance analyses (as explained in the following section 3.6) and correlation analyses with data filtered for two different time scales (as explained later, in section 3.7).

3.6 I: Trend analysis

3.6.1 Mann-Kendall test and the Theil-Sen slope

I use the Mann-Kendall test (MK test) to evaluate the statistical significance of a trend. The MK test is widely used in the study of hydrometeorological time series (Yue and Wang, 2002; Luiz Silva et al., 2019; Bari et al., 2016).

The aim of the MK trend test is to distinguish between randomness and trend in a time series, where the null hypothesis is that the variation in the time series is random, and do not follow a trend (Mann, 1945). Note that the MK test only determines whether there exists a trend in the data, as well as the sign of the trend, but do not estimate the *strength* of the trend. The test only determines the sign and the statistical significance.

The strength of the trends are therefore estimated by a Theil-Sen estimator/slope, as defined by Theil (1950) and Sen (1968). The Theil-Sen slope is the slope of a fitted regression line, found by calculating the median of the $\frac{y_j - y_i}{x_j - x_i}$ for all pair of sample points (x_i, y_i) and (x_j, y_j) of distinct x-values (Sen, 1968). Compared to the least-square regression line, the Theil-Sen estimator slope is less sensitive to outliers, and do not require the assumptions
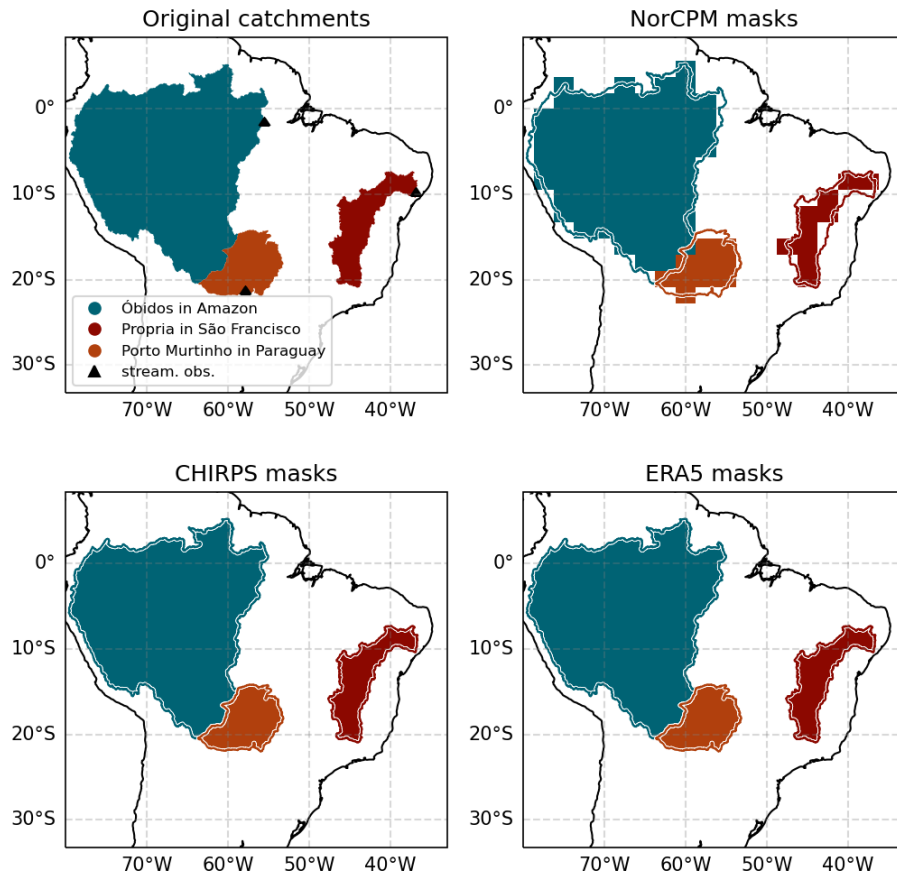
Figure 3.1: Original catchments and masks for the three types of gridded datasets of different resolution. The overlaying lines on the masks are the boarders from the original catchment data. The black triangles are locations of streamflow observations corresponding to the catchment areas.

that the variables are normally distributed and have constant variance, and hence is applicable to a wider range of data sets (Theil, 1950).

I have used the `pymannkendall` package on Python to conduct both the Mann-Kendall significance trend test and calculate the Theil-Sen slope (https://pypi.org/project/pymannkendall/). Below is the mathematical framework behind the Mann-Kendall significance test, using the equations 3.2, 3.3, 3.4 and 3.5, presented like in (Luiz Silva et al., 2019, pp. 356-357):

A positive (negative) trend is indicated by a positive (negative) value of Z, expressed like this:

$$Z = \frac{(S+u)}{\sqrt{VAR(S)}} \qquad (3.2)$$

Where VAR(S) is the variance, u = -1 if S > 0; u = 0 if S = 0; u = +1 if S < 0 thus:

$$S = \sum_{k=1}^{n-1} \sum_{j=k+1}^{n} signal(x_j - x_k) \qquad (3.3)$$

Where

$$\begin{aligned}
signal(x_j - x_k) = 1 \quad & if \quad x_j - x_k > 0; \\
signal(x_j - x_k) = 0 \quad & if \quad x_j - x_k = 0; \\
signal(x_j - x_k) = -1 \quad & if \quad x_j - x_k < 0;
\end{aligned} \qquad (3.4)$$

and x is the time series from k to n and $j = k + 1$.

$$VAS(S) = \frac{1}{18}[n \cdot (n-1) \cdot (2n-5) - \Sigma_{p=1}^{g} t_p \cdot (t_p - 1) \cdot (2t_p + 5)] \qquad (3.5)$$

Where g is the number of repeated value groups, p is the number of groups, t is the number of repeated values values in each group.

If the probability p of the Mann-Kendall test is equal to or less than the significance level α in a bilateral test, the null hypothesis (that there is just random change in the time series) is rejected, and a significant trend exists.

The significance levels I use in this analysis is $\alpha = 0.1$, corresponding to a confidence level of 90 %. This means that, for the trends I treat in this thesis, the probability that there is actually no trend in the data when I assume there is one (type I error), should be below 10 %. The lower the p-value of each individual test, the lower the probability that the null hypothesis is falsely rejected and that there in fact is no trend in the data. A type II error, is the opposite, when the null hypothesis is not rejected, and no trend is assumed to exist even though there actually is an existing trend.

Wang et al. (2020) argue that type II errors are equally important as type I errors in some cases, for instance in hydropower station design. A recommended way to increase the power of the MK test for detecting monotonic trends in hydro-meteorological time series is to increase the α from 0.05 to 0.1 (Wang et al., 2020), and thereby decreasing the significance level. This is what I do.

3.6.2 Identifying trends and internal variability with the MK test

I use the MK test and Theil-Sen slope to identify trends and internal variability at different time scales and with different timing. Short-term trends - for instance over just seven or nine years - can be understood as parts of year-to-year oscillations in the climate systems. Especially when the short-term trends oscillate between positive and negative values when varying the center year of the trend period with a couple of years. Differently, where the trend magnitude and direction is consistent when varying the center years, this can be interpreted to be detection of a consistent trend that is longer than the selected trend length.

The MK test and Theil-Sen slope will be used to compare trends and variability between the different experiments of modelled precipitation and evaporation data and observational data for each catchment. I have chosen to present the trends and variations in the units of percentage change per year. This presentation makes it easier to compare variations in the model and in the observations in locations where the model mean is different to the observed mean. Additionally, it makes it easier to compare between precipitation and evaporation (which originally have units mm/month) and streamflow (with the unit monthly mean m^3/s), without having to account for the different sizes of the catchment.

3.7 II: Correlation analysis and filtering

The second methodology I use - after the trend slope analysis - is to find correlations between observed precipitation variability, modelled precipitation variability and variations in observed streamflow. I use the correlations to detect similarities and relationships between the streamflow and precipitation. Additionally, I have correlated precipitation variability - of key seasons in each catchment - with global SST for the same season (and with the same filtering). This is to try to connect the variability in precipitation that is found to be important for the streamflow with global variability originating in the ocean.

3.7.1 Butterworth filtering

Because I am interested in separating the streamflow's dependency on precipitation variability of different time scales, I have used two different filters to isolate the variability. Decadal variability is captured with a low-pass fil-

ter, which has a threshold at > 9 years. Interannual variability is defined as the variability in the band-pass filter with periods in the range 2-9 years. The low-pass filter is made to not include the ENSO variability, that has the strongest variability of the range 2-7 years (see more in section ?? about ENSO).

Filtering is a method where selected frequencies in the time series are discarded. For low-pass filters, high frequency data is discarded. For a band-bass filter, only frequencies within the given band pass range are kept and both lower and higher frequencies are discarded. Filtering is closely related to a Fourier transform, followed by an inverse Fourier transform, where the data is transformed to the frequency domain by approximating a combination of several sinusoidal functions to fit the original data, and the data which have frequencies within the given domain (below the frequency limit in the low-pass filtering, and within the given range for the band-pass filtering) are kept to construct the filtered time series (Thomson and Emery, 2014).

The maximum frequency that can be detected with a filter is limited by the Nyquist frequency, which is $\omega_N = \frac{\pi}{\Delta T}$ where ΔT is the length of the time step (Thomson and Emery, 2014, pp. 598). The highest frequency detectable for yearly data will then be $\frac{\pi}{year}$, which equals a period of 2 years.

The minimum frequency that can be detected with a filter is limited by the fundamental frequency $\omega_1 = \frac{2\pi}{T}$ where $T = N\Delta T$, hence the max-limit period is T - the length of the record (Thomson and Emery, 2014, pp. 598). For yearly or seasonal data of 30 years, the longest detectable period will be that of 30 years, and all oscillations that are longer will be interpreted as trends with the given 30-year resolution, and not be included in the filtered series.

An ideal low-pass filter should i) remove all unwanted high frequencies, ii) keep all wanted low frequencies unchanged, iii) avoid creating spurious oscillations, iv) have no phase shift and v) have reasonable computational time (Thomson and Emery, 2014, pp. 594). There exist several types of filters, each of them with different trade-offs between the listed ideal qualities. The filter I chose to use in my analysis is the Butterworth filter, originally proposed by Butterworth (1930). The Python package I use is `scipy.signal.butter`.

I apply the filters after i) detrending, ii) calculating anomalies (subtracting the climatology reference period mean) of the time series and iii) normalizing them (dividing by the standard deviation) - in that order.

I choose 1981-2011 as the reference climatology period. There are two reasons for this choice. The first reason is that this is the earliest possible 30-year period to exist for all datasets (ERA5, CHIRPS, NorCPM historical, NorCPM assim-i1 and most inflow data). The second reason is that

I am especially interested in the changes over the last ten years. That is approximately from 2012 until 2022. To have a reference period prior to this decade of interest makes it convenient to look for changes from the 30-year reference period to (and within the) the ten year period from 2012-2022. I use the same climatological reference period to compare the model data with the observational data. I calculate model bias by subtracting CHIRPS data for precipitation and ERA5 data for evaporation.

3.7.2 Correlation and p-values with reduced degrees of freedom

After filtering the data, I correlate the time series with each other - the seasonal streamflow of each region with each of the seasonal precipitation data for the same region - and the precipitation time series with the global SSTs. I use a lag between the streamflow and the precipitation for most catchment, because the time it takes from it rains until the water has flowed to the bottom of the catchment can exceed one month. The lag varies from catchment to catchment - according to size and topography among others - ans is indicated in the figures. I have checked the time series for 1-month, 2-month, 3-month, 4-month, 5-month and 6-month lags - as well as no lag - and chosen the lag that gives the highest correlations in the specific catchment. The lags are indicated in the figures in the result section.

The aim of the correlation analysis is to obtain a correlation coefficient that contains information on the linear relationship between two variables - i) streamflow and precipitation and ii) precipitation and SSTs - and the strength of the relationship. A correlation coefficient is unit-less, and in the range [-1,1], where -1 is a perfect negative relationship, 0 is no relationship and +1 is a perfect positive relationship (Snedecor, 1956, pp. 162). I use the Pearson product-moment correlation coefficient, which is calculated with the following formula:

$$R_{X,Y} = \frac{cov(X,Y)}{\sigma_X \sigma_Y} \tag{3.6}$$

Where $R_{X,Y}$ is the correlation coefficient between time series X and Y when cov(X,Y) is the covariance between time series X and Y, and σ_X and σ_Y are the standard deviations of time series X and Y respectively.

After filtering, the time series of inflow and precipitation obtain autocorrealtion. Hence, when calculating p-values for the correlations between time series, this must be taken into account (Bretherton et al., 1999). The method I use, is to compute the autocorrelation for each time series and using the

38

autocorrealtion values to reduce the degrees of freedom by a factor given in equation 3.7 (Bretherton et al., 1999).

$$N_{eff} = N\frac{1 - p_X p_Y}{1 + p_X p_Y} \qquad (3.7)$$

In equation 3.7, N_{eff} are the effective degrees of freedom in the correlation between two time series, when N is the number of observation time steps, and p_X and p_Y are the one-lagged autocorrelation of time series X and Y respectively.

Then, the new (effective) degrees of freedom is used to find the t-statistic value for a two-sided t-test (equation 3.8; Snedecor, 1956).

$$t = R\frac{\sqrt{N_{eff}}}{\sqrt{1 - R^2}} \qquad (3.8)$$

Equation 3.8 describes the t-statistic, t, when R is the correlation coefficient between two time series, N_{eff} are the effective degrees of freedom when autocorrelations are taken into account (equation 3.7). Ultimately, I compute the p-value of the correlation, given the t-score (equation 3.8) and effective degrees of freedom (equation 3.7).

I will compare the correlation maps between filtered precipitation time series and global SSTs by assessing the (dis)similarities between the modelled and the observed correlation patterns in the tropical basins. The spatial extent of by definitions of the tropical basins is shown on figure 3.2.

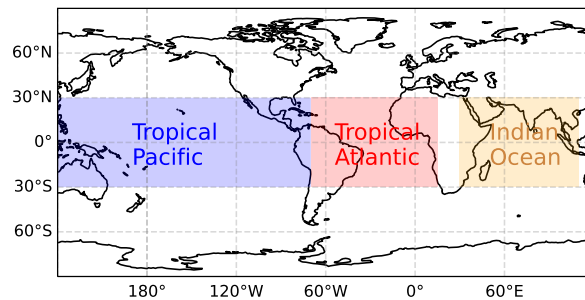Figure 3.2: Extent of the definitions of the tropical ocean basins that I use in the pattern correlation analysis, when comparing the modelled and observed precipitation-SST correlation maps. Tropical Pacific ocean is defined between 120°E and 80°W, Tropical Atlantic Ocean between 80°W and 10°E, Indian Ocean between 30°E and 110°E. The meridional extent of all three basins is from 30°N to 30°S

.

Chapter 4

Results

In this chapter, I will present the results of the thesis, which I have divided into two parts.

In the first part (section 4.1), I will present the streamflow trends during the 34-year period from 1981 to 2014, and compare these to precipitation and evaporation trends in the same period both modelled and observed data. This will lead to a conclusion on whether this specific 34-year trend is likely linked to modes of variability in the ocean or not (in each of the catchments).

The next part (section 4.2) will consist of the interannual and decadal variability of the streamflow, precipitation and evaporation in each catchment. I will compare the modelled and observed trends on multiple timescales and with different lengths. Also, I filter the data with different cut-off periods, correlate the precipitation variations in each season on each of the time scales with both the streamflow time series and global SST maps. This part shows results that indicate the origin of the modes of variability that influence the streamflow in each of the catchments - and on what time scale and in which season.

4.1   Trend 1981-2014

Since 1981 to 2014 is the longest common period of the data used in the thesis, limited by CHIRPS that start in 1981 and the historical simulation in NorCPM that stops in 2014, I will look at this specific 34-year trend for each of the basins.

I will show the trends for mean streamflow, precipitation and evaporation for the respective catchments within this period, and compare the observed values to the modelled ones.

The trends for the mean in each catchment in then followed by the trend

maps for the whole country - of each of the gridded data sets (CHIRPS for precipitation, ERA5 for evaporation and the NorCPM experiments for both). These trend maps will show trend variations *within* the catchments, helping us understand when the model experiment trends come from part of the catchments that differs from the observations. Also, the trend maps will provide information on where the trends in the assim-i1 ensemble are different for those in the NorCPM historical ensemble, and hence more specific regions where ocean anomalies changed the trend.

4.1.1 Amazon

In the period from 1981 to 2014, the streamflow out of Óbidos catchment has risen with a statistically significant trend of 513 m^3/s per year, which sums up to a total of 10 % increase in inflow over that 34-years period (figure 4.1a). During the 1981-2014 period - although there are local trend differences within the catchment that I will come back to in section 4.1.4 - the mean precipitation in the catchment has increased with 4.5 mm/year according to the CHIRPS data (figure 4.1b), corresponding to an increase of 7 % over the period.

The NorCPM ensemble means both contain an increase in precipitation over the same period as well, but of lower magnitude: The historical rainfall trend is 0.69 mm/year (statistically significant) compared to the 0.77 mm/year (statistically insignificant) increase for the assim-i1. Although the trends seem to be of similar magnitudes, the trend is not significant for the assim-i1 ensemble because this ensemble mean holds more year-to-year variability. Ocean anomaly assimilation in the assim-i1 experiment is not changing the 34-year trend in Amazon region substantially. Hence, the 1981-2014 increasing rainfall trend in the Amazon Óbidos region in the model, seems to be tied to the forcing that the historical and assim-i1 ensemble have in common (GHGs, aerosols, volcanic eruptions, solar radiance etc.), and not ocean variability. That is, according to the model result, the multi-decadal increase in precipitation in Amazon Óbidos is *not* mainly driven by internal variation originating in the ocean.

For the evaporation trends (figure 4.1c), GLEAM data show that the Amazon Óbidos basin had a mean increasing trend from 1981 to 2014, with a magnitude of 1.4 mm/year (about 3 % total increase). The ERA5 evaporation trend is also positive, but it is not statistically significant. Contrastingly, the decreasing evaporation trends in both of the model ensembles are statistically significant. In both of the NorCPM experiments, this seems to be caused by an abrupt drop in the evaporation around 1990 (figure 4.1c) that is not contained in the observational data. This drop in the model - and

the following evaporation decrease - might have to do with changes in model boundary forcing conditions, since is it similar for both the historical and the assim-i1 ensemble means.

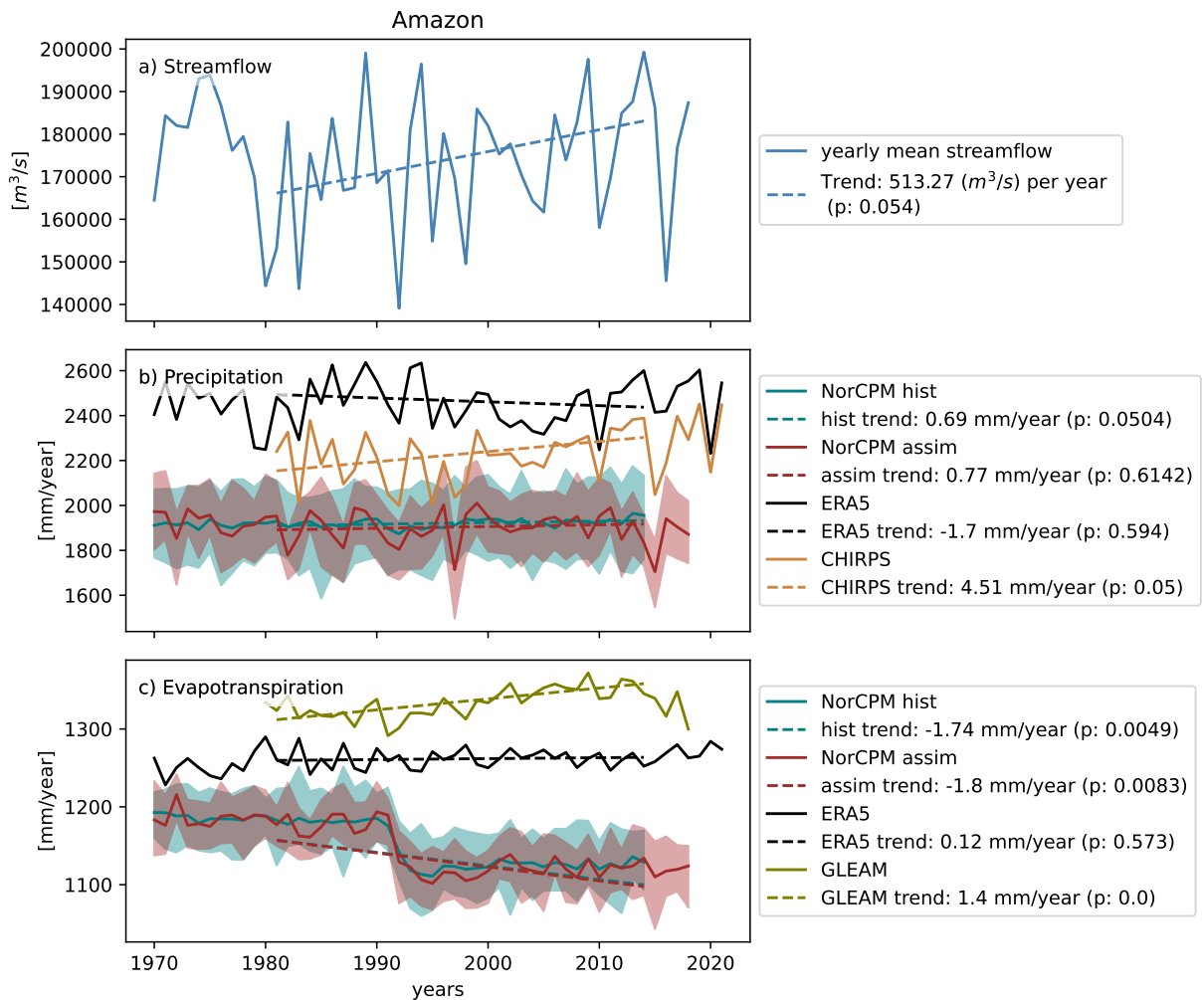Figure 4.1: Annual a) mean streamflow b) total precipitation and c) total evapotranspiration in Óbidos catchment in Amazon region (see location in figure 3.1). The stippled lines are the trends from 1981-2014. The magnitude of the trend (Theil-Sen slope), with the corresponding p-value from the Mann-Kendall trend test is in the legend. NorCPM historical and NorCPM assim refer to the ensemble means.

4.1.2 São Francisco

Propria catchment in São Francisco has experienced a strongly decreasing streamflow over the last decades (figure 4.2a). Over the period from 1981 to 2014, the streamflow has decreased with a rate of 25.7 m^3/s per year, corresponding to a total decrease of about 43 % over those years. During the same period, both observational data sets have measured decreasing precipitation trends, but not at significant levels. The lack of significance could be due to the high year-to-year variations.

NorCPM assim-i1 ensemble contains a significantly decreasing rainfall trend of -2.24 mm/year, which adds up to 22 % over the time period. This trend is not present in the historical experiment (figure 4.2b), and must therefore be added information by the ocean assimilation. This result suggest that the 34-year precipitation decrease in São Francisco is (partly) caused by variations in the ocean, because synchronizing ocean anomalies to observations in the assim-i1 experiment has induced a trend that was not present in the historical experiment with only external forcing.

The evaporation trends are statistically significant and decreasing in both of the model experiments (figure 4.2c), but the assim-i1 decrease is stronger. The assim-i1 ensemble mean evaporation trend measures -2.21 mm/year (total decrease of about 21 %) and the historical ensemble mean trend measures -0.32 mm/year (total decrease of about 3 %). The observation products are not consistent when it comes to the evaporation changes in São Francisco, but the ERA5 reanalysis measured decreasing evaporation (-2.53 mm/year, about 10 %, statistically significant).

The evaporation trends seem to be closely linked to the precipitation trends: Where the precipitation is decreasing, the evaporation is decreasing too. This makes sense, because São Francisco is partly in a semi-arid area, where evaporation is expected to be limited by evaporation. Hence, the assim-i1 results that improve the evaporation trends in the basin can simply be caused by the improvement of the rainfall trend by assim-i1 in the basin, and therefore also indirectly by ocean variation assimilation.

Figure 4.2: Annual a) mean streamflow b) total precipitation and c) total evapotranspiration in Propria catchment in São Francisco region (see location in figure 3.1). The stippled lines are the trends from 1981-2014. The magnitude of the trend (Theil-Sen slope), with the corresponding p-value from the Mann-Kendall trend test is in the legend. NorCPM historical and NorCPM assim refer to the ensemble means.

4.1.3 Paraguay

Porto Murtinho catchment shows a strong decline in streamflow over the last decades. From 1981 to 2014, the declining trend is in the range of -42.33 m^3/s per year, which corresponds to a total of about 67 % decline of streamflow (figure 4.3a). The rainfall in the catchment in the same period has

decreased in a rate of -9.15 mm/year (ERA5, statistically significant, about 24 %) and -2.00 mm/year (CHIRPS, not statistically significant, about 6 %). Surprisingly, the trend of the ensemble mean of the historical NorCPM experiment is statistically significant and positive (1.09 mm/year) over the same period. This increase in rainfall modelled by the historical ensemble adds up to 4 % increase in total over the period. The NorCPM assim-i1 trend is weakly negative ($< 1\%$ over the period) and not statistically significant (figure 4.3b).

Assim-i1 did remove the wrong positive trend in the NorCPM historical ensemble. Despite removing the wrong trend, the assim-i1 experiment did not obtain a 1981-2014 precipitation trend in the Paraguay catchment that resembles the observed one. This could mean that, neither the external forcing included in the experiments, nor the ocean variations, are the driving cause of the precipitation changes over the period. Other possible explanations are that the model is not able to reproduce the mechanics in the region over the period sufficiently to create the trend or that the modelled precipitation in the region is not responding correctly to the external forcing. I will come back to where in the basin and at what seasons the trends differ in the next section with the trend maps (section 4.1.4), and how the model biases might have influenced the analysis in the discussion part (section 5.2).

For the evaporation trends (figure 4.3c), the observations are not consistent: GLEAM has a non-significant weak positive trend, while ERA5 has a statistically significant decrease of 1.77 mm/year (about 4 %). In accordance with the modelled precipitation trends, the NorCPM historical ensemble mean has an increasing evaporation trend (more precipitation leads to more evaporation) and NorCPM assim-i1 has a non-significant decreasing evaporation trend (less precipitation leads to less evaporation).
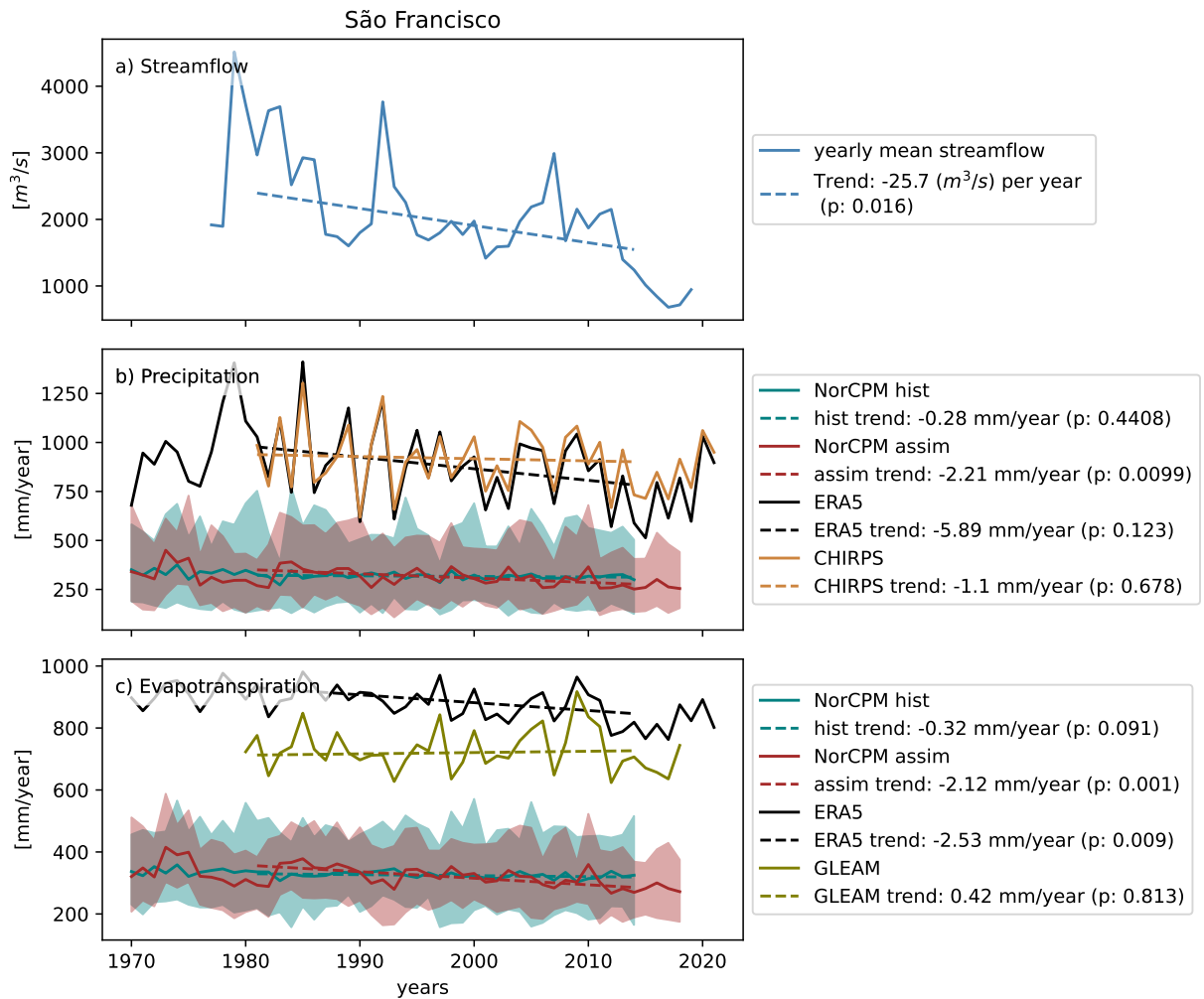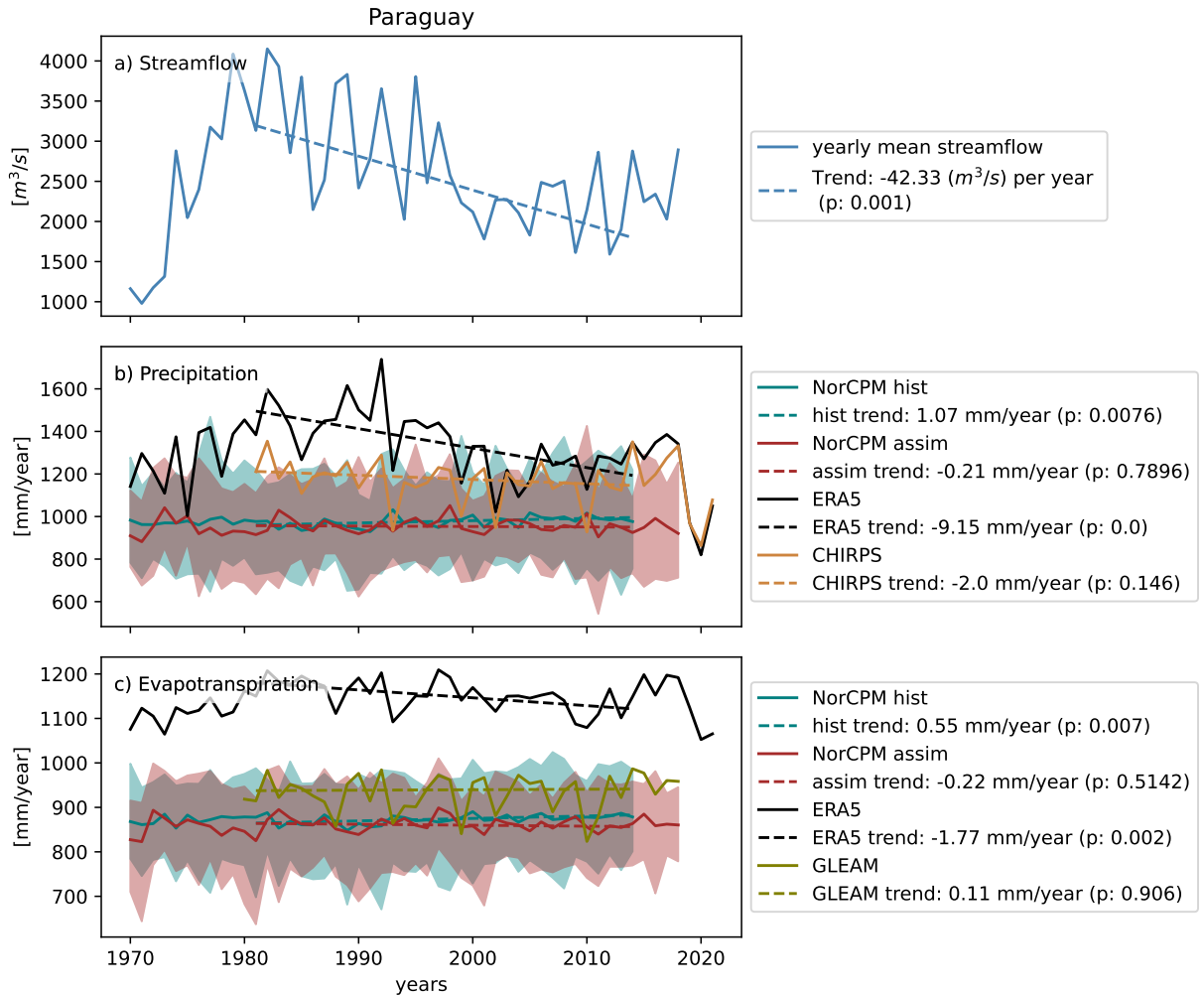
Figure 4.3: Annual a) mean streamflow b) total precipitation and c) total evapotranspiration in Porto Murtinho catchment in Paraguay region (see location in figure 3.1). The stippled lines are the trends from 1981-2014. The magnitude of the trend (Theil-Sen slope), with the corresponding p-value from the Mann-Kendall trend test is in the legend. NorCPM historical and NorCPM assim refer to the ensemble means.

4.1.4   Trend maps

To investigate the seasons and subareas of the catchments where the discussed trends come from, the spatial distribution of the precipitation trends from 1981 to 2014 are shown for NorCPM historical ensemble mean, NorCPM assim-i1 ensemble mean and CHIRPS (figure 4.4). Inspecting the differences

46

between the historical ensemble trend (figure 4.4a-d) and the assim-i1 ensemble trend (figure 4.4e-h), there are some notable similarities and differences for the basins that is sometimes bringing the assim-i1 modelled trends closer to the observed trends and sometimes not.

For Amazon catchment (the blue region in the figures, where the streamflow has increased), the historical ensemble and the assim-i1 ensemble had similar magnitude mean precipitation trends (as showed in section 4.1), so the ocean assimilation in assim-i1 seemed to make little difference to the main trend in the catchment.

When inspecting the trend maps, it is visible that both the historical ensemble (figure 4.4a-d) and assim-i1 ensemble (figure 4.4e-h) have a strongly increasing trend over the Andes mountain range throughout the rainy season (SON, DJF, MAM) in the western and southwestern part of the Amazon basin. This trend over the Andes in the west and southeast of the basin is only partly replicated in the CHIRPS observations (figure 4.4i-l). For the observed trends, there are significant contributions to the positive mean trend in the northern part of the basin - especially in MAM - and in the interior of the basin - especially in DJF. The observed precipitation trends in the interior of the basin are patchy with lots of local variations. The trend in the interior of the basin in the historical experiment, on the contrary, is uniformly negative (figure 4.4).

The assim-i1 experiment (figure 4.4i-l) seems to have removed some of the negative trends from the historical experiment - especially in the northwestern part - and thereby making the trends less different from the observations. Assim-i1 obtains a weak positive trend in the very north of the basin - in accordance with observations.

The assim-i1 ensemble also seems to be closer to capture the strengthening of the ITCZ that seems to have happened during the 34-year period according to the observations, although the positive trends in the ITCZ band seems to be displaced in the assim-i1 model so that they are outside the Amazon basin.

Despite these corrections by the assim-i1 experiment, the increase over the Andes mountain in the model seems to be what is driving the mean catchment trend for both the historical and assim-i1 ensembles, and therefore providing a trend that contains only parts of the dynamics causing the observed trend. The model does not replicate the trend in the northern and interior part of the Amazon sufficiently, which could be the reason why both experiments have lower percentage increase than observations. NorCPM only seem to get part of the trend right - and exaggerate the trend over Andes. Also important to note is that the trend over the Andes mountain range is not altered by ocean assimilation in assim-i1, and must therefore be caused by external forcing that is common for the two model experiments.

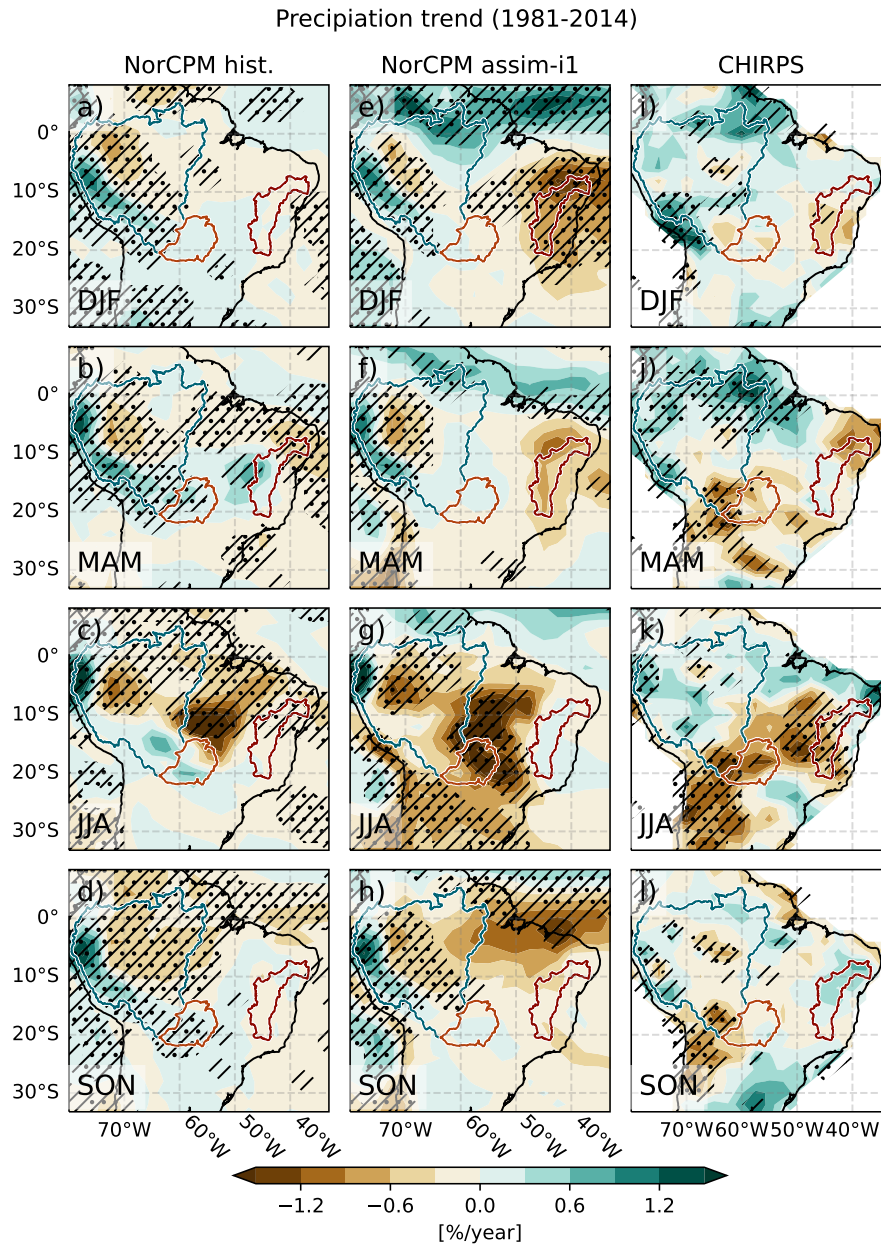Figure 4.4: 1981-2014 seasonal precipitation trends for NorCPM ensemble mean (a-d), assim-i1 ensemble mean (e-h) and CHIRPS (i-l). Hatched areas are significant with $\alpha = 0.1$, and dotted areas are confident with $\alpha = 0.05$, calculated with the MK test. The colored boarders indicated are the catchments treated in this master thesis: Blue is Amazon, red is São Francisco and orange is Paraguay.

For São Francisco (red region in the figures, with a decrease in stream-flow), the most striking difference between the trend in the two model experiments is the decreasing trend in the entire basin in DJF, which is non-existing in the historical experiment (figure 4.4a) and added in the assim-i1 experiemnt (figure 4.4e), bringing assim-i1 closer to the observed trends (figure 4.4j), which also show a statistically significant drying trend in the center of the basin.

Moreover, the assim-i1 experiment is bringing the modelled JJA trend somewhat closer to the observations by removing a statistical significant drying trend in the north of the basin (4.4c), which is of opposite sign in the observations (4.4k). In JJA, assim-i1 is not able to reproduce the observed drying trend that is measured in the observation, but this does not contribute much to the yearly mean values, since the JJA is a low-rainfall season in the region, and measured in % per year, the trends look stronger than they actually are measured in mm/year.

The assim-i1 corrections of the historical experiment trends show that when the assim-i1 experiment creates a negative mean yearly trend for the catchment that is not present in the historical - and thereby getting closer to the observed decreasing trend - the changed mean yearly trend is due to some of the right reasons: The yearly trends in the assim-i1 experiment is driven by the DJF trends, and in northern part of the basin in MAM, and so is the CHIRPS trend to a large extent. This strengthens the hypothesis that was raised when inspecting the mean trends in section 4.1.2, that the decreasing São Francisco rainfall trend from 1981 to 2014 is connected to ocean variations.

For Paraguay (orange region, with a strong decrease in streamflow), the historical ensemble has *increasing* rainfall trends throughout the year, that are significant in MAM and SON (figure 4.4b and 4.4d). In the assim-i1 ensemble, on the contrary, these increasing trends are not present. Instead, assim-i1 ensemble has a weak significant drying trend in the northeastern part of Paraguay basin in JJA (figure 4.4g).

Assim-i1 ensemble seasonal trends are closer to the observations, which also has a significantly drying trend of the similar magnitude during JJA (figure 4.4k), and non-significant trends in the other seasons in Paraguay basin, in accordance with the observations. Hence, the assimilation with ocean anomalies in assim-i1 is bringing the modelled trends closer to observed 34-year trend. This result indicates that the 1981-2014 precipitation trend in Paraguay is influenced by ocean variation.

Although the mean trend for the catchment in the assim-i1 experiment between 1981 and 2014 is not significant in Paraguay - as showed in section 4.1.3 - the dynamics seems to be in line with the observed trends in terms of

seasonal timing and location of the precipitation trend within the the basin.

4.2 Decadal and interannual variability

4.2.1 Amazon

Figure 4.5 shows the results from the MK test trend analysis on streamflow observations in the Óbidos catchment in Amazon. Each of the squares in the diagram visualizes the trend of a part of the time series, each square with a different combination of interval length (y-axis) and center year of the interval (x-axis). The color on the square indicates the magnitude of the trend, calculated with the Theil-Sen slope, and the stippled squares are the trends that are significant according to the MK test.

Towards the bottom of the diagram, the shorter trends are located. The pattern of these trends show interannual variability in the time series, and have the strongest trends measured in % per year. The trends that are farther to the top of the diagram are weaker in % change per year, which is consistent with the suppression of the interannual timescales when considering longer time scale trends. We can recognize parts of the significantly increasing streamflow trend in the basin in the 1981-2014 period in the weak positive values in the top right of the diagram.

Figure 4.5: Observed streamflow trends in Óbidos catchment in Amazon (ANA data) of several lengths and timescales. The trends are calculated with the Theil-Sen estimator/slope. Hatched areas are significant within the 90 % interval, and is calculated with the Mann-Kendall test. The change is given in % change per year, compared to the mean streamflow over the exact time period for the given trend.

Figure 4.6 is the similar visualization of the MK trend tests on the catchment *precipitation* time series. The same trend test procedure has been conducted on both of the modelled ensemble means: historical (a) and assim-i1 (b), and both observational datasets: ERA (c) and CHIPRS (d).

Figure 4.6: Precipitation trends in Óbidos catchment in Amazon of several lengths and timescales. The trends are calculated with the Theil-Sen estimator/slope. Hatched areas are significant within the 90 % interval, and is calculated with the Mann-Kendall test. a) NorCPM historical ensemble mean, b) NorCPM assim-i1 ensemble mean, c) ERA5 and d) CHIRPS. e) is observed streamflow (ANA data). The change is given in % change per year, compared to the mean precipitation over the exact time period for the given trend and with the given dataset.

51

It is visible in figure 4.6 that NorCPM assim-i1 ensemble mean contains stronger interannual precipitation variability (> 2 %) in the Amazon region than the historical ensemble (< 0.5 %). The assim-i1 ensemble contains interannual variability in the same magnitude as the observed precipitation data sets. This shows that assimilating ocean anomalies does add interannual precipitation variability in the region, and it seems like the effect from the anomaly assimilation is consistent among the assim-i1 model runs (since the variations are not averaged out in the assim-i1 ensemble mean, as they are for the historical ensemble mean). Hence, the variability of the variation in the region on time scales of 7- and 9-years period (and to some extent 11-years periods) is affected by ocean variation in Amazon.

The *timing* of the positive and negative short (7 years) variation trends of the assim-i1 mean seems to match up with the observed variations at several points, but not all (figure 4.6). For instance, center year 2002 has a significant declining trend, and 2006 has a significant increasing trend in both assim-i1 ensembles and in the observational data. Hence, the NorCPM assim-i1 seems to add information about the interannual precipitation variations in the area, compared to historical ensemble, although it does not always match up with observations. For instance, the last observed trends are positive for both of the datasets, while the assim-i1 trends are negative.

When it comes to the 13-, 15- and 21- year variations, the magnitudes of the variations are weaker in the assim-i1 experiment than in the observations. The observations also contain a higher number of significant trends. The timing of the trends on this time scales do not match well with the observations either. This could either mean that the precipitation variation on these time scales are caused by other factors than ocean variation or the forcing included in the model. Or it could mean that the model is not able to reproduce the longer oscillations that are connected to the ocean variability. I will come back to this when analysing the correlation maps for Amazon later in this section.

Figure 4.7 shows the test results for *evaporation* time series. The test in conducted is the same way as for streamflow and precipitation, varying the center year and interval length of the time series, before estimating the trends and their significance.

For the evaporation variations on different time scales, the model experiments (figure 4.7a-b) look more similar to each other than assim-i1 does to the observations (figure 4.7c-d). This is mainly due to the sudden drop of evaporation in the catchment that seem to be linked to model boundary condition, as I have previously discussed (in section 4.1.1).

Apart from that, the NorCPM assim-i1 ensemble mean has some variation on the 7- and 9-year interval length that is of stronger magnitude than the

historical ensemble mean. Some of the variation seem to match up quite well, but not all.
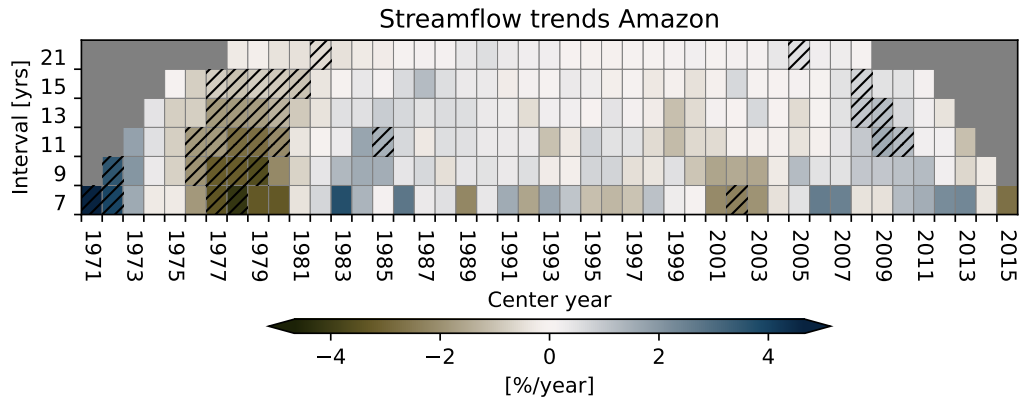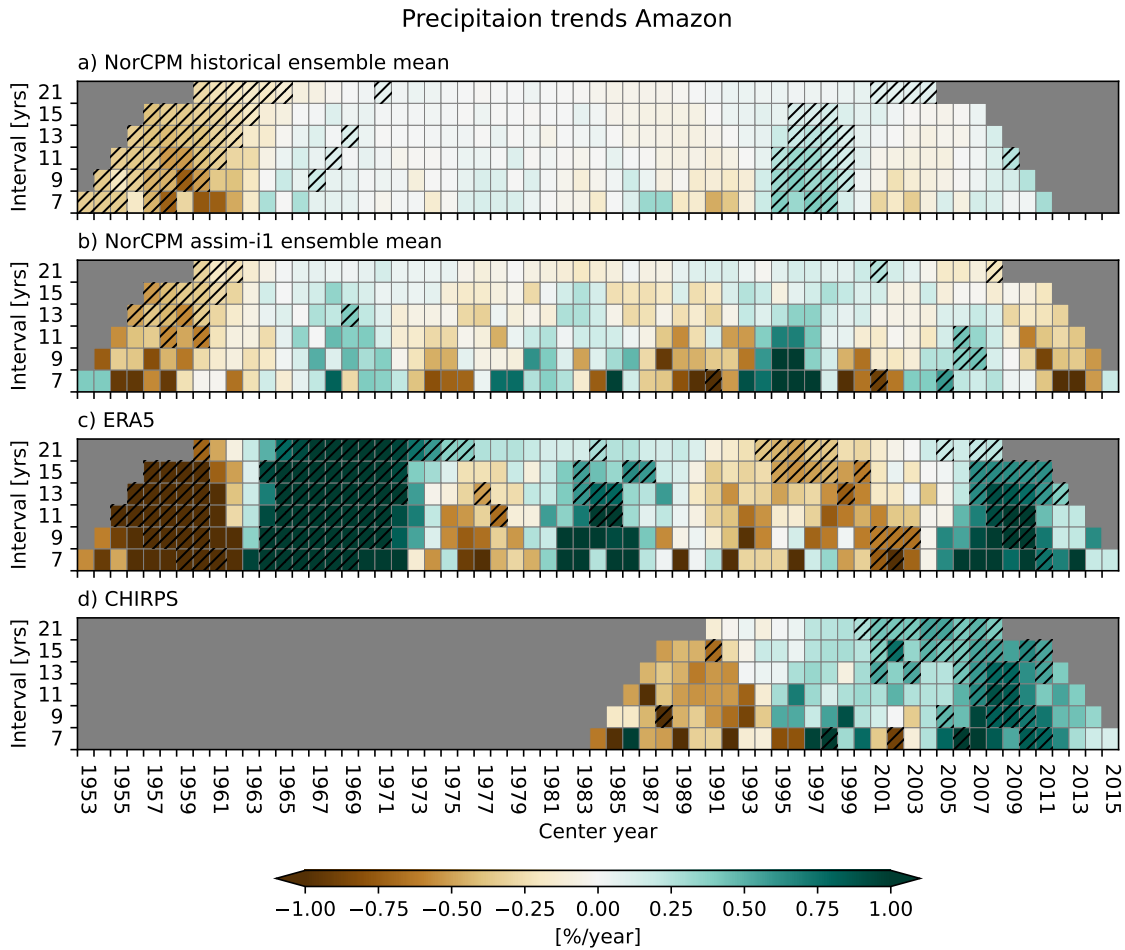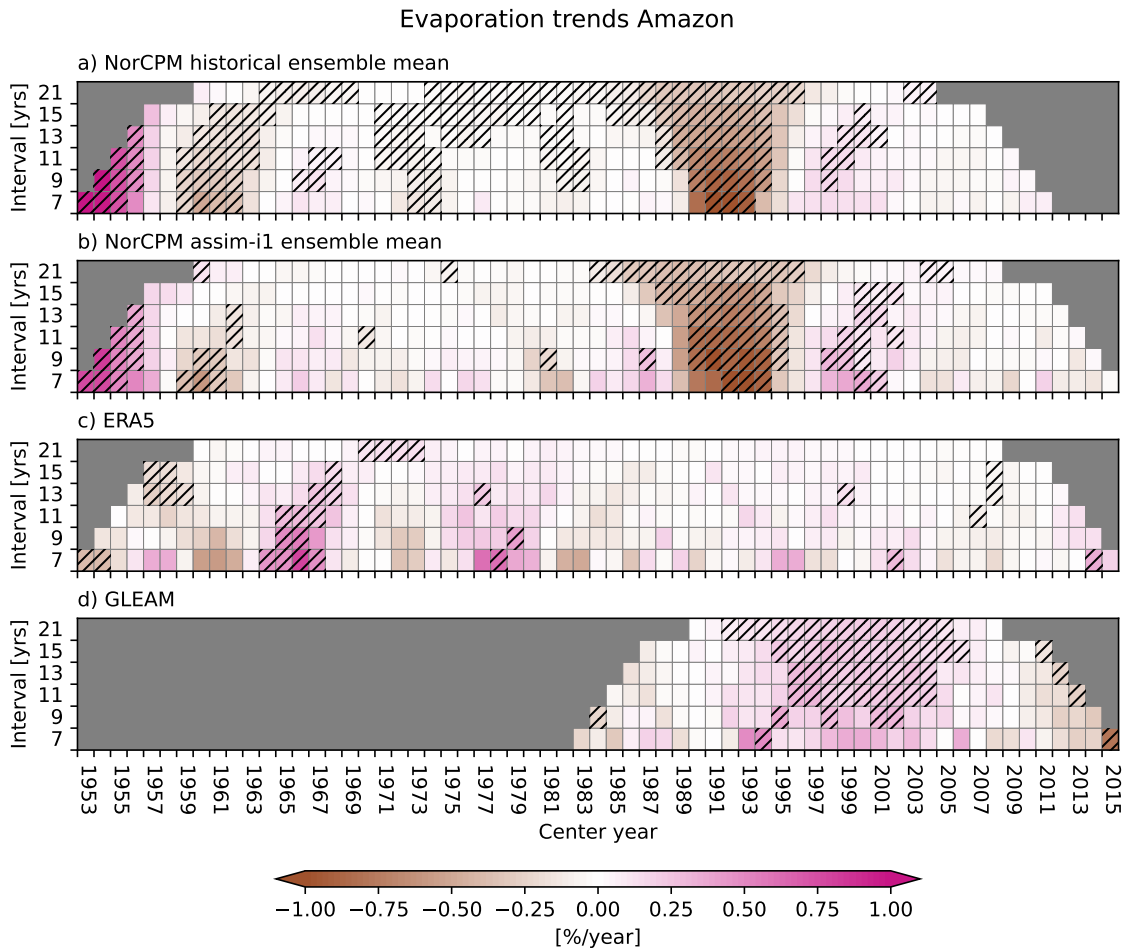

Figure 4.7: Evaporation trends in Óbidos catchment in Amazon of several lengths and timescales. The trends are calculated with the Theil-Sen estimator/slope. Hatched areas are significant within the 90 % interval, and is calculated with the Mann-Kendall test. a) NorCPM historical ensemble mean, b) NorCPM assim-i1 ensemble mean, c) ERA5 and d) GLEAM. e) is observed streamflow (ANA data). The change is given in % change per year, compared to the mean precipitation over the exact time period for the given trend and with the given dataset.

The visual inspection of the trends and variations of the Amazon time series shows that - for both precipitation and evaporation - the assim-i1 ensemble mean adds internal variability. But it is not clear whether the inter-

nal variability is an *improvement* that have brought the modelled variability closer to the observations.

Therefore, in the following part II of the analysis, I split the time series into seasonal time series (December-January-February: DJF, March-April-May: MAM, June-July-August: JJA, September-October-November: SON), filter them on two different time scales, and correlate these seasonal and filtered time series - both from the model and from observations - with the streamflow time series that are filtered on the same time scales. With this analysis, I will be able to identify at what time scales and what seasons the model is improving the correlation with the streamflow.

Then, to understand more about *why* the assim-i1 experiment alters the the variation magnitude and timing for the variation on each of the time scales and seasons, I want to investigate the relationship between the variation in the time series and the variation of SST. I do this for observations too, to compare the model SST-precipitation dynamics with the observations.

If (i) the correlation with the lagged streamflow is improved for a specific season and a specific time scale of variability, and (ii) the correlation map of assim-i1 ensemble shows the same pattern as the observations, then it is confirmed what dynamics or origin of variability in the ocean that is affecting the streamflow variations.

For the Óbidos catchment, I have used a lag of 3 months when correlating the time series. This is the lag that gives the highest correlation, when I tested for flow season that was 1, 2, 3, 4, 5 and 6 months shifted forward as well as unlagged. Because the catchment is large, it will take several months from the rain falls into the outskirts of the catchment before it reaches the outflow point where the streamflow measurements are taken. So this lag is logical.

The correlation coefficients between precipitation and streamflow in Óbidos in Amazon, for time scales of > 9 years, are listed in table 4.1. There are some interesting results here:

Firstly, precipiation variations on time scales longer than 9 years in the NorCPM assim-i1 experiment seem to improve correlations with observed streamflow variations on the same time scales (lagged), compared to the historical experiment. NorCPM assim-i1 has higher correlation coefficient in all seasons except MAM, reaching values that are comparable to those of ERA5. This means that the timing of the precipitation variation in the assim-i1 experiment contain as much long term variability of the right timing as ERA5 does.

Secondly, NorCPM assim-i1 obtains a *statistically significant* correlation between JJA precipitation and SON streamflow out of the Amazon basin of 0.66 (p: 0.064, table 4.1), that is not contained in the historical experiment

(R: -0.04, p: 1.061, table 4.1). Hence, this could be a time scale and season where the ocean anomalies are driving decadal precipitation variations, which again are driving streamflow variation in the Amazon Óbidos catchment.

Table 4.1: Correlation coefficients (with corresponding p-values) between 9 years-lowpass filtered seasonal precipitation and 3 months-lagged streamflow in Óbidos catchment in Amazon. All data is detrended and normalized prior to correlation calculation. Significant correlations are marked in bold.

	ERA5	CHIRPS	NorCPM hist.	NorCPM assim-i1
DJF				
R	0.61	**0.96**	-0.26	0.2
p	0.1132	0.0055	0.5931	0.6857
MAM				
R	**0.69**	0.45	-0.02	-0.4
p	0.073	0.2692	0.9553	0.3452
JJA				
R	0.34	**0.81**	-0.0	**0.66**
p	0.4027	0.0482	0.994	0.0458
SON				
R	0.38	0.54	-0.03	0.41
p	0.4571	0.1288	0.9456	0.3578

Figure 4.8 shows the correlation map between the lowpass-filtered SST and precipitation time series for CHIRPS and assim-i1 - the same that were correlated with streamflow in in table 4.1. Table 4.2 shows the corresponding pattern correlations between observed and modelled correlation maps. There are similar features in the observational correlation maps (figure 4.8a-d) and the assim-i1 correlation map (figure 4.8e-h) for some seasons.

In JJA, NorCPM assim-i1 ensemble has statistically significant negative correlations in the eastern tropical south Pacific (0.6-0.8, figure 4.8c), which is present in the CHIRPS correlation map as well (> 0.8, figure 4.8g). Also, NorCPM assim-i1 and CHIRPS both have significant positive correlations in the south Atlantic Ocean: CHIRPS around 30°S (0.6-0.8) and assim-i1 in the entire south Tropical Atlantic (0.4-0.8). Additionally, they both have positive statistically significant correlations in the Indian Ocean (0.4-0.8).
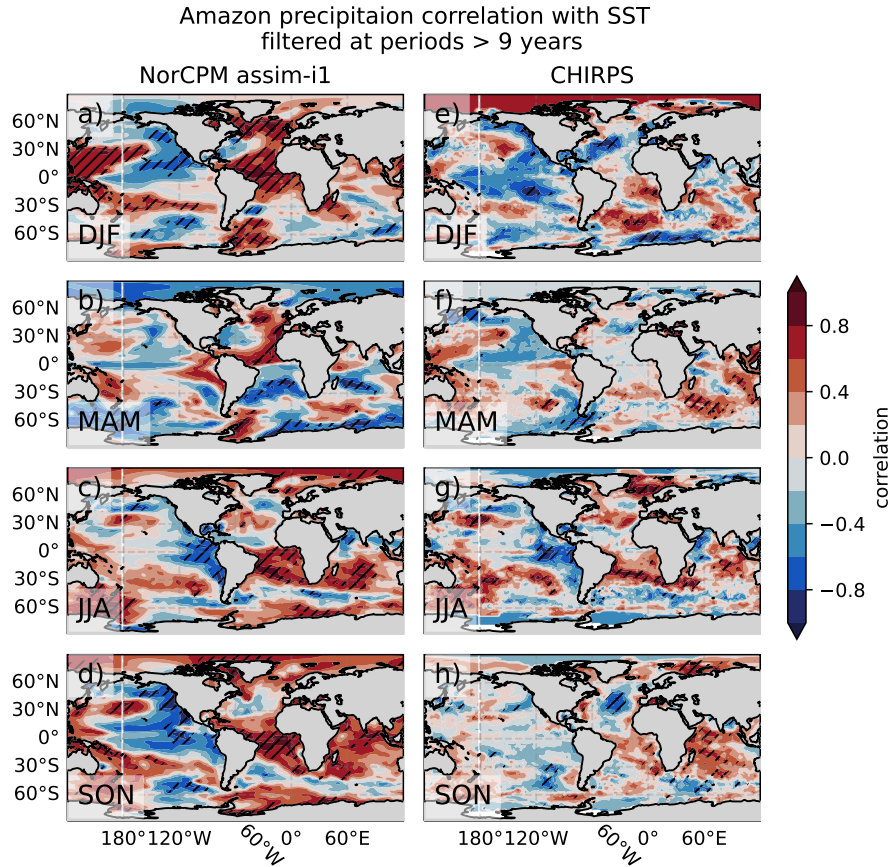
Figure 4.8: Correlation values between seasonal precipitation time series in Óbidos catchment in Amazon and global seasonal SSTs for NorCPM assim-i1 ensemble mean (a-d) and CHIRPS correlated with ERA5 SSTs (e-h). All time series are normalized and filtered for periods > 9 years before the correlations are calculated. The time series run from 1981-2018. Hatched areas are significant with $\alpha = 0.1$.

Table 4.2: Pattern correlations between correlation maps for CHIRPS and NorCPM assim-i1 in figure 4.8. The boundaries of the ocean basins are shown in figure 3.2 in the method section. The tropical ocean band is defined between 30°S and 30°N.

	DJF	MAM	JJA	SON
Tropical Pacific	0.13	-0.1	0.57	0.43
Tropical Atlantic	0.39	0.17	0.4	0.07
Indian Ocean	0.2	0.32	0.78	0.08
Tropical Ocean Band	0.45	0.19	0.69	0.5

In JJA, the SST patterns for the observations and model seem to be most similar in Tropical Pacific and Indian ocean, according to the pattern correlation shown in table 4.2. The total JJA pattern correlation in the tropical ocean band is 0.69 between the model and observations, which shows that the model to a large extent replicates the tropical SST pattern in JJA. The similarity of the JJA correlation patterns indicates that the model teleconnections that connect SST variations on decadal time scales and JJA precipitation variation in Amazon is similar to the observed teleconnections. Both in the model and in the observations, the JJA precipitation and therefore SON streamflow - seem to be influenced by variations in the Pacific, Atlantic and Indian ocean. In the Pacific, the correlation pattern might resemble some type of negative PDO mode. That is, colder waters in the east Pacific (negative PDO) lead to more precipitation - and therefore more lagged inflow in the Óbidos catchment. Note that JJA is the driest season in the region.

For the other seasons, the assim-i1 ensemble tends to overestimate the impact of the Tropical Atlantic SST variation impact on the Amazon rainfall variation. CHIRPS has some correlations in the Tropical Atlantic too, but to a smaller extent. In an important part of the wet season, DJF, CHIRPS shows a PDO pattern in the Pacific, with negative correlations in a comma-shape in the tropical and norther pert of the Pacific basin. The assim-i1 model ensemble does replicate this partly, but the model simultaneously have high correlations with the Tropical Atlantic and North Atlantic basin ($>$ 0.6) which is not similar to observations. The model is syncing the Amazon DJF precipitation variation up with the Atlantic ocean variations when the observations indicate that this pattern should not be as important as in the model.

In MAM, the pattern correlation between the correlation maps of assim-i1 and CHIRPS is 0.19 (table 4.2), which indicate a idssimilar correlation pattern between the model and observations in the tropical band. This might be a reason why the model was not able to reach high correlations between the precipitation and streamflow variations on decadal time scales.

Table 4.3 contains the correlation coefficients between lagged streamflow and precipitation filtered for interannual variability. Filtered on the 2-9 year time scales, the correlations between observed precipitation and streamflow are strongly positive for all seasons (for both datasets, in the range of 0.56 - 0.84), showing that there is a strong link between year-to-year rainfall variability and streamflow in Óbidos catchment in Amazon.

Table 4.3: Correlation coefficients (with corresponding p-values) between 2-9 years-bandpass filtered seasonal precipitation and 3 months-lagged stream-flow in Óbidos catchment in Amazon. All data is normalized and detrended prior to correlation calculation. Significant correlations are marked in bold.

	ERA5	CHIRPS	NorCPM hist.	NorCPM assim-i1
DJF				
R	**0.56**	**0.63**	0.27	0.28
p	0.0025	0.003	0.1708	0.1313
MAM				
R	**0.74**	**0.59**	0.33	**-0.4**
p	0.0	0.0034	0.1179	0.0415
JJA				
R	**0.84**	**0.71**	0.01	**0.72**
p	0.0	0.0002	0.9507	0.0004
SON				
R	**0.8**	**0.79**	-0.23	0.28
p	0.0	0.0	0.2792	0.132

The assim-i1 ensemble improves the correlation with lagged streamflow compared to the historical correlations in JJA. In JJA, NorCPM assim-i1 has a correlation coefficient, R, of 0.72 (p: 0.0004), which is similar to that of CHIRPS (R: 0.71) and ERA5 (R: 0.84, table 4.3). Hence, JJA is the only season where the interannual variation in rainfall over Amazon region is significantly improved in the NorCPM assim-i1 ensemble compared to the historical ensemble. According to these model results, interannual anomalies of JJA precipitation over Amazon might be tightly connected to ocean anomalies, and these anomalies are in turn correlated with SON streamflow out of the Óbidos catchment.

When looking at the correlation maps between JJA precipitation and JJA SSTs filtered on the same time scales (2-9 years, figure 4.9c and 4.9g), assim-i1 ensemble correlation map looks close to resmble the pattern in the observation dataset. For the observations and in assim-i1, there are significant positive correlations in the south Tropical Atlantic ocean, with correlation coefficients in the range 0.4-0.6 for CHIRPS and 0.4-0.8 for the model. Also, both CHIRPS (figure 4.9c) and assim-i1 (figure 4.9g) have significant positive correlations in the Atlantic between 30°N and 60 °N. By and large, the assim-i1 SST correlation pattern is similar to the observed one, and the patter correlation coefficients between the model and observation are high in all basins (0.81, 0.6, and 0.82 in Tropical Pacific, Tropical Atlantic and

Indian Ocean respectively, table 4.4), which strengthens the confidence that the influence on interannual precipitation is originating in the ocean (in JJA).

Also the DJF correlation maps look similar for the model (figure 4.9a) and the observations (figure 4.9e). The pattern correlations are also high in all basins during DJF (0.58 for Tropical Pacific, 0.7 for Tropical Atlantic and 0.73 for Indian Ocean; table 4.4). This shows that the model establishes similar teleconnection patterns between the global ocean anomalies and precipitation in Amazon.
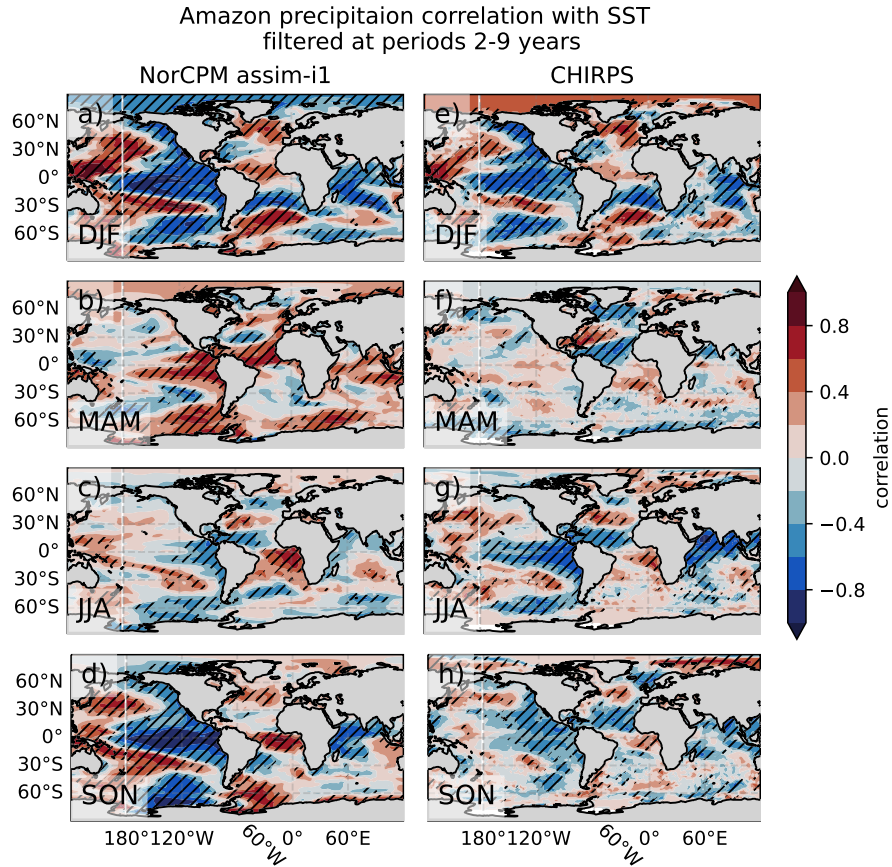
Figure 4.9: Correlation values between seasonal precipitation time series in Óbidos catchment in Amazon and global seasonal SSTs for NorCPM assim-i1 ensemble mean (a-d) and CHIRPS correlated with ERA5 SSTs (e-h). All time series are normalized and filtered for periods 2-9 years before the correlations are calculated. The time series run from 1981-2018. Hatched areas are significant with $\alpha = 0.1$.

Table 4.4: Pattern correlations between correlation maps for CHIRPS and NorCPM assim-i1 in figure 4.9. The boundaries of catchments are shown in figure 3.2 in the method section. The tropical ocean band is defined between 30°S and 30°N.

	DJF	MAM	JJA	SON
Tropical Pacific	0.58	-0.25	0.81	0.41
Tropical Atlantic	0.7	0.14	0.6	0.25
Indian Ocean	0.73	0.03	0.82	0.34
Tropical Ocean Band	0.79	-0.08	0.77	0.48

4.2.2 São Francisco

Figure 4.10 shows the overview over trends and their significance - with different timings and lengths - for observed streamflow in Propria catchment in São Francisco. This is the catchment with the largest magnitude of the interannual variability. Note that the range of the colorbar is ±20 % per year, as compared to ±5 % per year in the Amazon plot. There is significant streamflow variability on all evaluated time scales, and patterns that looks like oscillations.

The record of the observations at Propria catchment is shorter than those for Amazon and Paraguay, and does not start until 1977. This limits the ability to identify oscillating patterns on the longer time scales than that in the diagram.

There seem to have been a strong decrease in streamflow over the last decade, where the trends get increasingly stronger when moving from center year 2005 until center year 2016 (figure 4.10c-d). This means that even after the decreasing trend between 1981 and 2014 that was discussed earlier (in section 4.1.2), this catchment has had even steeper decreasing trends in the recent past. There are declining streamflow rates on all time scales leading up to 2019.
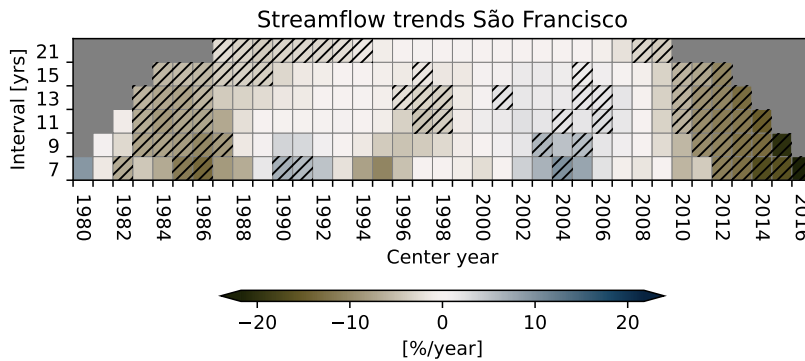
Figure 4.10: Same as figure 4.5, but for Propria catchment in São Francisco.

There is a steep recent decline in the *precipitation* on all time scales as well (as seen in figure 4.11c-d). This decreasing trend of precipitation in the late decade in the catchment is not contained in the historical NorPCM experiment at all (as seen in figure 4.11a). Again, it becomes clear that the drying of São Francisco basin is not solely due to external forcing: neither the 1981-2014 longer trend, nor the trends on shorter time scales is present in the historical NorCPM experiment.

The assim-i1 experiment contains interannual variations of the same magnitude as the observations, when assessing the results in the units % per year. Note that São Francisco is located in an area where the model largely underestimates the rainfall, so the trend estimates in mm/year are more different between the model and observations.
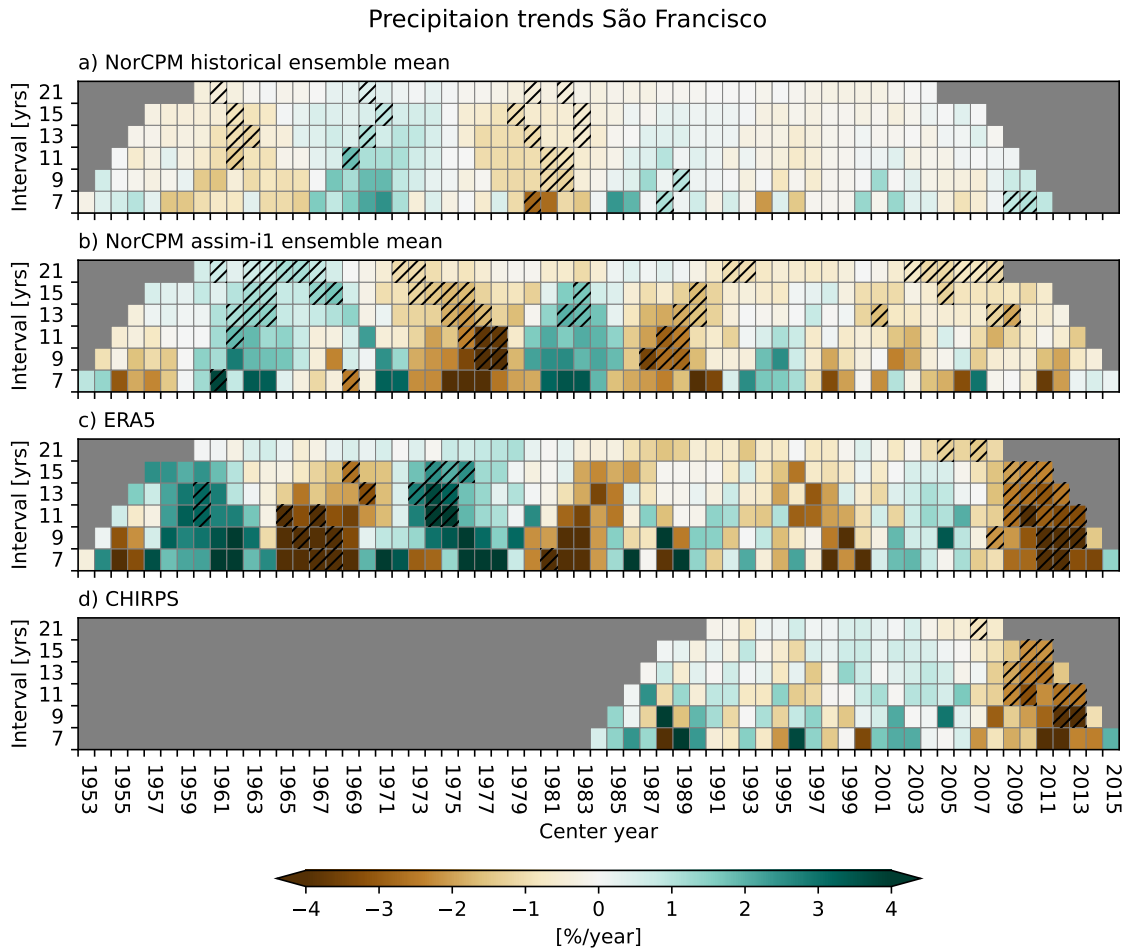
Figure 4.11: Same as figure 4.6, but for Propria catchment in São Francisco.

The timing of the variability of the assim-i1 experiment does match better up with the drying trends over the last decade, but not completely (as seen in figure 4.11b). The trends on shorter time scales than 21 years are weaker than observations. Several of the recent trends - on all time scales - are not as strong as in observations either.

The 21-year trends in the assim-i1 experiment are different from the ones in historical experiment several times. Since the assim-i1 ensemble catch the

negative decreasing 21-year trend from about 1995 and until 2018 that the historical ensemble does not (upper right in each panel in figure 4.11), these trends are induced by ocean variation in the model. Parts of the explanation for the drying trends in the basin from the 1990s to the 2010s is therefore likely to be ocean variability. The AMO has for instance changed sign from negative to positive throughout that time period. A possible explanation would be that the changes are connected to this variation. I will come back to this later in this section, when assessing the correlation maps.

The same diagram for evaporation trends and variation in São Francisco (figure 4.12) has similar looking patterns as the precipitation in the model experiments. This supports the earlier given argument that evaporation is limited by precipitation in the semi-arid region, and therefore the evaporation variation on most time scales seem to follow the precipitation variation.
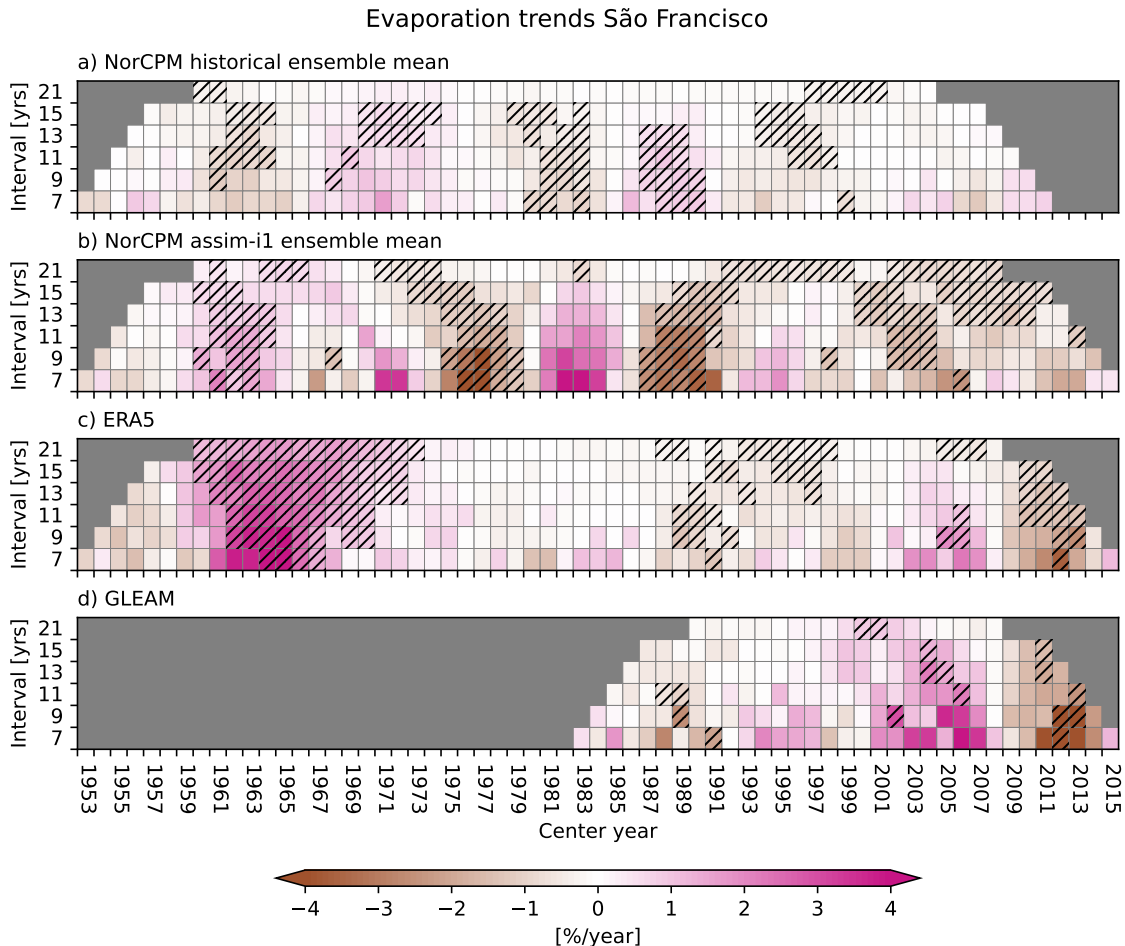

Figure 4.12: Same as figure 4.7, but for Propria catchment in São Francisco.

63

For evaporation, like with precipitation, the assim-i1 experiment induce more variation on shorter time scales that look different from the historical ensemble variation. And during the recent decade, the evaporation is decreasing in the the assim-i1 experiment on several time scales, coinciding with observations.

To investigate the seasons and time scales of variability, and to identify the origin of the ocean induced variability in the assim-i1 experiment and in observations, I present correlations between seasonal filtered time series and correlation maps.

When filtered on longer time scales, > 9 years, the assim-i1 experiment does not improve correlations in any seasons between the observed inflow and modelled precipitation variation, as compared to the historical experiment (table 4.5). For the slow variation in MAM, the correlation between observed rainfall and lagged inflow are high (ERA5: 0.55, CHIRPS: 0.75), but the assim-i1 has an negative correlation (statistically insignificant). These low correlation values indicate that the modelled precipitation variation on these time scales might not be connected to the right dynamics in the model, as the variations are so different.

Table 4.5: Correlation coefficients (with corresponding p-values) between 9 year-lowpass filtered seasonal precipitation and 1 month-lagged streamflow in Propria catchment in the São Francisco region. All data is normalized and detrended prior to correlation calculation. Significant correlations are marked in bold.

	ERA5	CHIRPS	NorCPM hist.	NorCPM assim-i1
DJF				
R	0.37	0.63	0.42	**-0.77**
p	0.4163	0.2018	0.3747	0.0789
MAM				
R	0.55	0.75	0.6	-0.04
p	0.2127	0.1637	0.1563	0.9317
JJA				
R	-0.59	-0.12	-0.11	-0.27
p	0.3965	0.8237	0.8452	0.6419
SON				
R	-0.14	0.16	**-0.75**	-0.13
p	0.8256	0.7547	0.0578	0.847

When assessing the correlation map filtered on the same time scales (low-pass, 9 years, figure 4.13), it can be seen that both assim-i1 and observed data show a negative PDO-like pattern, with a "comma"-shape of negative correlations in the North Pacific basin in MAM, JJA and SON. The correlations between SSTs in the Tropical Pacific and precipitation variation in São Francisco reach stronger correlations in the model than in the observations. In the observations, no Tropical Pacific correlations are statistically significant during MAM and JJA for instance.

For the beginning of the wet season, DJF, the model show few statistically significant correlations with the SST variations on decadal time scales. The model does not replicate the correlation pattern of the observations in the tropical band either (pattern correlation between modelled and observed correlation maps is 0.04; table 4.6). Hence, even tough the model is assimilated with the observed SSTs, the *model dynamics* are not replicating the right dynamical patterns to replicate the precipitation variation in DJF on decadal time scales. This can be why the assim-i1 experiment does not improve the interannual variations well enough to reach significant correlations between DJF precipitation and lagged streamflow.
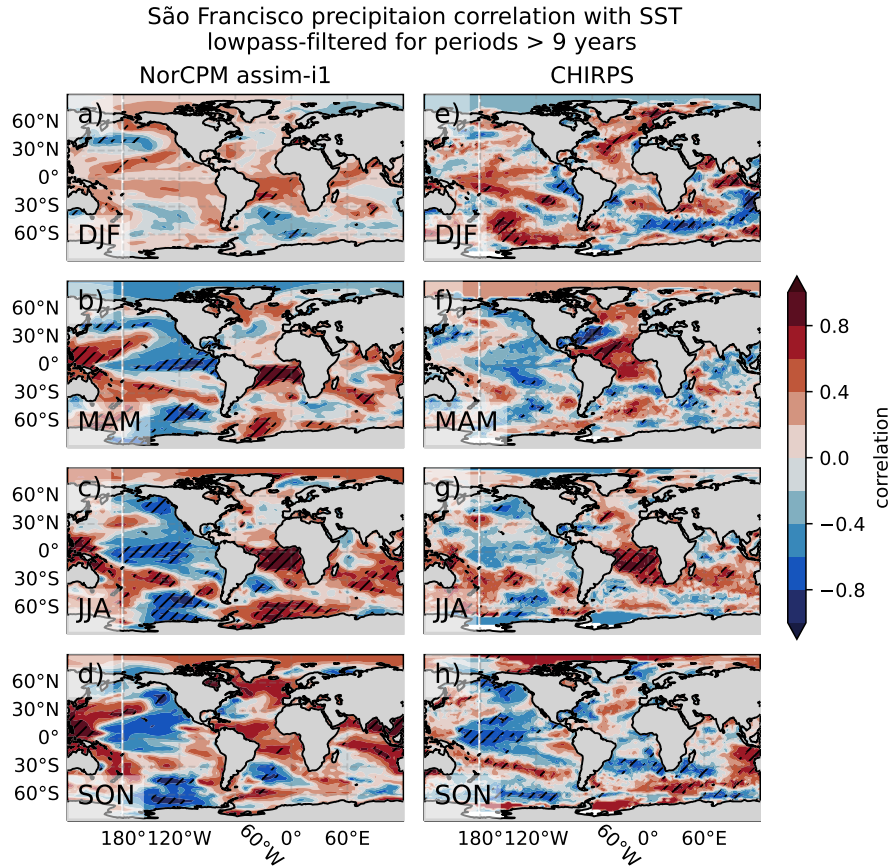
Figure 4.13: Correlation values between seasonal precipitation time series in Propria catchment in São Francisco and global seasonal SSTs for NorCPM assim-i1 ensemble mean (a-d) and CHIRPS correlated with ERA5 SSTs (e-h). All time series are normalized and lowpass-filtered for periods > 9 years before the correlations are calculated. The time series run from 1981-2018. Hatched areas are significant with $\alpha = 0.1$.

Table 4.6: Pattern correlations between the correlation maps of NorCPM assim-i1 and CHIRPS in figure 4.13. The spatial extent of the tropical Oceans basins are defined in figure 3.2. The tropical ocean band is defined as ocean between 30°N and 30°S.

	DJF	MAM	JJA	SON
Tropical Pacific Ocean	-0.09	0.11	0.73	0.39
Tropical Atlantic Ocean	0.23	0.33	0.64	0.55
Indian Ocean	0.02	0.24	0.5	0.61
Tropical Ocean Band	0.04	0.45	0.78	0.62

Table 4.7 shows the correlation between the seasonal precipitation and the streamflow filtered on *interannual* time scales, between 2-9 years. Both the decadal and interannual filtered streamflow is lagged with 1 month in the correlation analyses, since this was the lag that gave the highest correlations in São Francisco catchment. It makes sense that the lead time is shorter in São Francisco than Amazon, as the basin is considerably smaller.

Table 4.7: Correlation coefficients (with corresponding p-values) between 2-9 years-bandpass filtered seasonal precipitation and 1 month-lagged streamflow in Propria catchment in the São Francisco region. All data is normalized and detrended prior to correlation calculation. Significant correlations are marked in bold.

	ERA5	CHIRPS	NorCPM hist.	NorCPM assim-i1
DJF				
R	**0.79**	**0.53**	0.25	-0.24
p	0.0004	0.0451	0.356	0.3348
MAM				
R	-0.06	-0.19	0.31	**-0.48**
p	0.8465	0.5142	0.2257	0.086
JJA				
R	**-0.41**	**-0.46**	**0.49**	-0.17
p	0.0561	0.0422	0.0644	0.4971
SON				
R	0.25	0.09	-0.18	-0.34
p	0.3489	0.7433	0.5276	0.135

Apart from the DJF rainfall, it is striking that the correlation between observed (CHIRPS, ERA5) precipitation and streamflow filtered on this time scale reach such low correlations. The correlations of streamflow with CHIRPS and ERA5 in MAM, JJA and SON are either negative (does not make logically sense; less rain would not lead to higher streamflow) or very low, and all of them insignificant. Hence, interannual variations in streamflow does not seem to be much influenced by the interannual variations in MAM, JJA and SON rainfall. I will suggest some possible explanations for this lack of relaitonship between rainfall and streamflow in the region in the discussion.

The only significant correlation with streamflow in the basin on interannual time scales, is between observed precipitation in DJF and streamflow in JFM (1-month-lagged season; ERA5: 0.79, CHIRPS: 0.53, table 4.7). DJF

is part of the wet season in São Francisco. The correlation in DJF is not replicated in the assim-i1 experiment (R: -0.28, p: 1.73).

When assessing the correlation map between DJF SSTs and precipitation, filtered on the same time scale, it is visible that the NorCPM-assim has a different correlation distribution in the Pacific than the observations. The NorCPM assim-i1 experiment (figure 4.14a) has stronger correlations, in larger and shifted areas compared to the observation correlation map (figure 4.14e). The pattern correlation between the two DJF maps in the Tropical Pacific region is -0.17, and the pattern correlation for the tropical band included is 0.25 (table 4.8). Even though NorCPM is assimilated with observed SSTs in the assim-i1 experiment, the precipitation variation in the São Francisco basin is not affected by the same anomalies in the model as seen in the observations. This could be an explanation for why the year-to-year variations in the model DJF precipitation does not correlate well with variations in the lagged observed streamflow, when the observations do. The lack of correlations might also be caused by model bias (as I will come back to in the discussion).
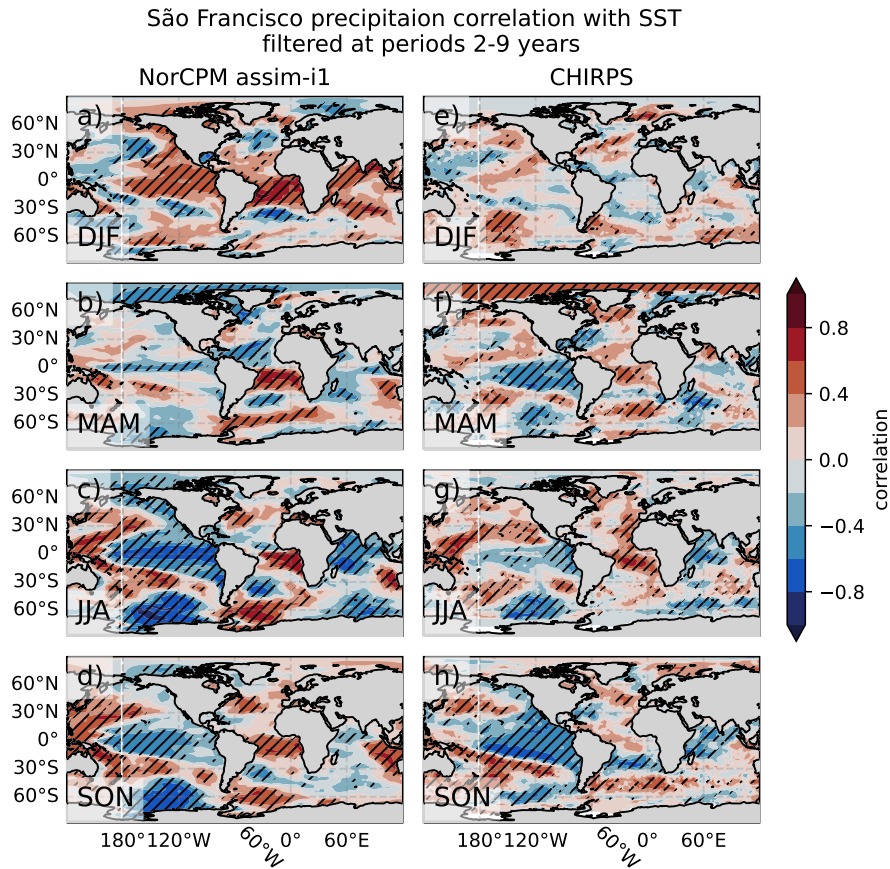
Figure 4.14: Correlation values between seasonal precipitation time series in Propria catchment in São Francisco and global seasonal SSTs for NorCPM assim-i1 ensemble mean (a-d) and CHIRPS correlated with ERA5 SSTs (e-h). All time series are normalized and filtered for periods 2-9 years before the correlations are calculated. The data run from 1981-2018. Hatched areas are significant with $\alpha = 0.1$.

Table 4.8: Pattern correlations between the correlation maps of NorCPM assim-i1 and CHIRPS in figure 4.14 for selected areas. The spatial extent of the tropical Oceans basins are defined in figure 3.2. The tropical ocean band is defined as ocean between 30°N and 30°S.

	DJF	MAM	JJA	SON
Tropical Pacific Ocean	-0.17	0.15	0.59	0.45
Tropical Atlantic Ocean	0.48	0.01	0.51	0.39
Indian Ocean	0.23	0.16	0.63	0.67
Tropical Ocean Band	0.25	0.14	0.64	0.65

4.2.3 Paraguay

Figure 4.15 shows a summary of the trends on different time scales and with different timings for observed streamflow out of Paraguay catchment. From the figure, it is visible that the catchment has oscillations on all time scales, that are significant. The streamflow measurements in this basin reach further back than 1950, but I have included the trends from that period, because it is easier comparable with the precipitation data (NorCPM assim-i1 and ERA5 both start in 1950).

The long record allows the slow oscillations in the flow to be visible. There are several periods of either increasing of decreasing flow that are significant when varying the center of the period, which show that the trends are significant on length scale exceeding the 21-year trend.
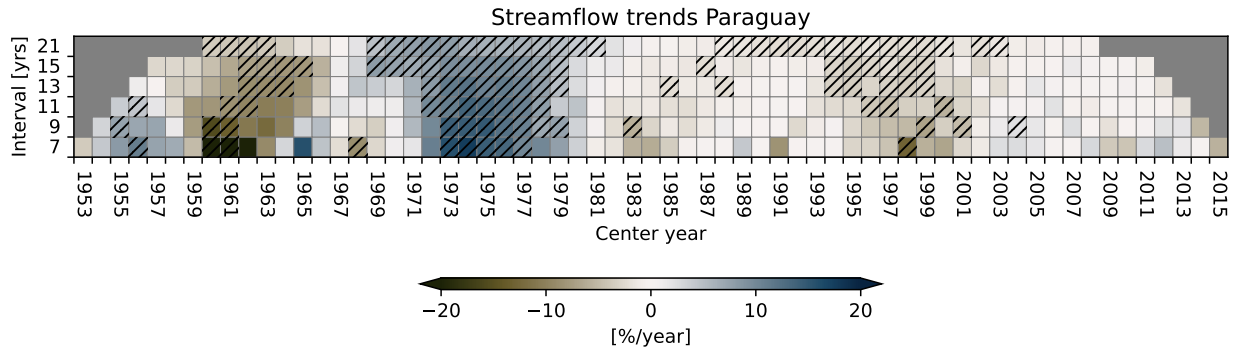

Figure 4.15: Same as figure 4.5, but for Porto Murtinho catchment in Paraguay.

Figure 4.16 shows the trend diagram for the precipitation in the Paraguay basin. It is visible that the assim-i1 ensemble adds variation and oscillations on the shorter time scales, in a magnitude somewhere between ERA5 (with higher magnitude variations) and CHIRPS (with lower magnitude variations). ERA5 and CHIRPS seem to estimate quite different precipitation variations within this catchment. It is important to keep in mind that ERA5 is a reanalysis product that is not based on direct observations of precipitation like CHIRPS is. This might be the reason for the differences, and hence CHIRPS should be trusted more in the region. Assim-i1 agrees on some of the same short scale oscillations as CHIRPS, but not all.

When comparing the significant precipitation trends and their magnitudes with the streamflow variation in the area (figure 4.15), the oscillations on all time scales seem to match quite well between the observed flow and the observed precipitation. The exception is the recent past, where ERA5 has

measured increasing rainfall on all time scales, and CHIRPS significantly increasing rainfall on shorter time scales. There are no statistically significant increasing streamflow trends on shorter time scales in the recent past (figure 4.15).
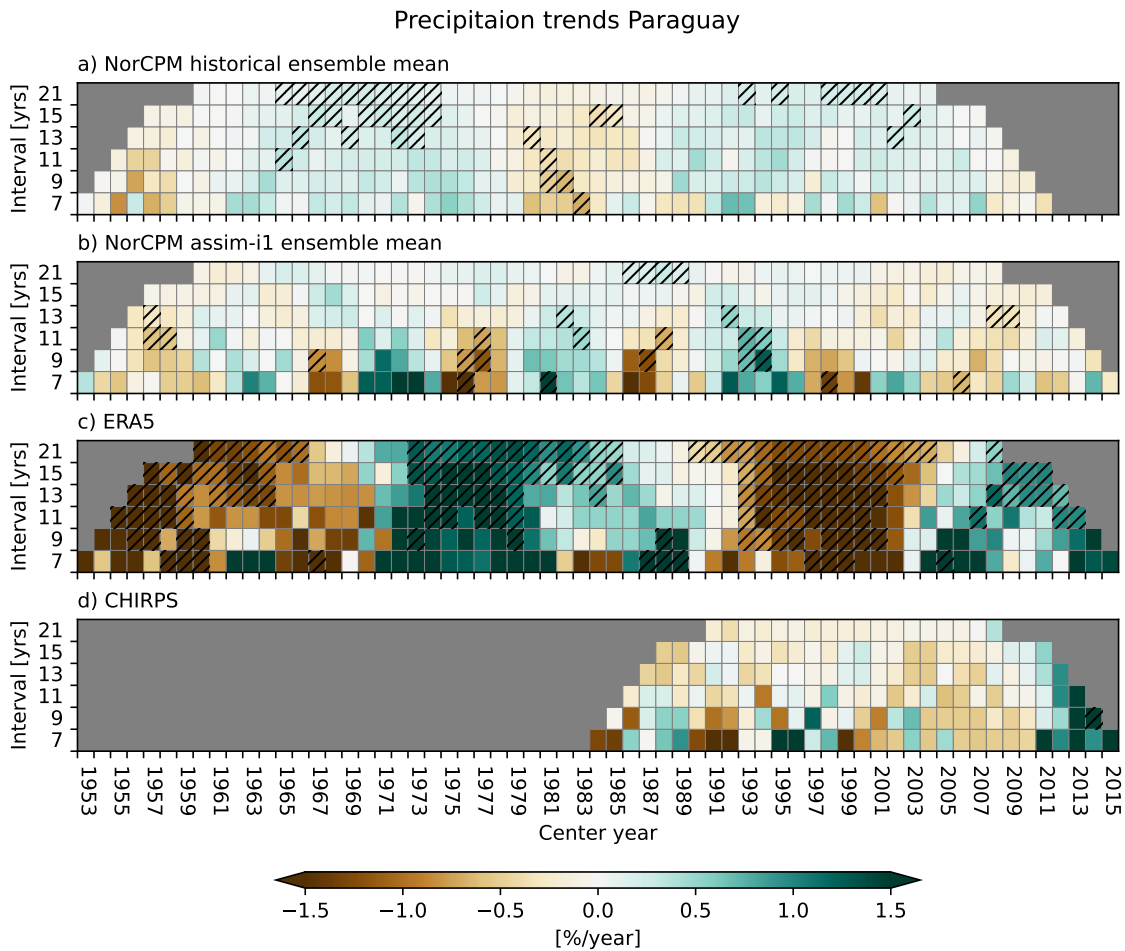
Figure 4.16: Same as figure 4.6, but for Porto Murtinho catchment in Paraguay region.

A reasonable explanation for that the recent increases in rainfall has not resulted in significant increases on streamflow on the same time scale, could be the seen in the evaporation trend diagram for Paraguay (figure 4.17): At the same timing and time scale as the precipitation has increased, the evaporation has increased too.

Assessing the evaporation diagram further, it can be seen that the assim-i1 experiment is altering the strength and timing of evaporation variation in

71

the Paraguay region: First and foremost by introducing stronger variations
on the shorter time scales, that match up with the timing of the observations
on several occasions, although they are somewhat weak. Assim-i1 experiment
is also changing the long-term oscillations, by removing some long-term in-
creasing evaporation trends that are included in the historical experiment.
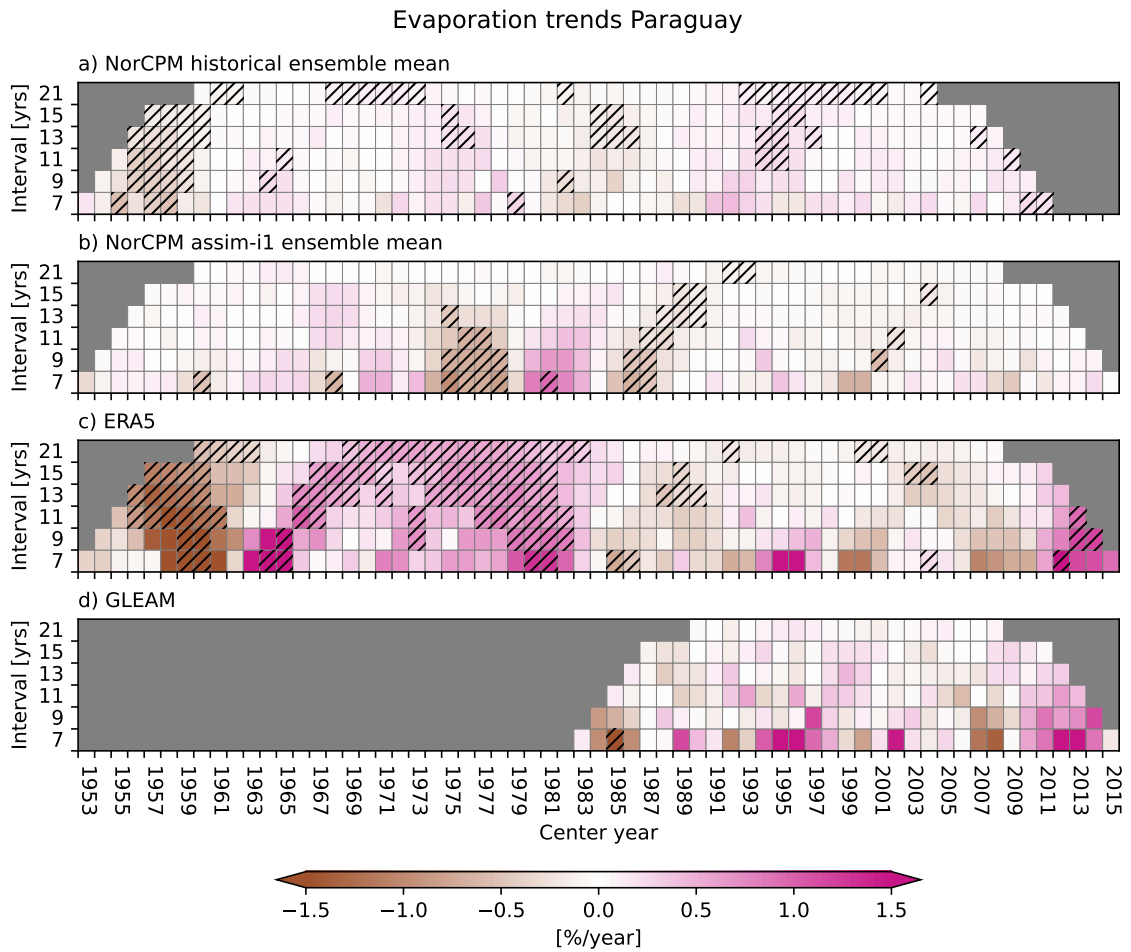
Figure 4.17: Same as figure 4.7, but for Porto Murtinho catchment in
Paraguay region.

For the correlation between the lowpassed filtered precipitation and and
streamflow time series in the Paraguay catchment, there are no statistically
significant correlations (table 4.9). Although not at statistically significant
levels, NorCPM assim-i1 improves the correlation in JJA, which is the dry
season. The correlation maps for low-pass filtered (> 9 years) precipitation
in Paraguay for both assim-i1 and CHIRPS in all seasons are show in figure

4.18. The correlation pattern do not seem to be so consistent between the model and the observations. The pattern correlations in table 4.10 further underlines that the correlations patterns differ. All the pattern correlations between modelled and observed precipitation patterns have negative correlations in the tropical ocean band.

Table 4.9: Correlation coefficients (with corresponding p-values) between > 9 years-lowpass filtered seasonal precipitation and 6 months-lagged streamflow in Porto Murtinho catchment in the Paraguay region. All data is normalized and detrended prior to correlation calculation. Significant correlations are marked in bold.

	ERA5	CHIRPS	NorCPM hist.	NorCPM assim-i1
DJF	(6-month	lag)		
R	0.42	-0.52	-0.27	0.02
p	0.5334	0.4713	0.5835	0.9692
MAM	(6-month	lag)		
R	0.61	0.52	0.08	-0.08
p	0.4128	0.3748	0.9014	0.8586
JJA	(6-month	lag)		
R	0.75	0.11	-0.1	0.56
p	0.1661	0.8584	0.887	0.3156
SON	(2-month	lag)		
R	0.68	0.57	0.14	0.18
p	0.2419	0.2405	0.7934	0.7082

The correlation maps between SON SSTs and SON rainfall in Paraguay catchment look especially different: The CHIRPS data show high significant correlations in the Pacific ocean, with correlation values > 0.6 in large parts of the basin, and > 0.8 in the tropical Pacific (figure 4.18h). The pattern resembles a positive mode of the PDO. In the model (figure 4.18d), on the contrary, the SON correlation pattern has negative values Tropical Pacific. This can be a reason for why the precipitation variations on decadal time scales in the assim-i1 ensemble does not correlate with the observed lagged streamflow in the catchment, even though there is supposed to be a correlation according to observational data (table 4.9). The assim-i1 runs are assimilated with observed ocean anomalies, but do not contain a pattern that replicates the influence of SSTs on Paraguay SON precipitation on decadal time scales, according to observations.
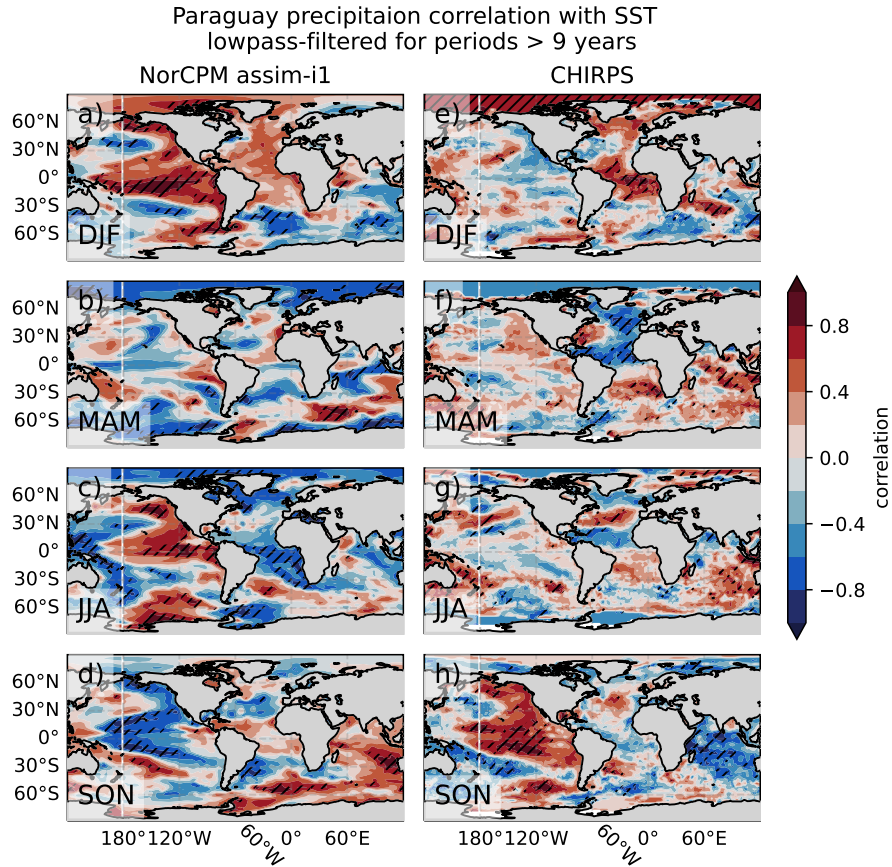
Figure 4.18: Correlation values between seasonal precipitation time series in Porto Murtinho catchment in Paraguay and global seasonal SSTs for Nor-CPM assim-i1 ensemble mean (a-d) and CHIRPS correlated with ERA5 SSTs (e-h). All time series are normalized and lowpass-filtered for periods > 9 years before the correlations are calculated. Time series are from 1981-2018. Hatched areas are significant with $\alpha = 0.1$.

Table 4.10: Pattern correlations between the correlation maps of NorCPM assim-i1 and CHIRPS in figure 4.13 for selected areas. The spatial extent of the tropical Oceans basins are defined in figure 3.2. The tropical ocean band is defined as ocean between 30°N and 30°S.

	DJF	MAM	JJA	SON
Tropical Pacific Ocean	0.14	-0.13	-0.18	-0.64
Tropical Atlantic Ocean	-0.21	-0.18	-0.07	-0.66
Indian Ocean	0.02	-0.11	0.12	-0.57
Tropical Ocean Band	-0.21	-0.13	-0.22	-0.75

74

In the lagged analysis of streamflow observations and precipitation in Paraguay basin (table 4.9 and table 4.11), the highest correlations values were found to be at a 6 month lag, except for in the SON season, where 2 months were found to be the lag that gave the highest correlations. This different lag throughout the season could be explained by different positions of the rainfall maxima. If the rainfall events are close to the outlet of the basin (in the south), the lag will be smaller than when the rainfall happened far from the bottom of the drainage area. A 6 month lag between streamflow and rainfall is quite long, but can be reasonable since the water in the rivers also consists of groundwater flow. If the ground water has a seasonal storage cycle of around 6 months, it makes sense that the river flow has its maximum correlation with the rain 6 months earlier.

Table 4.11 shows the seasonal correlation values between precipitation and lagged streamflow on *interannual* time scales. While the decadal streamflow variability for Paraguay catchment is not statistically significant correlated with precipitation variability, the correlations between streamflow and precipitation filtered on interannual time scale - 2-9 years - is significant at some seasons: SON (beginning of rainy season) for both observational data sets, and MAM and JJA (end of rainy season and dry season) for ERA5 only and DJF (rainy season, CHIRPS). NorCPM assim-i1 experiment improves the correlations compared to NorCPM historical - in the dry season JJA (statistically significant, to R:0.57) and in the beginning of the wet season SON (statistically significant, to R:0.34).

Therefore, SON season in Paraguay basin might be a season and a time where the interannual oscillations (2-9 years) in the oceans are influencing the JJA and SON rainfall, which again are highly correlated with the 6- and 2 month-lagged seasonal streamflow out of the basin (DJF and NDJ; austral summer season).

75

Table 4.11: Correlation coefficients (with corresponding p-values) between 2-9 years-bandpass filtered seasonal precipitation and 6 months-lagged streamflow in Porto Murtinho catchment in Paraguay basin. All data is normalized and detrended prior to correlation calculation. Significant correlations are marked in bold.

	ERA5	CHIRPS	NorCPM hist.	NorCPM assim-i1
DJF	(6-month	lag)		
R	0.31	**0.57**	**-0.3**	0.05
p	0.1105	0.0142	0.099	0.7794
MAM	(6-month	lag)		
R	**0.32**	0.27	-0.0	0.05
p	0.0922	0.2835	0.997	0.8242
JJA	(6-month	lag)		
R	**0.49**	0.15	0.12	**0.57**
p	0.0036	0.5394	0.4724	0.0001
SON	(2-month	lag)		
R	**0.51**	**0.58**	0.13	**0.34**
p	0.0024	0.0152	0.5195	0.0503

Figure 4.19 shows the correlation maps between Paraguay precipitation and global SSTs for assim-i1 and CHIRPS. Generally, these maps look more different to each other. This is also supported by the pattern correlations, which yield low values for the pattern correlations between modelled and observed SST correlation patterns (DJF: -0.26, MAM: 0.22 and JJA: -0.25, table 4.12).

SON was one of the seasons where the filtered correlation with streamflow was improved in the assim-i1 experiment. When looking at the correlation map of SON, assim-i1 experiment (figure 4.19d) has a somewhat similar pattern of SST correlations as the observations (figure 4.19h). Apart from the positive correlation with the Indian ocean in the assim-i1 run that is not in the observations, and the stronger magnitude of the correlations in the model, the correlation patterns have similarities. There are positive correlations in the range of 0.2-0.6 in the Tropical Pacific in both observational and assim-i1 data. For both observations and assim-i1, there is also a southwest/northeast anomaly gradient in the tropical Atlantic that seem to influence the interannual variability of precipation in Paraguay.
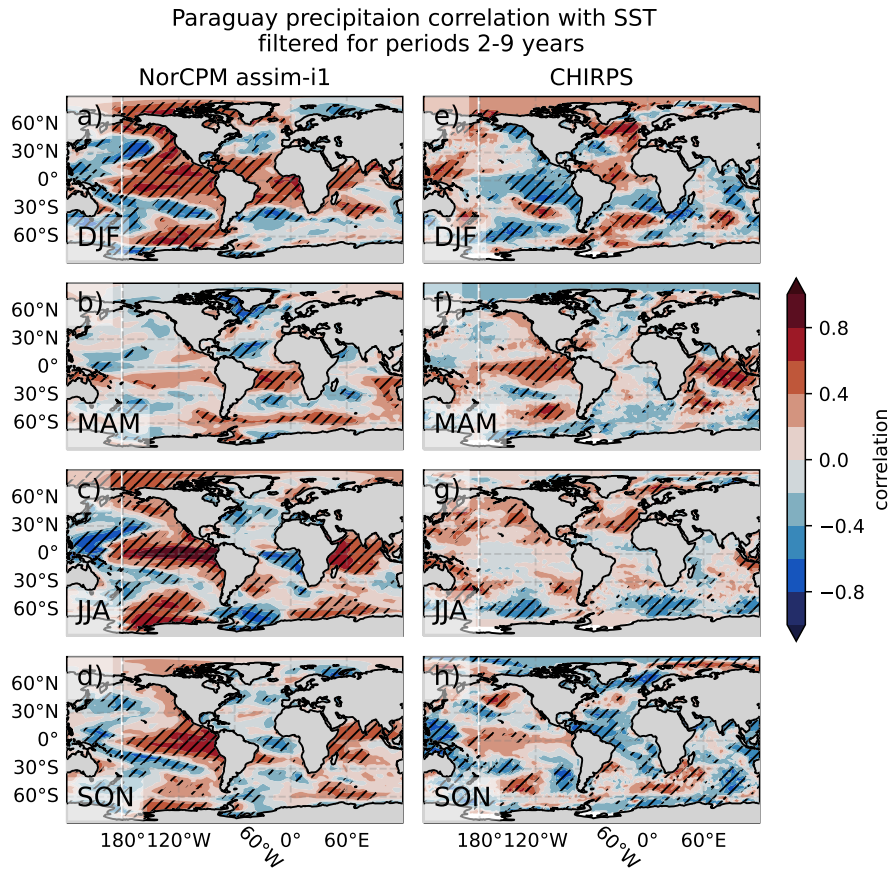
Figure 4.19: Correlation values between seasonal precipitation time series in Porto Murtinho catchment in Paraguay and global seasonal SSTs for NorCPM assim-i1 ensemble mean (a-d) and CHIRPS correlated with ERA5 SSTs (e-h). All time series are normalized and filtered for periods 2-9 years before the correlations are calculated. Data period is 1981-2018. Hatched areas are significant with $\alpha = 0.1$.

Table 4.12: Pattern correlations between the correlation maps of NorCPM assim-i1 and CHIRPS in figure 4.14 for selected areas. The spatial extent of the tropical ocean basins are defined in figure 3.2. The tropical ocean band is defined as ocean between 30°N and 30°S.

	DJF	MAM	JJA	SON
Tropical Pacific Ocean	0.33	0.09	-0.13	0.24
Tropical Atlantic Ocean	-0.44	0.49	-0.14	-0.19
Indian Ocean	-0.14	0.28	-0.15	0.49
Tropical Ocean Band	-0.26	0.22	-0.25	0.29

Chapter 5

Discussion

The method I use in the thesis; comparing output from an ocean assimilated climate model with a non-assimilated climate model to detect influence from ocean variability, has not been used on the case of hydropower production in Brazil before. I will therefore compare the conclusions that this method indicate with results from other studies for the same regions, to see whether the thesis method yields reasonable results compared with the literature.

Then, I will discuss possible explanations for some of the cases where the model did not reproduce the observed variability, or the origin of variability, by assessing the model biases.

Lastly, I will discuss human factors that could have influenced the amount and timing of the streamflow in the catchments, and thereby disturb the analysis of water flow and precipitation. These additional factors might also continue to influence the catchment streamflow in the future, and therefore be important when seeking to understand future streamflow for hydropower production planning.

5.1 Modes of variability and trends affecting streamflow

5.1.1 Amazon

The model results show that the SST variation is a main contributor to the JJA precipitation variations in Amazon basin - and therefore also to the 3-month-lagged flow out of the catchment - both on interannual and decadal time scales. The analysis showed correlations both in the Pacific and Atlantic ocean.

Reboita et al. (2021) found that JJA precipitation in the northern part of the Amazon basin (around 3°S and northward) shows positive rainfall anomalies in the range of 55-75 mm/day when analysing the years between 1979-2019 at times when SST anomalies in the tropical south Atlantic were positive (under neutral ENSO conditions). With different precipitation data sets and SST datasets and methods, I reach the same conclusion in my result, strengthening the result by Reboita et al. (2021), as well as the confidence in the model results in the JJA season in Amazon. Furthermore, since I split the variation in the time series into periods > 9 years and < 9 years, I am able to identify that the most important time scale of variation for the SSTs in the south tropical Atlantic influence on northern Amazon precipitation is on interannual time scales, not on decadal (where the correlation map between precipitation and SSTs did not show the same consistent pattern in the Atlantic ocean as it did in the 2-9 years period filtered correlation map).

The Atlantic ocean SST dipole can modulate the position of the ITCZ, which is the main weather system causing precipitation in Amazon basin, as well as intensity of the trade winds that bring moisture to the Amazon region from the Atlantic (Hastenrath, 1984). This variability has implications for hydropower planning, since the SON flow in Óbidos is also well correlated with the JJA precipitation in the region, the decadal variations of the SON flow can be well detected by predicting the south tropical Atlantic SSTs.

Even though the assim-i1 experiment was able to improve the correlation between the streamflow and the modelled precipitation anomalies in the Amazon basin for most seasons, there were some seasons where the origin of the SST variability connected to the changes were different from the observed one. For decadal variability in DJF for instance, the pattern correlation in the Tropical Pacific was low between model and observations, and the model had higher correlations in the Atlantic than the observations.

The CHIRPS data suggested a negative PDO pattern to be influential for the streamflow variations on longer time scales. It has already been established that slow oscillations in the Pacific ocean with the same pattern as in the CHIRPS correlation map leads to positive rainfall anomalies in Amazon on decadal time scales (Reboita et al., 2021) and inter-decadal time scales (Villamayor et al., 2018). Hence, the observed CHIRPS pattern in the thesis analysis is consistent with previous research - despite the short record of the CHIRPS data. Even though the model resembles part of the pattern, the tropical part of the signal is not different to the observed one. I can hence conclude that the model lack some dynamics to include the decadal and inter-decadal variations originating in the tropical parts of the Pacific ocean on the Amazon DJF precipitation variations. Hence, there are likely some long-term variations that are underplayed in the analysis, which must

be kept in mind in the conclusion.

But the multi-decadal trend from 1981 to 2014 of both of the NorCPM experiments are nevertheless positive, indicating that at least parts of the longer term trend in the basin is due to external forcing. It is reasonable to believe that there is a forced trend that have led to increased rainfall in the Amazon region: The strength of the ITCZ has increased in response to climate change (Byrne et al., 2018 and references therein). Since the rain in Amazon is mostly impacted by this large-scale weather pattern, the increase that was seen in the historical NorCPM experiment makes sense. Thermodynamic relations can be an explanation to the changes: warmer atmosphere can hold more water. Note that global climate models do not agree on the projected changes of the ITCZ (Byrne et al., 2018), which will have implications for future streamflow in the Amazon.

5.1.2 São Francisco

The (strong) decline in streamflow from 2010 until today is coinciding with the phase of AMO, which has gone from a positive to negative phase in the same time span, shifting around year 2000 (Reboita et al., 2021). Also, the correlation map show that there are high correlations with the long oscillations(> 9 years period) between MAM rainfall and SSTs in the tropical Atlantic ocean.

At the same time, the model is syncing up only partly with the tropical Atlantic ocean on this time scale variability (only the western part), and show higher correlations with SSTs in the western part of Pacific, so the model might be right for the wrong reasons. Precipitation does decrease more in the time span due to the ocean variability, but the model makes the area drier because of the wrong physical processes (possibly). This will be discussed further when assessing the model bias (section 5.2).

Propria catchment in São Francisco basin seem to get a lot of its DJF precipitation variability from the Pacific ocean on interannual time scales (2-9 years period) and a lot of the variability on decadal time scales (> 9 years period) seem to originate in the Atlantic ocean, possibly connected to AMO.

Villamayor et al. (2018) found that multidecadal variability in the Atlantic ocean is drying the Northeast part of Brazil (but they investigate an area that is slightly northwards from the São Francisco basin, and therefore is not completely in line with the São Fransciso basin trends). Luiz-Silva et al. (2021) have also found that rainfall in Northeast Brazil is strongly modulated by atmospheric dynamics that are influenced by SSTs in the Pacific Ocean and in the South Atlantic Ocean.

5.1.3 Paraguay

The correlation pattern between SON rainfall in Paraguay and SSTs looks like a typical PDO pattern when assessing the CHIRPS data (figure 4.18 d). The strong streamflow decrease since 1980 and towards 2010 (figure 4.3) is matching well with the switch from the warm phase to the cold phase of PDO, with the switch centered around approximately 1998 (Reboita et al., 2021). The historical NorCPM ensemble contained positive precipitation trends for this region over the last decades, and assim-i1 ensemble did not. The assim-i1 ensemble did not, however manage to recreate the observed *negative precipitation trends*, and a plausible explanation for this shortcoming lies in this poorly correlations with the Pacific basin anomalies. Even though the NorCPM is assimilated with the right SST anomalies in the assim-i1 experiments, the *model mechanics* lack teleconnection patterns that is detectable in the observed precipitation variations for Paraguay - namely the PDO influence on Paraguay rainfall, which seemed to be differing among the seasons, which is also found by Reboita et al. (2021).

5.2 How model biases have influenced the analysis

5.2.1 Precipitation bias

In some areas, the assim-i1 did not replicate the precipitation or evaporation variations that were observed. This could be due to the bias in the model. In the following section, I will therefore show how the differences between the model climatology and the observed climatology might have influenced the results.

The first step is to look at the large scale weather patterns in the model. Figure 5.1a-d shows the seasonal precipitation climatology for the NorCPM assim-i1 ensemble mean for all seasons. The model contains the ITCZ, a band of maximum precipitation that is oscillating the meridional direction, with a maximum southward position in DJF and northward position in JJA. The model also contains the SACZ in DJF and SON and to some extent MAM, with a diagonal band of precipitation in the northeast/southwest orientation from the Amazon to the Atlantic ocean. Compared to the observations (figure 5.1e-h), the model ITCZ looks narrower, and the semi-arid area in the interior of northeast looks bigger and drier. Also, the SACZ seems to not reach as far south as observed.

Figure 5.1i-l shows the bias for precipitation climatology for assim-i1. The

brown areas are where the model is drier than observations, and the green areas are where the model is wetter than the observations. The model precipitation bias has a range of ± 700 mm seasonal difference, and the model values are significantly different from the observed values in the whole country.
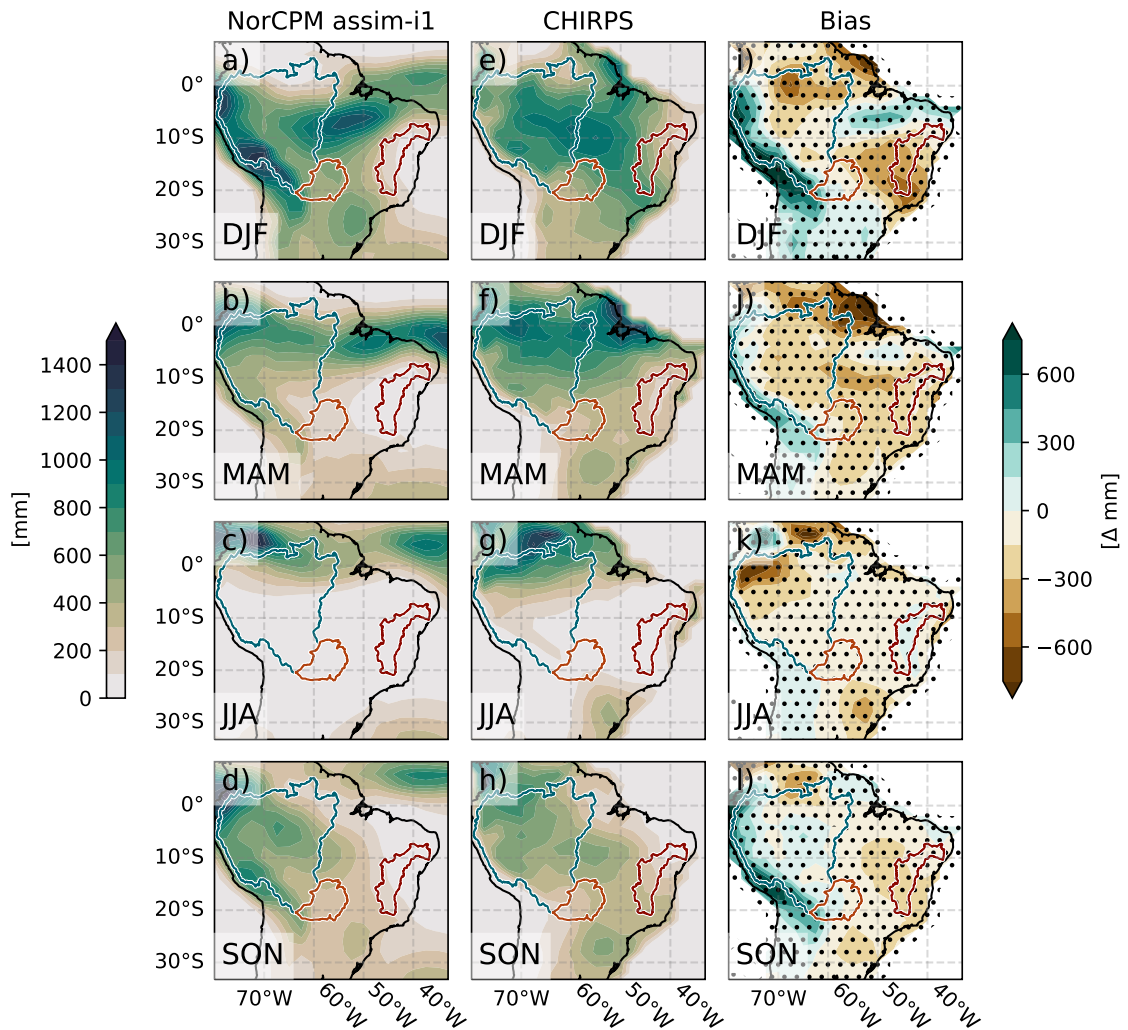

Figure 5.1: Mean seasonal total precipitation model bias (i-l), defined as the CHIRPS mean precipitation (e-h) subtracted from the NorCPM assim-i1 ensemble mean (a-d) precipitation for the cliamtological period 1981-2011. Dotted areas are significant at a 95 % confidence level. The area indicated areas are the three catchments treated in this thesis.

There are two features that stands out. First, the model is generally too dry, especially in the northeastern region, where the São Francisco basin

is located (red region on figure 5.1). This is one of the driest areas in the country, and still the dry biases measured in mm are largest here.

The modelled precipitation cycle in the São Francisco region (figure 5.2b), is highly affected by the dry bias of the model in the northeast of the country. The model estimates only about a third of the observed precipitation values in the basin though large parts of the wet season. The model is closer to the observed values in the dry season, where both observations and model approach zero. Although the timing of the rainy season in São Francisco basin in the model seems to fit quite well, the rainy season is way too dry. It was also during the rainy season that the model did not correlate well with the observed lagged streamflow variability on either of the time-scales. The reason might be the dry bias in the region in the season.
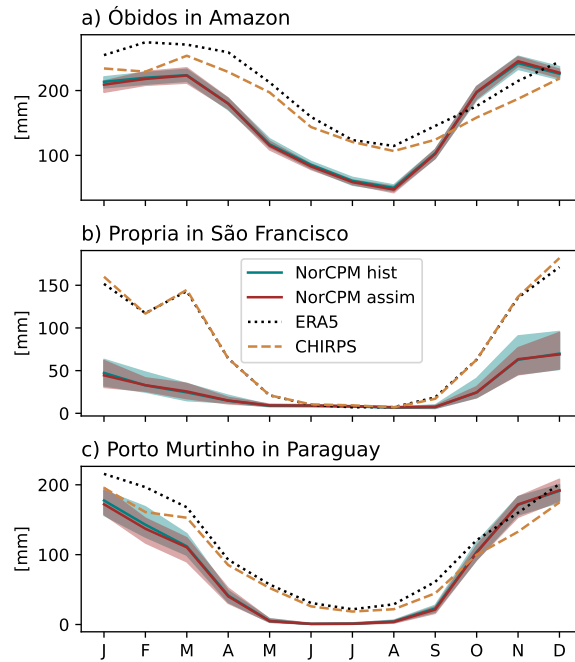
Figure 5.2: 1981-2011 climatological mean annual precipitation cycle for Óbidos catchment in Amazon, Propria catchment in São Francisco, and Porto Murtinho catchment in Paraguay. For the NorCPM data, solid line is the ensemble mean, and shaded area is the ensemble spread.

The analysis of variability during the rainy season in São Francisco is also a part of the results where model precipitation did not match with the streamflow. For instance, DJF modelled precipitation - filtered for interannual time scales - and the MAM modelled precipitation - filtered for decadal

time scales - did not correlate with the lagged streamflow, even though the observed precipitation did. The strong dry bias in the São Francisco basin might have been the reason for this lack of correlations in the analysis.

Second, the model has a strong wet bias in the Andes mountain range, with values > 750 mm in DJF, 150-300 mm in MAM and 300-600 mm in SON. These biases are within the Amazon Óbidos catchemnt (blue region on figure 5.1). In the rest of the Óbidos catchment, the model is too dry in the northeastern part of the basin during the wet season - DJF and MAM - and too dry in the northwestern part of the basin in JJA.

When investigating the climatological seasonal cycle Amazon (figure 5.2a), the catchment has the right magnitude of precipitation throughout the year in the model experiments, but the onset of the wet season is too early in the model compared with observations. This could be because the model over-estimates rainfall in the Andes mountain range and underestimates rainfall in the northern part of the basin - as discussed above. The positive and negative biases within the region cancel each other out - hence the magnitude of the *mean* catchment rainfall is similar to observations, but the seasonal rainfall cycle is shifted since a higher proportion of the rainfall in the model comes from the south of the basin and less from the north - compared to observations.

This bias seem to have affected the analysis, as the Andes mountain range was an area where the model overestimated the precipitation trends over the 1981-2014 region. This bias seem to have given this part of the catchment proportionally more influence on the mean precipitation time series, which is used when assessing the trends and variations of different time scales and timings. The results for the analyses in the Amazon basin must therefore be understood as representing trends and variations in the eastern part of the basin more than it represents trends and variations over the Amazon forest and in the northern part of the basin. The latter areas are also important for the streamflow variations out of the catchment.

The biases in Paraguay catchment (orange region on figure **??**) are smaller than for the other catchments, with the model reaching a 150-300 mm difference only in the northeastern part of the basin during MAM, and biases $< \pm 150$ mm throughout the rest of the year. For the mean precipitation in the region, the Paraguay catchment also seem to have the right amount of rainfall and the right timing of the seasonal cycle (figure 5.2c).

5.2.2 Evaporation bias

The model also contains less evaporation than observations in large parts of
the country (figure 5.3). The biases are in the right panel of figure 5.3, and the
brown areas are where the model has less evaporation than the observations,
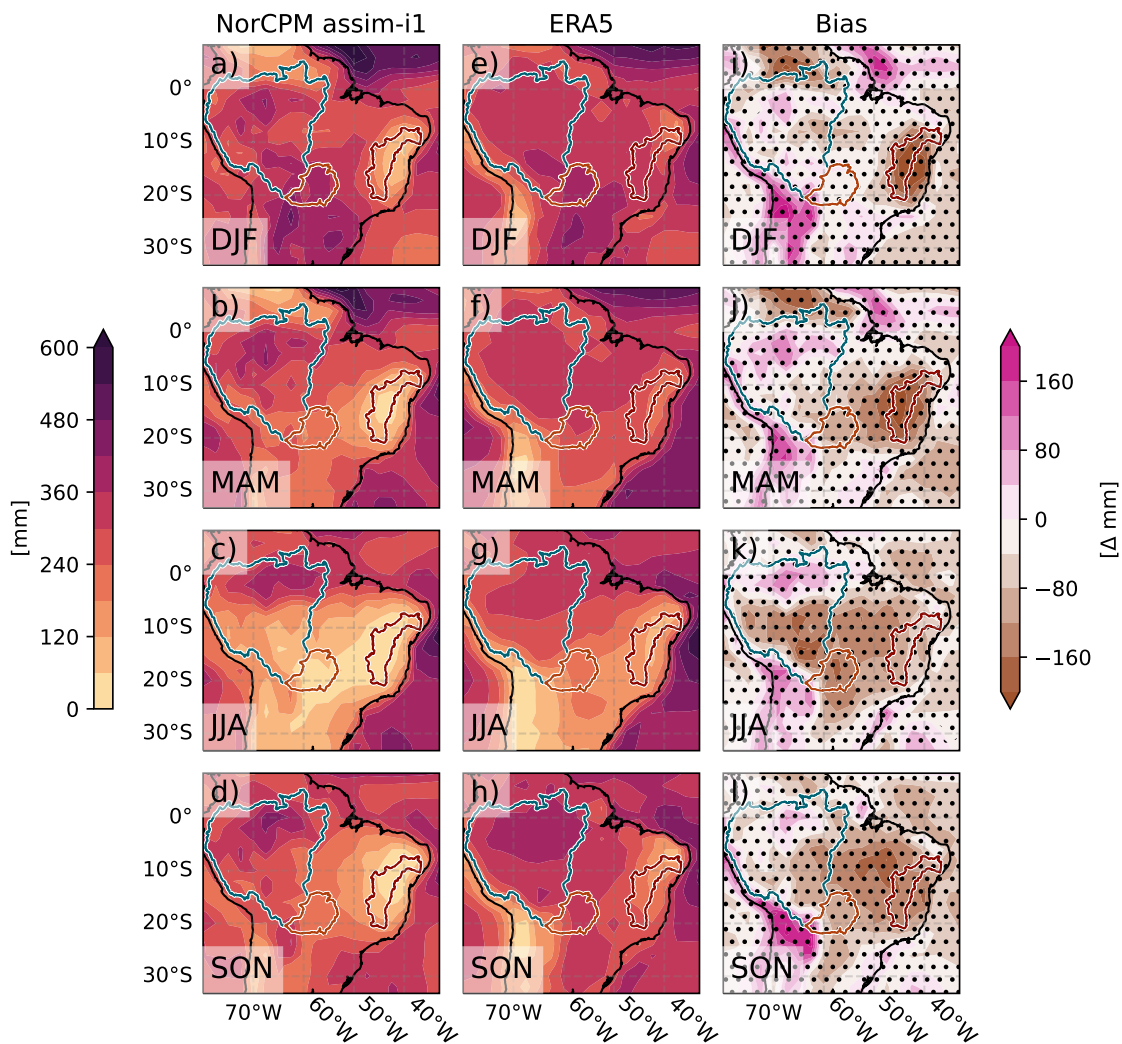and the magenta areas are where the model has more evaporation.

Figure 5.3: Mean seasonal total evaporation model bias (i-l), defined as the
ERA5 mean precipitation (e-h) subtracted from the NorCPM assim-i1 ensem-
ble mean (a-d) precipitation for the cliamtological period 1981-2011. Dotted
areas are significant at a 95 % confidence level. The areas indicated are the
three catchments treated in this master thesis.

The evaporation climatology bias in the NorCPM is about 150-600 mm per year in large part of the country. Especially in the SACZ region during the rainy season (DJF and to some extent MAM and SON; figure 5.3i, 5.3j and 5.3l respectively), there is a bias of too little evaporation. Since the model has too little precipitation in the same areas for the same seasons, this is the likely cause. There is likely too little moisture in the atmosphere over large parts of Brazil in the model, causing too little evaporation and too little precipitation. This might have influenced the trends in the 1981-2014 analysis: Especially in the São Francisco, where the model bias is large.

The seasonal timings of the evaporation maxima and minima in the three basins are not too far off, even if the values are low (especially in São Francisco, and in some parts of the year in Amazon, figure 5.4). Hence, the evaporation magnitude is likely to have affected the analysis more than the seasonal timing bias, since the latter seem to be more in line with observations.
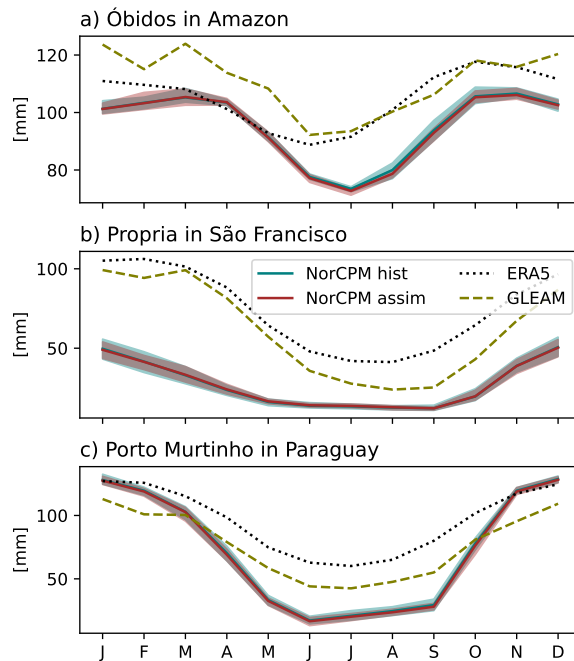

Figure 5.4: 1981-2011 climatological mean annual evaporation cycle for Óbidos catchment in Amazon, Propria catchment in São Francisco, and Porto Murtinho catchment in Paraguay. For the NorCPM data, solid line is the ensemble mean, and shaded area is the ensemble spread.

5.3 Other ways the model might have influenced the analysis

5.3.1 Differences in model climatology between the two experiments

In addition to adding ocean variability of the right timing in the assim-i1 experiment, the assimilated ocean variables also change the climatology of the model (slightly, figure 5.5).

Therefore, another possible interpretation of when the assim-i1 ensemble is synchronizing with the observed longer trends could be that the local dynamics or the placements of the large scale systems are improved in the assim-i1 model, since the temperatures of the ocean are connected to the large scale systems as well. The location of the SACZ (oceanic component) is for instance related to the SSTs in South Atlantic, in a two-way relationship (Jorgetti et al., 2014).

In figure 5.5, the differences between the two precipitation climatologies of the experiments are presented. Although the modelled large scale rainfall patterns are very similar for the historical and the assim-i1 ensemble means, there are some differences that might have affected the analysis. The brown areas in the figure are where the assim-i1 mean is drier than the historical mean, and the green areas are where the assim-i1 mean is wetter than the historical mean. The magnitude of the difference between these two is within the range of ± 50 mm seasonal difference (figure 5.5).

For the Amazon Óbidos catchment (blue region on figure 5.5), the assim-i1 is significantly drier in the northern half of the basin during JJA. This indicates that the ITCZ in the assim-i1 runs is displaced a bit northwards, or that the ITCZ causes less rainfall in that season in the assim-i1 runs. During DJF, the SACZ band is drier in the assim-i1 ensemble mean. This affects the southern half of the Paraguay basin (orange region on figure 5.5). Furthermore, assim-i1 climatology is wetter than the historical model climatology in the southern part of São Francisco basin (red region on figure 5.5).
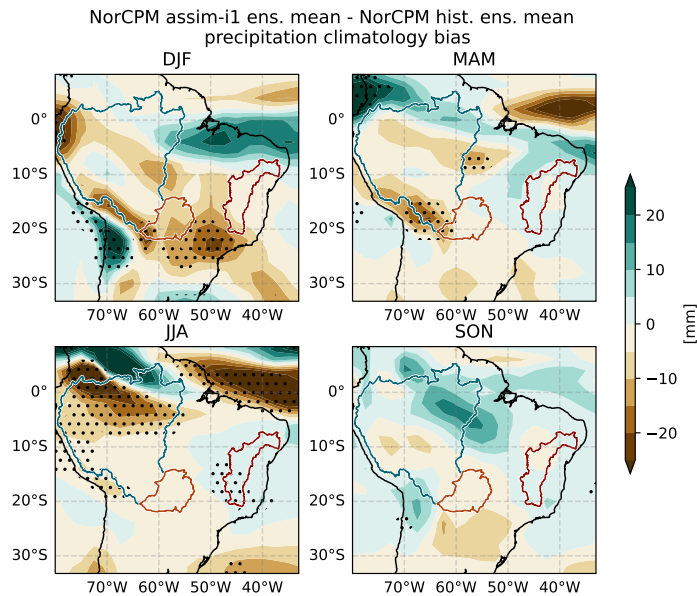
Figure 5.5: 1981-2011 mean seasonal total precipitation difference NorCPM assim-i1 ensemble mean - NorCPM historical ensemble mean. Dotted areas are significant at a 95 % confidence level.

5.3.2 Influence of resolution

The scarce resolution of the model - compared to observations - will have influenced the results. Such scarce resolution cannot resolve the same details in topography and precipitation systems as the CHIRPS and ERA5 is able to do, with the higher resolution of 0.05°and 0.25 °respectively.

The resolution of the model limited my choices for catchment areas to analyse. I had to pick out catchments that were large enough to at least covering an area that consists of more than one grid cell, and thereby I had to analyse catchment areas there are not uniform in climate type. Additionally, larger catchments have longer lags and less correlation between inflow and precipitation (Luiz-Silva et al., 2021). Both the São Francico catchment and the Paraguay catchment consist of 10 grid cells, while the Amazon catchment consists of around 90 grid cells.

5.4 Human activities that have influenced river flow in Brazil

In Brazil, basins that have received increasing (decreasing) rainfall amounts do not always correspond with the basins that have received increasing (decreasing) inflow into the dams (Luiz-Silva et al., 2021), indicating that other variables are also key to understanding the inflow rates in the country.

In coherence with this, what I found, is that there are many regions and seasons where the correlations between precipitation and streamflow were not significant for the observational data, even when lags are included. For instance for interannual variability in the São Francisco reservoir outside the rainy season, there seem to be other influences affecting the streamflow magnitudes.

In Paraguay for longer time scale variation, there should also be additional explanations for the changes in river flow according to the results. Since the correlation between observed precipitation and streamflow are significant for the 2-9 year band-pass filtered data (for all seasons except MAM, table 4.11), but not for the low-pass filtered time series (table 4.9), the year-to-year precipitation variability might be more influential than decadal variability on the variability of streamflow in the region. But the decdal and longer variations might require a different explanation. Especially since the measurements show that the streamflow decline is very steep over the last decades, and the precipitation observations are not as steep.

Some possible explanations for these two cases - and their alike - might impacts by human activities, including farming, deforestation and hydropower production from other dams in upstream reservoirs.

5.4.1 Upstream reservoirs

Many of these streamflow observations have other reservoirs or hydropower plants upstream from the measurement location. That means that the production (and therefore the streamflow out of the dam) from these upstream reservoirs also influence the streamflow measured at the bottom of the catchment. Since producers might let out water into the river at different timings, this affect the seasonal cycle of river flow, and thereby introducing large variations in the seasonal flow from year to year. São Francisco basin has the Sobradinho dam upstream from the Propria measuring point, which is one of the largest dams in the country. This might have influenced the measurements and the connection between precipitation and streamflow substantially in this region.

Especially, since the lowest precipitation-flow correlations are between the dry season precipitation and the lagged flow, it seems like the river flow could depend on for instance how much water that was saved in the reservoirs during the wet season rather than how much it was raining during the dry season. This might give a year-to-year variability that does not match up with the dry season anomalies.

5.4.2 Land use changes and water consumption

Land use changes might impact the river flow directly - through increased water consumption by agricultural activities - and indirectly through deforestation, which changes the soil infiltration and evaporation patterns. Across the three basins, there have been different influences on the river flow from different types of human activities, that have changes the river flows in the period which is analyse in this thesis.

In the Pantanal, in the upper part of the Paraguay basin, there has been a growth of water-intensive agriculture over the last decade: Between 2000 and 2008, the agricultural land cover increased with 28 % (Marques et al., 2021), since natural biomes were converted to farm land and pasture. The water consumption along the river by the farming activities, could be an explanation to why the precipitation in the region has increased on all time scales in the recent decade, but the streamflow has not.

In Amazon, there has been extensive deforestation over the last decades (Chagas et al., 2022). Conversion from rain forest to cropland changes both the soil - and therefore the timing of the river flow - and the evaporation pattern. As explained in the background part, the Amazon is a region where a lot of the precipitation originates in the rain forest itself, and has been recycled through the transpiration by the forest. Hence, these changes over the last decades could also have been - and continue to be - an influence on the river flow out of Óbidos catchment.

Chagas et al. (2022) found that large-scale deforestation is a cause of decreased river minimum flow in the southern Amazon. In the northern part of the basin, on the other hand, the minimum flows were found to having increased, with the reason being an increase in precipitation-evaporation (P-E). The streamflow in the northern Amazon was little affected by land management, probably due to more undisturbed areas (Chagas et al., 2022).

In the Brazilian highlands (southern part of the São Francisco basin, an area with high concentration of agriculture and the main origin of water in the São Francisco river), both the meteorological decrease of water availability and increasing water use have led to decreasing minimum and maximum flow in the river, but from the year 2000 and onward, a rapid increase in water

use has been the cause of decreasing amounts of river flow in drought flows
(Chagas et al., 2022). This means, that even though I with this thesis am able
to separate the changes in river flow that is caused by external forcing from
that of internal variability, the anthropological factors could be as important
as the meteorological ones for the recent and future flow.

Chapter 6

Summary and conclusion

In this thesis, I have aimed to separate internal variability from trends in three hydrographic catchments in Brazil. I have assessed trends and variability of precipitation and evaporation in an ocean anomaly assimilated NorCPM experiment, and compared them to observed precipitation, evaporation and streamflow trends and variability for catchments in Amazon, São Francisco and Paraguay. Additionally, I have correlated modelled and observed seasonal precipitation time series for each catchment with observed lagged streamflow and modelled and observed global SSTs for two separated filtered time-scales.

I have found that the Amazon region is a catchment where the streamflow has been increasing over the last decades and over the last years at statistically significant levels on several time scales. The thesis results suggests that part of the mean inflow increase over the last decades is related to external forcing that has caused precipitation increase. I have also shown that JJA precipitation variation - on decadal and interannual time-scales - is tightly linked to variations originating in the ocean *and* to observed streamflow out of the Amazon Óbidos catchment in SON. NorCPM replicates the global SST variation pattern well on both interannual and decadal time scales for the JJA precipitation. For hydropower planing in Amazon, the connection between global JJA SSTs and SON streamflow can be used to improve predictions of future streamflow. For the future of hydropower in the region, the thesis results indicate that the long-term trend of increased inflow will persist, but with substantial decadal and interannual variations.

For the São Francisco basin, the streamflow has been decreasing over the last decades, and steeply since about year 2000. All recent decrease is at statistical significant levels. According to the analysis conducted in the thesis, the inter-decadal decreasing trend might be linked to variability originating in the ocean. At the same time, low correlations between observed

92

streamflow and rainfall in Propria in Saõ Francisco, indicate that decadal streamflow variability is influenced profoundly by other factors than rainfall as well. There is statistically significant variability that originates in the Atlantic, Pacific and Indian oceans that affect rainfall variations in São Francisco. Interannual precipitation variability during parts of the wet season, DJF, is tightly linked to streamflow variability out of São Francisco. The model is not able to represent the teleconnections that connects SST variability in the ocean to DJF precipitation variability the catchment, mainly due to a lack of the right correlation pattern in the tropical Pacific ocean and the Indian Ocean. For hydropower production planning in São Francisco, the water levels can be expected to (partly) restore in future, as the results indicate that the inter-decal decreasing trend seem to have been caused by internal variation. Stakeholders should also monitor other influences in the region - such as human activities - to predict the water balance of the future.

Streamflow out of Paraguay catchment has decreased strongly at statistical significant levels over the last decades. It is not clear from the results whether the steep reduction in streamflow over the last decades is caused by internal variability or external forcing. Decadal streamflow variations seem to be strongly influenced by other factors than precipitation variation, due to insignificant correlations between observed streamflow and precipitation in all seasons. On interannual time scales, the results show that JJA and SON precipitation variation in Porto Murtinho catchment in Paraguay is tightly connected to ocean variability *and* to streamflow variability in the austral summer. The correlation maps showed that significant variability is connected to warm anomalies in the tropical Pacific and southwest/northeast anomaly gradient in the tropical Atlantic. To understand the future long-term trend and decadal variations of streamflow in Paraguay, other variables in addition to precipitation should be monitored. Hydropower production planners can utilize the verified connection between global JJA and SON SST variations on austral summer streamflow on interannual time scales, to predict future flow.

The NorCPM wet bias over the Andes mountains in Amazon, and the dry bias in São Francisco have affected the analysis in the two regions. In the all basins, the model lack some of the right teleconnection responses to global SST anomalies, especially in the rainy season MAM in São Francisco and Amazon, and in all seasons in Paraguay. For all catchments, JJA is the season where NorCPM ocean anomaly assimilation improves the correlation with streamflow the most, and MAM is the season where the ocean anomalies generally improves the precipitaiton the least. These model restrictions have affected the analysis.

Chapter 7

Future work

Substantial further knowledge on how trends and variability affect hydropower production in Brazil is still needed. In this thesis, only three catchments were assessed, and only one earth system model analysed. As discussed, the results in this thesis are limited by the performance of this model. In the future, it would therefore be very interesting to conduct the same analysis with an *ensemble* of different earth system models, which were all assimilated with the same observed ocean variability. This might remove some of the errors resulting from the systematic biases that comes from using a single model.

Additionally, a more comprehensive understanding of the interaction between precipitation, evaporation and streamflow could be obtained by looking into the water fluxes from land to ocean in the model, and compare that with the observed streamflow data from the large rivers. It would also be interesting to conduct a similar experiment, where ocean variability in only parts of the global oceans were assimilated, to further distinguish between ocean variability origins.

More studies of the interaction between climate change, variability and human influence would be very useful for hydropwer planning in Brazil. Recommended future work is to design a more comprehensive analysis by using data on water consumption and streamflow from upstream reservoirs that is provided in the CAMELS-BR collection.

Using the modelled precipitation and evaporation as input into a hydrological model would also be very interesting. This would reveal more precise streamflow responses to precipitation and evaporation variations, since hydrological models can model the actual flow - including deep infiltration into the soil - in a much more detailed manner. Using a hydrological model would also enable experiments that test the sensitivity between land use change effects and rainfall variability and different combinations of the two.

Bibliography

A. A. Abatan, S. F. Tett, B. Dong, C. Cunningham, C. M. Rudorff, N. P. Klingaman, and R. C. de Abreu. Drivers and physical processes of drought events over the State of São Paulo, Brazil. *Climate Dynamics*, 58(11-12): 3105–3119, 6 2022. ISSN 14320894. doi: 10.1007/s00382-021-06091-2.

A. Almagro, P. T. S. Oliveira, and L. Brocca. Assessment of bottom-up satellite rainfall products on estimating river discharge and hydrologic signatures in Brazilian catchments. *Journal of Hydrology*, 603, 12 2021. ISSN 00221694. doi: 10.1016/j.jhydrol.2021.126897.

L. M. Alves, R. Chadwick, A. Moise, J. Brown, and J. A. Marengo. Assessment of rainfall variability and future change in Brazil across multiple timescales. *International Journal of Climatology*, pages 1875–1888, 2020.

ANA - Brazilian National Water Agency. HIDROWEB, 3 2023.

S. H. Bari, M. T. U. Rahman, M. A. Hoque, and M. M. Hussain. Analysis of seasonal and annual rainfall trends in the northern region of Bangladesh. *Atmospheric Research*, 176-177:148–158, 7 2016. ISSN 01698095. doi: 10.1016/j.atmosres.2016.02.008.

H. E. Beck, E. F. Wood, M. Pan, C. K. Fisher, D. G. Miralles, A. I. J. M. van Dijk, T. R. McVicar, and R. F. Adler. MSWEP V2 Global 3-Hourly 0.1° Precipitation: Methodology and Quantitative Assessment. *Bulletin of the American Meteorological Society*, 100(3):473–500, 3 2019. ISSN 0003-0007. doi: 10.1175/BAMS-D-17-0138.1.

M. Bentsen, I. Bethke, J. B. Debernard, T. Iversen, A. Kirkevåg, Seland, H. Drange, C. Roelandt, I. A. Seierstad, C. Hoose, and J. E. Kristjánsson. The Norwegian Earth System Model, NorESM1-M – Part 1: Description and basic evaluation of the physical climate. *Geoscientific Model Development*, 6(3):687–720, 5 2013. doi: 10.5194/gmd-6-687-2013.

I. Bethke, Y. Wang, F. Counillon, N. Keenlyside, M. Kimmritz, F. Fransner, A. Samuelsen, H. Langehaug, L. Svendsen, P.-G. Chiu, L. Passos, M. Bentsen, C. Guo, A. Gupta, J. Tjiputra, A. Kirkevåg, D. Olivié, Seland, J. Solsvik Vågane, Y. Fan, and T. Eldevik. NorCPM1 and its contribution to CMIP6 DCPP. *Geoscientific Model Development*, 14(11):7073–7116, 2021. doi: 10.5194/gmd-14-7073-2021. URL `https://gmd.copernicus.org/articles/14/7073/2021/`.

C. S. Bretherton, M. Widmann, V. P. Dymnikov, J. M. Wallace, and I. Bladé. The Effective Number of Spatial Degrees of Freedom of a Time-Varying Field. pages 1990–2009, 1999.

S. Butterworth. On the Theory of Filter Amplifiers . *Experimental Wireless and the Wireless Engineer*, 7:536–541, 10 1930.

M. P. Byrne, A. G. Pendergrass, A. D. Rapp, and K. R. Wodzicki. Response of the Intertropical Convergence Zone to Climate Change: Location, Width, and Strength. *Current Climate Change Reports*, 4(4):355–370, 12 2018. ISSN 2198-6061. doi: 10.1007/s40641-018-0110-5.

W. Cai, M. J. McPhaden, A. M. Grimm, R. R. Rodrigues, A. S. Taschetto, R. D. Garreaud, B. Dewitte, G. Poveda, Y. G. Ham, A. Santoso, B. Ng, W. Anderson, G. Wang, T. Geng, H. S. Jo, J. A. Marengo, L. M. Alves, M. Osman, S. Li, L. Wu, C. Karamperidou, K. Takahashi, and C. Vera. Climate impacts of the El Niño–Southern Oscillation on South America, 4 2020. ISSN 2662138X.

M. A. Caretta, A. Mukherji, M. Arfanuzzaman, R. A. Betts, A. Gelfan, Y. Hirabayashi, T. K. Lissner, J. Liu, E. L. Gunn, R. Morgan, S. Mwanga, S. Supratid, H.-O. Pörtner, D. C. Roberts, M. Tignor, E. S. Poloczanska, K. Mintenbeck, A. Alegría, M. Craig, S. Langsdorf, S. Löschke, V. Möller, A. Okem, and B. Rama. Water. In H.-O. Pörtner, D. Roberts, M. Tignor, E. Poloczanska, K. Mintenbeck, A. Alegría, M. Craig, S. Langsdorf, S. Löschke, V. Möller, A. Okem, and B. Rama, editors, *Climate Change 2022: Impacts, Adaptation and Vulnerability. Contribution of Working Group II to the Sixth Assessment Report of the Intergovernmental Panel on Climate Change.*, chapter Water, pages 551–712. Cambridge University Press, Cambridge, 2022. doi: 10.1017/9781009325844.006.

V. B. Chagas, P. L. B. Chaffe, N. Addor, F. M. Fan, A. S. Fleischmann, R. C. D. Paiva, and V. A. Siqueira. CAMELS-BR: Hydrometeorological time series and landscape attributes for 897 catchments in Brazil.

Earth System Science Data, 12(3):2075–2096, 9 2020. ISSN 18663516. doi: 10.5194/essd-12-2075-2020.

V. B. P. Chagas, P. L. B. Chaffe, and G. Blöschl. Climate and land management accelerate the Brazilian water cycle. *Nature Communications*, 13(1): 5136, 9 2022. ISSN 2041-1723. doi: 10.1038/s41467-022-32580-x.

W. L. F. Correia Filho, J. F. de Oliveira-Júnior, C. A. da Silva Junior, and D. d. B. Santiago. Influence of the El Niño–Southern Oscillation and the sypnotic systems on the rainfall variability over the Brazilian Cerrado via Climate Hazard Group InfraRed Precipitation with Station data. *International Journal of Climatology*, 42(6):3308–3322, 5 2022. ISSN 10970088. doi: 10.1002/joc.7417.

J. C. Costa, G. Pereira, M. E. Siqueira, F. Da Silva Cardozo, and V. V. Da Silva. VALIDAÇÃO DOS DADOS DE PRECIPITAÇÃO ESTIMADOS PELO CHIRPS PARA O BRASIL. *Revista Brasileira de Climatologia*, 24, 6 2019. ISSN 1980-055X. doi: 10.5380/abclima.v24i0.60237.

A. P. M. Cunha, M. Zeri, K. D. Leal, L. Costa, L. A. Cuartas, J. A. Marengo, J. Tomasella, R. M. Vieira, A. A. Barbosa, C. Cunningham, J. V. Cal Garcia, E. Broedel, R. Alvalá, and G. Ribeiro-Neto. Extreme drought events over Brazil from 2011 to 2019. *Atmosphere*, 10(11), 11 2019. ISSN 20734433. doi: 10.3390/atmos10110642.

J. F. de Oliveira-Júnior, C. A. da Silva Junior, P. E. Teodoro, F. S. Rossi, C. J. C. Blanco, M. Lima, G. de Gois, W. L. F. Correia Filho, D. de Barros Santiago, and M. H. G. dos Santos Vanderley. Confronting CHIRPS dataset and in situ stations in the detection of wet and drought conditions in the Brazilian Midwest. *International Journal of Climatology*, 41 (9):4478–4493, 7 2021. ISSN 10970088. doi: 10.1002/joc.7080.

V. d. S. Dias, M. P. da Luz, G. M. Medero, and D. T. F. Nascimento. An overview of hydropower reservoirs in Brazil: Current situation, future perspectives and impacts of climate change, 5 2018. ISSN 20734441.

C. Funk, P. Peterson, M. Landsfeld, D. Pedreros, J. Verdin, S. Shukla, G. Husak, J. Rowland, L. Harrison, A. Hoell, and J. Michaelsen. The climate hazards infrared precipitation with stations - A new environmental record for monitoring extremes. *Scientific Data*, 2, 12 2015. ISSN 20524463. doi: 10.1038/sdata.2015.66.

R. D. Garreaud, M. Vuille, R. Compagnucci, and J. Marengo. Present-day South American climate. *Palaeogeography, Palaeoclimatology,*

Palaeoecology, 281(3-4):180–195, 10 2009. ISSN 00310182. doi: 10.1016/j.palaeo.2007.10.032.

S. A. Good, M. J. Martin, and N. A. Rayner. EN4: Quality controlled ocean temperature and salinity profiles and monthly objective analyses with uncertainty estimates. *Journal of Geophysical Research: Oceans*, 118 (12):6704–6716, 12 2013. ISSN 21699275. doi: 10.1002/2013JC009067.

A. M. Grimm. The El Niño Impact on the Summer Monsoon in Brazil. *Source: Journal of Climate*, 16(2):263–280, 2003. doi: 10.2307/26249547.

D. L. Hartmann. Global physical climatology, 2016.

S. Hastenrath. Interannual Variability and Annual Cycle: Mechanisms of Circulation and Climate in the Tropical Atlantic Sector. *Monthly Weather Review*, 112(6):1097–1107, 6 1984. ISSN 0027-0644. doi: 10.1175/1520-0493(1984)112¡1097:IVAACM¿2.0.CO;2.

H. Hersbach, B. Bell, P. Berrisford, S. Hirahara, A. Horányi, J. Muñoz-Sabater, J. Nicolas, C. Peubey, R. Radu, D. Schepers, A. Simmons, C. Soci, S. Abdalla, X. Abellan, G. Balsamo, P. Bechtold, G. Biavati, J. Bidlot, M. Bonavita, G. De Chiara, P. Dahlgren, D. Dee, M. Diamantakis, R. Dragani, J. Flemming, R. Forbes, M. Fuentes, A. Geer, L. Haimberger, S. Healy, R. J. Hogan, E. Hólm, M. Janisková, S. Keeley, P. Laloyaux, P. Lopez, C. Lupu, G. Radnoti, P. de Rosnay, I. Rozum, F. Vamborg, S. Villaume, and J.-N. Thépaut. The ERA5 global reanalysis. *Quarterly Journal of the Royal Meteorological Society*, 146(730):1999–2049, 2020. doi: https://doi.org/10.1002/qj.3803. URL `https://rmets.onlinelibrary.wiley.com/doi/abs/10.1002/qj.3803`.

International Energy Agency. *Hydropower*. IEA Technology Roadmaps. OECD, 11 2012. ISBN 9789264189201. doi: 10.1787/9789264189201-en. URL `https://www.oecd-ilibrary.org/energy/hydropower`$_9$`789264189201 − en`.

International Energy Agency. Brazil Energy Statistics, 2 2022a.

International Energy Agency. Renewables, 2 2022b. URL `https://www.iea.org/fuels-and-technologies/renewables`.

R. L. Jaffe. Energy from moving water: Hydropower. In *The physics of energy*, pages 591–594. Cambridge University Press, Cambridge, 2018. ISBN 9781107016651.

P. D. Jones, D. H. Lister, C. Harpham, M. Rusticucci, and O. Penalba. Construction of a daily precipitation grid for southeastern South America for the period 1961-2000. *International Journal of Climatology*, 33(11): 2508–2519, 9 2013. ISSN 08998418. doi: 10.1002/joc.3605.

T. Jorgetti, P. L. da Silva Dias, and E. D. de Freitas. The relationship between South Atlantic SST and SACZ intensity and positioning. *Climate Dynamics*, 42(11-12):3077–3086, 2014. ISSN 14320894. doi: 10.1007/s00382-013-1998-z.

Z. Liu and M. Alexander. Atmospheric bridge, oceanic tunnel, and global climatic teleconnections, 6 2007. ISSN 87551209.

H. Locher and A. Scanlon. Sustainable Hydropower – Issues and Approaches. In H. Samadi-Boroujeni, editor, *Hydropower: Practice and Application*, chapter 1, pages 1–22. NTECH d.o.o., Croatia, 2012.

C. López-Bermeo, R. D. Montoya, F. J. Caro-Lopera, and J. A. Díaz-García. Validation of the accuracy of the CHIRPS precipitation dataset at representing climate variability in a tropical mountainous region of South America. *Physics and Chemistry of the Earth*, 127, 10 2022. ISSN 14747065. doi: 10.1016/j.pce.2022.103184.

W. Luiz Silva, L. N. R. Xavier, M. E. P. Maceira, and O. C. Rotunno. Climatological and hydrological patterns and verified trends in precipitation and streamflow in the basins of Brazilian hydroelectric plants. *Theoretical and Applied Climatology*, 137(1-2):353–371, 7 2019. ISSN 14344483. doi: 10.1007/s00704-018-2600-8.

W. Luiz-Silva, A. C. Oscar-Júnior, I. F. A. Cavalcanti, and F. Treistman. An overview of precipitation climatology in Brazil: space-time variability of frequency and intensity associated with atmospheric systems. *Hydrological Sciences Journal*, 66(2):289–308, 2021. ISSN 21503435. doi: 10.1080/02626667.2020.1863969.

H. B. Mann. Nonparametric Tests Against Trend. *Econometrica*, 13(3): 245–259, 7 1945. URL https://www.jstor.org/stable/1907187.

J. F. Marques, M. B. Alves, C. F. Silveira, A. Amaral e Silva, T. A. Silva, V. J. dos Santos, and M. L. Calijuri. Fires dynamics in the Pantanal: Impacts of anthropogenic activities and climate change. *Journal of Environmental Management*, 299:113586, 2021. ISSN 0301-4797. doi: https://doi.org/10.1016/j.jenvman.2021.113586. URL https://www.sciencedirect.com/science/article/pii/S0301479721016480.

B. Martens, D. G. Miralles, H. Lievens, R. van der Schalie, R. A. M. de Jeu, D. Fernández-Prieto, H. E. Beck, W. A. Dorigo, and N. E. C. Verhoest. GLEAM v3: satellite-based land evaporation and root-zone soil moisture. *Geoscientific Model Development*, 10(5):1903–1925, 5 2017. ISSN 1991-9603. doi: 10.5194/gmd-10-1903-2017.

NOAA. Gridded Climate Data, 3 2023.

V. H. d. M. Paca, G. Espinoza-Dávalos, D. Moreira, and G. Comair. Variability of Trends in Precipitation across the Amazon River Basin Determined from the CHIRPS Precipitation Product and from Station Records. *Water*, 12(5):1244, 4 2020. ISSN 2073-4441. doi: 10.3390/w12051244.

F. J. Paredes-Trejo, H. A. Barbosa, and T. V. Lakshmi Kumar. Validating CHIRPS-based satellite precipitation estimates in Northeast Brazil. *Journal of Arid Environments*, 139:26–40, 4 2017. ISSN 1095922X. doi: 10.1016/j.jaridenv.2016.12.009.

M. S. Reboita, T. Ambrizzi, N. M. Crespo, L. M. M. Dutra, G. W. d. S. Ferreira, A. Rehbein, A. Drumond, R. P. da Rocha, and C. A. d. Souza. Impacts of teleconnection patterns on South America climate. *Annals of the New York Academy of Sciences*, 1504(1):116–153, 2021. ISSN 17496632. doi: 10.1111/nyas.14592.

M. S. Reboita, C. A. C. Kuki, V. H. Marrafon, C. A. de Souza, G. W. S. Ferreira, T. Teodoro, and J. W. M. Lima. South America climate change revealed through climate indices projected by GCMs and Eta-RCM ensembles. *Climate Dynamics*, 58(1-2):459–485, 1 2022. ISSN 14320894. doi: 10.1007/s00382-021-05918-2.

R. W. Reynolds, N. A. Rayner, T. M. Smith, D. C. Stokes, and W. Wang. An Improved In Situ and Satellite SST Analysis for Climate. *Journal of Climate*, 15(13):1609–1625, 7 2002. ISSN 0894-8755. doi: 10.1175/1520-0442(2002)015¡1609:AIISAS¿2.0.CO;2.

E. B. Rosa, L. P. Pezzi, M. F. L. d. Quadro, and N. Brunsell. Automated Detection Algorithm for SACZ, Oceanic SACZ, and Their Climatological Features. *Frontiers in Environmental Science*, 8, 2 2020. ISSN 2296665X. doi: 10.3389/fenvs.2020.00018.

P. K. Sen. Estimates of the Regression Coefficient Based on Kendall's Tau. *Journal of the American Statistical Association*, 63(324):1379–1389, 12 1968. ISSN 0162-1459. doi: 10.1080/01621459.1968.10480934.

V. A. Siqueira, R. C. D. Paiva, A. S. Fleischmann, F. M. Fan, A. L. Ruhoff, P. R. M. Pontes, A. Paris, S. Calmant, and W. Collischonn. Toward continental hydrologic–hydrodynamic modeling in South America. *Hydrology and Earth System Sciences*, 22(9):4815–4842, 9 2018. ISSN 1607-7938. doi: 10.5194/hess-22-4815-2018.

G. W. Snedecor. *Statistical Methods. Applied to Experiments in Agriculture and Biology.* The Iowa State University Press, Ames, 5 edition, 1956.

R. G. Tedeschi and M. Collins. The influence of ENSO on South American precipitation: simulation and projection in CMIP5 models. *International Journal of Climatology*, 37(8):3319–3339, 6 2017. ISSN 10970088. doi: 10.1002/joc.4919.

H. Theil. A rank-invariant method of linear and polynominal regression analysis (parts 1-3). *Ned. Akad. Wetensch. Proc. Ser. A*, 53:1397–1412, 1950.

R. E. Thomson and W. J. Emery. *Data Analysis Methods in Physical Oceanography.* Elsevier, 2014. ISBN 9780123877826. doi: 10.1016/C2010-0-66362-0.

J. Villamayor, T. Ambrizzi, and E. Mohino. Influence of decadal sea surface temperature variability on northern Brazil rainfall in CMIP5 simulations. *Climate Dynamics*, 51(1-2):563–579, 7 2018. ISSN 0930-7575. doi: 10.1007/s00382-017-3941-1.

R. J. Villela. The south Atlantic convergence zone: A critical view and overview, 2017. ISSN 21761892.

F. Wang, W. Shao, H. Yu, G. Kan, X. He, D. Zhang, M. Ren, and G. Wang. Re-evaluation of the Power of the Mann-Kendall Test for Detecting Monotonic Trends in Hydrometeorological Time Series. *Frontiers in Earth Science*, 8, 2 2020. ISSN 2296-6463. doi: 10.3389/feart.2020.00014.

A. Wörman. Hydrological Statistics for Regulating Hydropower. In H. Samadi-Boroujeni, editor, *Hydropower: Practice and Application*, chapter 3, pages 41–60. INTECH d.o.o., Croatia, 2012.

S. Yue and C. Y. Wang. Applicability of prewhitening to eliminate the influence of serial correlation on the Mann-Kendall test. *Water Resources Research*, 38(6):4–1, 6 2002. ISSN 00431397. doi: 10.1029/2001wr000861.

P. G. Zaninelli, C. G. Menéndez, M. Falco, N. López-Franca, and A. F. Carril. Future hydroclimatological changes in South America based on an ensemble of regional climate models. *Climate Dynamics*, 52(1-2):819–830, 1 2019. ISSN 14320894. doi: 10.1007/s00382-018-4225-0.

M. T. Zilli, L. M. Carvalho, and B. R. Lintner. The poleward shift of South Atlantic Convergence Zone in recent decades. *Climate Dynamics*, 52(5-6): 2545–2563, 3 2019. ISSN 14320894. doi: 10.1007/s00382-018-4277-1.